Departamento de Ingeniería Química y Tecnologías del Medio Ambiente
UNIVERSIDAD DE ZARAGOZA

DOCTORAL THESIS

CHEMICAL LOOPING COMBUSTION OF BIOMASS WITH NEGATIVE CO_2 EMISSIONS

Author: Antón C. Pérez Astray

Supervisors: M. Teresa Mendiara Negredo
Luis F. de Diego Poza

Zaragoza, December 2019

icb INSTITUTO DE CARBOQUIMICA

CSIC
CONSEJO SUPERIOR DE INVESTIGACIONES CIENTÍFICAS

M. Teresa Mendiara Negredo, Investigadora ‘‘Ramón y Cajal’’, y

Luis F. de Diego Poza, Investigador científico del CSIC,

CERTIFICAN:

que el trabajo titulado:

“Combustión de biomasa mediante transportadores de oxígeno con emisiones negativas de CO_2”

“Chemical Looping Combustion of biomass with negative CO_2 emissions”

Fue realizado por Antón C. Pérez Astray bajo la dirección de los abajo firmantes en el Instituto de Carboquímica (ICB-CSIC) en Zaragoza y se corresponde con el plan de investigación aceptado el 29 de septiembre de 2016 por la Comisión de Doctorado de la Universidad de Zaragoza. Así mismo, se autoriza a la presentación de la misma como compendio de publicaciones.

Y para que así conste, se firma el presente certificado,

Fdo: Dra. M. Teresa Mendiara Negredo Fdo: Dr. Luis F. de Diego Poza

en Zaragoza, a 12 de noviembre de 2019.

Combustión de biomasa con transportadores de osíxeno e emisións negativas de CO_2

Resumo

As emisións de CO_2 á atmosfera convertéronse nun importante problema ambiental debido ao quecemento global e ao consecuente cambio climático. O reto do cambio climático fai precisa a implicación e aplicación de estratexias combinadas entre institucións, gobernos e cidadás. Para alcanzárense os obxectivos fixados no Acordo de París (2015) cómpre reducir as emisións de gases de efecto invernadoiro e actualmente ningunha tecnoloxía é capaz de atinxir os obxectivos de redución por si mesma. A biomasa representa unha interesante alternativa como combustíbel con emisións neutras de CO_2. Deste xeito, se o CO_2 xerado durante a combustión de biomasa é capturado para ser almacenado, pódense acadar emisións negativas de CO_2 a través da bioenerxía con captura e almacenamento de CO_2. A combustión mediante transportadores de osíxeno destaca coma unha das tecnoloxías de captura de CO_2 máis prometedoras grazas á baixa penalización enerxética da separación do CO_2 e o consecuente baixo custo do proceso. A combustión mediante transportadores sólidos de osíxeno baséase na utilización de reactores de leito fluidizado, as reaccións de combustión teñen lugar no reactor de redución, onde o transportador sólido de osíxeno, normalmente un óxido metálico, redúcese. Despois de se reducir, o transportador de osíxeno chega ao reactor de oxidación, onde se volve oxidar en aire para comezar un novo ciclo redox.

O principal obxectivo desta tese é avaliar o potencial das tecnoloxías de combustión mediante transportadores sólidos de osíxeno con biomasa. O plan de investigación inclúe estudos a diferentes escalas, comezando a nivel de laboratorio, continuando con planta piloto de 1 kW_t e rematando coa operación en continuo dunha planta de 20 kW_t para demostrar a viabilidade e optimizar os rangos de operación precisos para o uso de distintos transportadores de osíxeno.

Algúns minerais, baseados en ferro ou en manganeso, foron seleccionados pola alta reactividade e baixo custo dos mesmos. Na planta 1 kW_t estudouse o efecto

de distintas variábeis de operación sobre o funcionamento do proceso baixo *In Situ* Gasification Chemical Looping Combustion (*i*G-CLC). Obtivéronse valores arredor do 100% de eficacia de captura de CO_2 cos tres tipos de biomasa estudados usando minerais como transportadores de osíxeno, e as demandas totais de osíxeno reducíronse coa substitución do transportador de osíxeno por outros máis reactivos así como pola optimización de diferentes variábeis de operación. Tamén se probou un óxido sintético mixto baseado en ferro e manganeso con capacidade de liberar osíxeno molecular durante o proceso de combustión. Neste caso estudouse tamén o efecto de distintas variábeis de operación sobre a eficacia de captura de CO_2 maila demanda total de osíxeno, atopando unha gran dependencia de ámbalas dúas tanto da temperatura no reactor de oxidación como do exceso de aire no mesmo reactor, chegando a valores arredor do 100% de eficacia de captura de CO_2 con demandas totais de osíxeno por volta do 5%. O uso dun óxido mixto baseado en cobre e manganeso estudouse tamén baixo o proceso coñecido como Chemical Looping with Oxygen Uncoupling (CLOU). Neste caso obtivéronse altos valores de eficacia de captura de CO_2 e demandas totais de osíxeno próximas a cero. Na planta de 20 kW_t, estudouse o efecto de diferentes variábeis de operación utilizando un mineral de ferro como transportador de osíxeno. Nesta planta acadáronse valores de demanda próximas ao 100% e demandas totais de osíxeno entre 15-20% malia as baixas temperaturas usadas.

Outros dos aspectos a seren considerados na combustión de biomasa son a formación de NO_x maila posible presenza de alcatráns na corrente gasosa de saída. Neste traballo compáranse os resultados obtidos mediante dous modos de operación, *i*G-CLC e CLOU.

Todos estes resultados amosan as posibilidades de integración de biocombustíbeis sólidos coas tecnoloxías de combustión mediante transportadores de osíxeno conseguindo unha tecnoloxía quen de producir un beneficio enerxético con emisións negativas de CO_2.

Palabras chave: Biomasa, NET, BECCS, CLC, *i*G-CLC, CLOU.

Combustión de biomasa mediante transportadores de oxígeno con emisiones negativas de CO_2

Resumen

Las emisiones de CO_2 a la atmósfera se han convertido en un importante problema ambiental debido al calentamiento global y el consecuente cambio climático. El reto del cambio climático hace necesaria la aplicación de estrategias combinadas entre instituciones, gobiernos y ciudadanos. Para alcanzar los objetivos fijados en el Acuerdo de París (2015) es necesario reducir las emisiones de gases de efecto invernadero y actualmente ninguna tecnología es capaz de alcanzar los objetivos de reducción por si sola. La biomasa representa una interesante alternativa como combustible con emisiones neutras de CO_2. Así mismo, si el CO_2 generado durante la combustión de biomasa es capturado para su almacenamiento, se pueden alcanzar emisiones negativas de CO_2 a través de la bioenergía con captura y almacenamiento de CO_2. La combustión mediante transportadores de oxígeno destaca como una de las tecnologías de captura de CO_2 más prometedoras gracias a la baja penalización energética debida a la separación del CO_2, y su consecuente bajo coste. La combustión mediante transportadores sólidos de oxígeno se basa en la utilización de reactores de lecho fluidizado. La combustión tiene lugar en el reactor de reducción, donde el transportador sólido de oxígeno, normalmente un óxido metálico, se reduce. Después de reducirse, el transportador de oxígeno llega al reactor de oxidación, donde se vuelve a oxidar en aire para comenzar un nuevo ciclo redox.

El principal objetivo de esta tesis es evaluar el potencial de las tecnologías de combustión mediante transportadores sólidos de oxígeno con biomasa. El plan de investigación incluye estudios a diferentes escalas, comenzando a nivel de laboratorio, continuando con planta piloto de 1 kW_t y finalizando con la operación en continuo de una planta de 20 kW_t para demostrar la viabilidad y optimizar los rangos de operación para el uso de distintos transportadores de oxígeno.

Algunos minerales basados en hierro, así como otros basados en manganeso, han sido seleccionados por su alta reactividad y bajo coste. En la planta 1 kW_t se

estudió el efecto de distintas variables de operación sobre el funcionamiento del proceso bajo *In Situ* Gasification Chemical Looping Combustion (*i*G-CLC). Se alcanzaron valores en torno al 100% de eficacia de captura de CO_2 con los tres tipos de biomasa estudiados usando minerales como transportadores de oxígeno, y las demandas totales de oxígeno se redujeron mediante la sustitución del transportador de oxígeno por otros más reactivos, así como por la optimización de diferentes variables de operación. También se ha probado un óxido sintético mixto basado en hierro y manganeso con capacidad de liberar oxígeno molecular durante el proceso de combustión. En este caso se estudió también el efecto de distintas variables de operación sobre la eficacia de captura de CO_2 y la demanda total de oxígeno, encontrando una gran dependencia tanto de la temperatura como del exceso de aire, ambos en el reactor de oxidación. Se alcanzaron valores en torno al 100% de eficacia de captura de CO_2 con demandas totales de oxígeno alrededor del 5%. El uso de un óxido mixto basado en cobre y manganeso ha sido estudiado también bajo el proceso conocido como Chemical Looping with Oxygen Uncoupling (CLOU). En este caso se alcanzaron altos valores de eficacia de captura de CO_2 y demandas totales de oxígeno próximas a cero. En la planta de 20 kW_t, se estudió el efecto de diferentes variables de operación utilizando un mineral de hierro como transportador de oxígeno. En esta planta se alcanzaron valores de demanda próximas al 100% y demandas totales de oxígeno en torno al 15-20% pese a las bajas temperaturas usadas.

Otros de los aspectos a ser considerados en la combustión de biomasa es la formación de NO_x y la posible presencia de alquitranes en la corriente gaseosa de salida. En este trabajo se comparan los resultados obtenidos mediante dos modos de operación, *i*G-CLC y CLOU.

Todos estos resultados muestran las posibilidades de integración de biocombustibles sólidos con las tecnologías de combustión mediante transportadores de oxígeno consiguiendo una tecnología de emisiones negativas de CO_2, capaz de producir un beneficio energético.

Palabras clave: Biomasa, NET, BECCS, CLC, *i*G-CLC, CLOU.

Chemical Looping Combustion of biomass with negative CO_2 emissions

Abstract

CO_2 emissions to the atmosphere became an important environmental problem because of the effect on the global warming and consequently, the climate change. The climate change challenge demands a commitment of combined strategies between global institutions, governments and citizens. To reach the objectives set in the Paris Agreement (2015), greenhouse gas emissions need to be reduced. No technology is currently able to achieve the necessary reductions in greenhouse gas emissions on its own. Biomass represents an interesting alternative fuel for heat and power production as a carbon dioxide-neutral fuel. Moreover, if the CO_2 generated during biomass combustion process is captured then negative-CO_2 emissions would be reached and these are named bioenergy with Carbon Capture and Storage (BECCS) technologies.

Chemical Looping Combustion (CLC) came up as one of the most promising CO_2 capture technologies thanks to the low energy penalty of the CO_2 separation and therefore, low-cost. CLC technologies are based in two interconnected fluidized bed reactors without gas mixing. The combustion takes place in the fuel reactor where the oxygen is supplied by a solid oxygen carrier, normally metal oxides. After being reduced, the oxygen carrier goes to the air reactor without gas mixing between reactors where it is oxidized again in air, and it is able for a new redox cycle starts.

The main objective of this thesis is to evaluate the biomass combustion with CLC technologies (bioCLC). The research plan covers studies different at different scales, starting at lab scale, through a 1 kW_{th} pilot plant, to the continuous operation in a 20 kW_{th} plant to demonstrate the viability and optimizing the operation range for different low-cost oxygen carriers and different types of biomass residues.

Iron based ores as well as manganese ores has been pointed as promising oxygen carriers because of their reactivity and low cost. Under *In Situ* Gasification

Chemical Looping Combustion (*i*G-CLC) mode, the performance of the process was studied focusing on the effect of different important operating variables in a 1 kW_{th} CLC unit. Values about 100% of carbon capture efficiency with the three types of biomass were obtained using ores as oxygen carrier and the total oxygen demand was reduced because of the different reactivity of each oxygen carrier and the operating conditions optimization. Also a synthetic iron-manganese mixed able to release molecular oxygen during the CLC process was used. The effect of the several operating variables was also studied finding a high dependency on the air excess and the temperature, both in the air reactor, on the CO_2 capture efficiency and the total oxygen demand. About 100% of CO_2 capture efficiency achieving values of total oxygen demand about 5%. The use of a mixed Cu-Mn oxide was also studied as a Chemical Looping with Oxygen Uncoupling (CLOU) oxygen carrier. High CO_2 capture efficiencies were obtained and close to null total oxygen demand was achieved.

The effect of the operating conditions on the performance of CLC was evaluated in a 20 kW_{th} CLC unit using an iron ore as oxygen carrier. A Spanish biomass residue was tested achieving values close to 100% and total oxygen demands between 15-20% despite the low temperature used, supporting the consideration of the CLC process with biomass (bioCLC) as a promising bioenergy with Carbon Capture (BECCS) technology.

One of the aspects to be considered in the combustion of biomass is the formation of NO_x and the possible existence of tar in the gaseous product stream. This work compares the results obtained with two different chemical looping combustion modes, *i*G-CLC and CLOU.

All these results show the feasibility of the integration of solid biofuels with CLC technologies achieving a negative emission technology able to produce an energy gain through a BECCS technology.

Keywords: Biomass, NET, BECCS, CLC, *i*G-CLC, CLOU.

List of publications

I. Mendiara, T., A. Pérez-Astray, M. T. Izquierdo, A. Abad, L.F. de Diego, F. García-Labiano, P. Gayán, J. Adánez. Chemical Looping Combustion of different types of biomass in a 0.5 kW_{th} unit. Fuel. 2018, 211, 868-875.

II. Pérez-Astray A, Mendiara T, de Diego L.F., Abad A, García-Labiano F, Izquierdo M.T., Adánez J. (2019a) Manganese ores as low-cost oxygen carriers for biomass chemical looping combustion in a 0.5 kW_{th} unit. *Submitted to Fuel Processing Technology.*

III. Pérez-Astray A, Mendiara T, de Diego L.F., Abad A, García-Labiano F, Izquierdo M.T., Adánez J. (2019b) CLC of biomass as a BECCS technology using a manganese-iron mixed oxide. *Submitted to Sep. Purif. Technol.*

IV. Adánez-Rubio, I., A. Pérez-Astray, T. Mendiara, M.T. Izquierdo, A. Abad, P. Gayán, L.F. de Diego, F. García-Labiano, J. Adánez. Chemical Looping Combustion of biomass: CLOU experiments with a Cu-Mn mixed oxide. Fuel Processing Technology. 2018, 172, 179-186.

V. Adánez-Rubio, I., A. Pérez-Astray, A. Abad, P. Gayán, L.F. de Diego, J. Adánez. Chemical Looping with oxygen uncoupling: an advanced biomass combustion technology to avoid CO_2 emissions. Mitigation and Adaptation Strategies for Climate Change. 2019. Article in press. doi: 10.1007/s11027-019-9840-5.

VI. Pérez-Astray, A., I. Adánez-Rubio, T. Mendiara, M.T. Izquierdo, A. Abad, P. Gayán, L. F. de Diego, F. García-Labiano, J. Adánez. Comparative study of fuel-N and tar evolution in chemical looping combustion of biomass under both *i*G-CLC and CLOU modes. Fuel. 2019, 236, 598-607.

Contribution report

- Co-author, responsible for the experimentation, data evaluation and writing. Papers I, IV, V.
- Principal author, responsible for the experimental work, data evaluation and writing. Papers II, III, VI.

Acknowledgements

The work developed for this PhD thesis was carried out at the Instituto de Carboquímica (ICB-CSIC), part of the Spanish National Research Council, during the years 2016-2019. In addition, the work here presented involves the experimental work carried out at the Technical University of Hamburg (Germany) during a four months research stay. Here, I would like to express my grateful to all people who have helped and supported me during this period.

The author thanks the Spanish Ministry of Economy and Competitiveness (MINECO) for the funding received from the projects ENE2014-56857-R and ENE2017-89473-R AEI/FEDER UE for the financial support. A. Pérez-Astray thanks MINECO for the BES-2015-074651 pre-doctoral fellowship co-financed by the European Social Fund. The author also thanks PROMINDSA and FerroAtlántica del Cinca SL for providing solid materials used in this work.

I would like to express my gratitude to my supervisors, Teresa and Luis, thanks a lot for all you showed me, your patient and the guidance. I also want to thank and appreciate to all the Combustion and Gasification Group, specially Paco, Mayte, Alberto, Pili and Juan for the opportunity you have given me as well as your time and help during these years. I would also thank all those others who contributed to this work by their comments and company. Iñaki, Jose, Marga, Arturo, Anabel, Kike, Iván, Óscar, Domingo y Alejandro, you created a friendly working environment where I really felt comfortable. I do not want to miss anyone of the ICB colleagues and every moments we spent together, thank you for everything. Thanks and appreciation to the all the Institute of Solids Process Engineering and Particle Technology in Hamburg. Thank you for receiving me so warmly, making me feeling as any of you.

Ás miñas e aos meus

e a quen credes na investigación pública.

Index

Figure index

Table index

INTRODUCTION

1.1 Earth's energy balance

Since the beginning of life, about 4000 million years ago, the Sun has been supplying energy to the planet Earth. Autotroph organisms use the Sun energy to convert inorganic compounds into organic ones that they use for their biological functions. The deposition of organic materials into geologic formations under specific conditions and during long-term periods favored the fossil fuel formation. Therefore, the Earth can be considered a fossil battery in which the irradiancy coming from the Sun represents the only energy input of about 1353 W/m^2 in average (Schramski et al. 2015). Biomass acts as the solar energy accumulation, and coal, oil and natural gas correspond to different evolution states of natural biomass deposits into the earth's crust forming these diverse hydrocarbons associated to geological formations.

In the Paleolithic era, humans controlled the fire using vegetable biomass residues. Biomass is here all the organic matter susceptible to produce energy excluding that accumulated into geological formations (ISO 2014). Protection, thermal comfort, better food usability or lighting were the first energy uses of the biomass, being the first energy source controlled by humans. The agricultural practice development allowed an energy surplus generation that also facilitated animal domestication. This achievement provided food and animal work, increasing the individual energy demand as well as satisfying new energy needs. Figure 1 shows the evolution of the estimated individual human exogenous energy consumption. The sail navigation developing and water mills utilization implied the kinetic and potential energy use. The transportation and new goods and materials appeared at that time as the new needs for humans. Moreover, the continuous improvement of technologies for the use of different energy sources correspond with the major step forward from advanced agricultural to industrial societies (Malanima 2014).

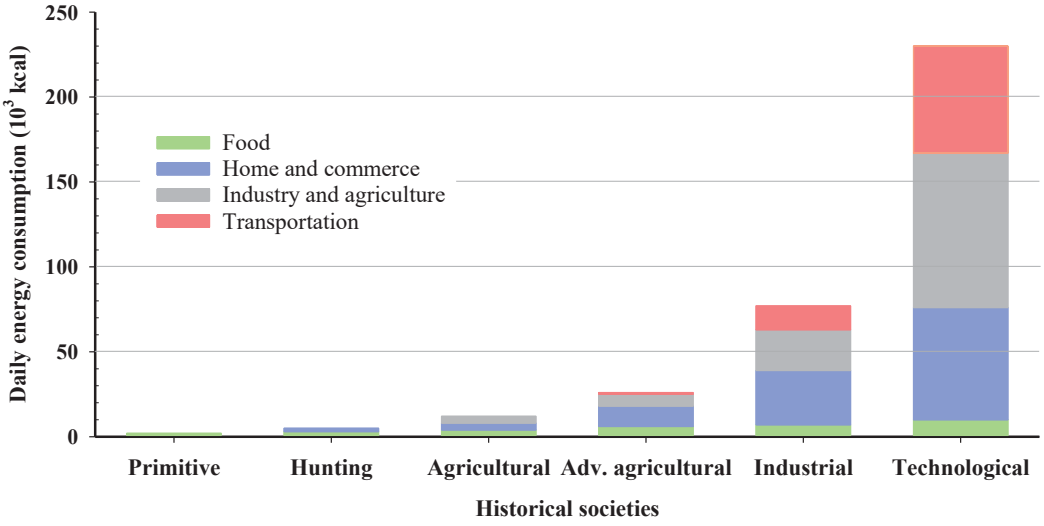

Figure 1. Evolution of estimated exogenous energy needs per capita.

Source: modified from Cook (1971).

The steam engine invention started the First Industrial Revolution. Coal began to be used for almost any mechanical activity and, in this way, the CO_2 previously captured in the fossil fuels from the ancient atmosphere during millions of years started being released modifying its concentration in the atmosphere (Schramski et al. 2015). The use of oil began the Second Industrial Revolution and

for hundreds of years the use of fossil fuels has been increasing along the increase of human energy needs. Figure 2 presents the evolution of energy consumption from Middle Ages to the present. The deployment of new more efficient and non-fossil-fueled technologies, started during the 20th century continuing until now. However, since the fire discovering, combustion processes jointly remain as the major contributors to the mix of primary energy consumption. Moreover, technological improvements allowed the use of more and more exogenous energy in different and complex activities in today's societies.

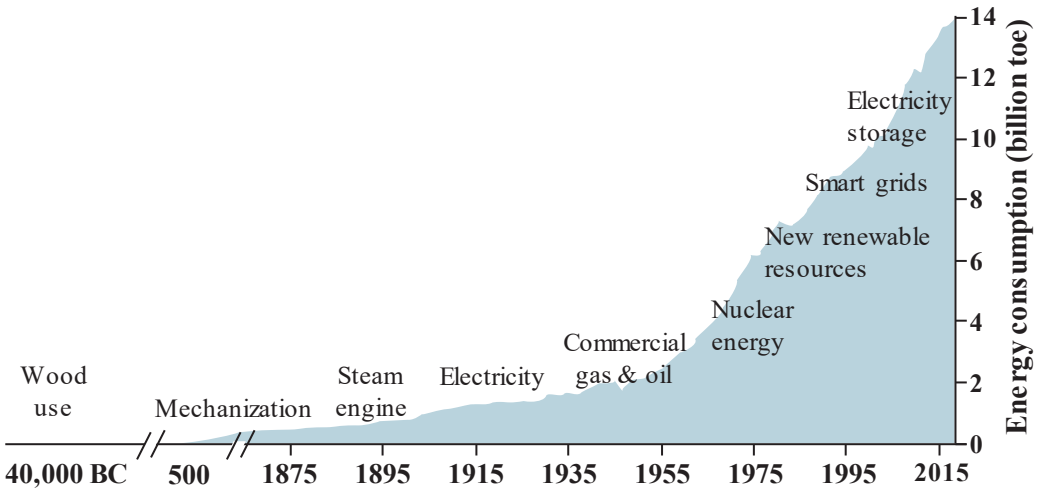

Figure 2. Evolution of energy sources consumption.

Source: modified from Belotskaia et al. (2016).

In addition to the energy source or even the technology used, human population must be considered in the analysis. Figure 3 shows the historical evolution of total energy consumption, population and energy consumption per capita. As it can be seen, the human population exponentially rose from Middle Ages to date. Similar conclusions can be extracted from the total energy consumption, During the last decades of the 20th century, the introduction of different more efficient technologies and electrification, mainly in developed countries, made the energy consumption per capita to increase less than the population or the total energy consumption.

The world's population and the energy consumption continue rising, however, this trend shows a great diversity around the world and the energy consumption has a strong dependence on the economic growth in different countries (Kander et al. 2014). Production and consumption systems need large amounts of energy and it is easy to observe the relationship between the energy consumption and the economy. Figure 4, provides an overview of the energy consumption and the Gross Domestic Product (GDP). As it can be seen, in a general trend, the economically richer a country is, the higher is the energy consumption in this territory.

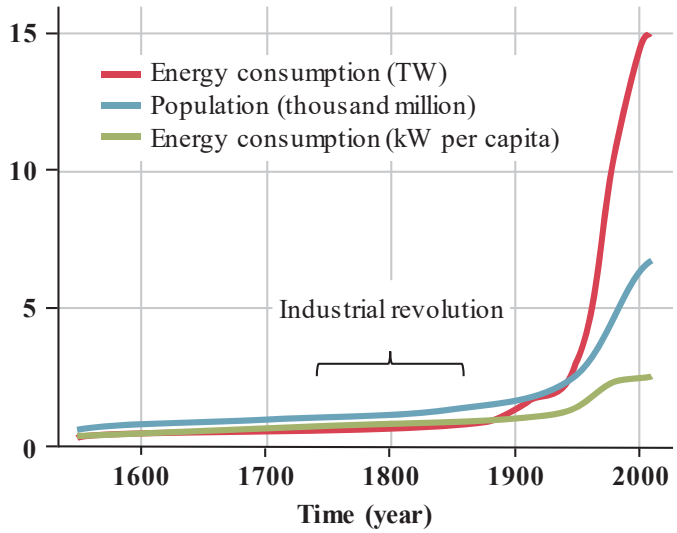

Figure 3. Evolution of total energy consumption, population and energy consumption per capita from Middle Ages.

Source: Ehrlich et al. (2012).

The Organization for Economic Co-operation and Development (OECD) is an international cooperation organization encompassing 36 States that covers about 70% of world markets and about 80% of the World Gross National Income (GNI). Since 2008, the energy consumption of non-OECD countries overcome that of OECD, moreover, the expected rising of non-OECD consumption will multiply by four that of OCDE during the next decades (BP 2019). Figure 5 gives the primary energy consumption per capita in the period 1980-2016 and the expected evolution up to 2040. A big difference between the United States of America (USA) and the

rest of the regions can be observed. A slight reduction in all the developed economies is expected changing the trend followed during the past decades. Meanwhile, the expected increase in the consumption per capita of developing economies (China and India) contrasts with the stability of the other non-OECD countries, based on the difficulty of these countries with high population growth rates to increase their energy consumption per capita.

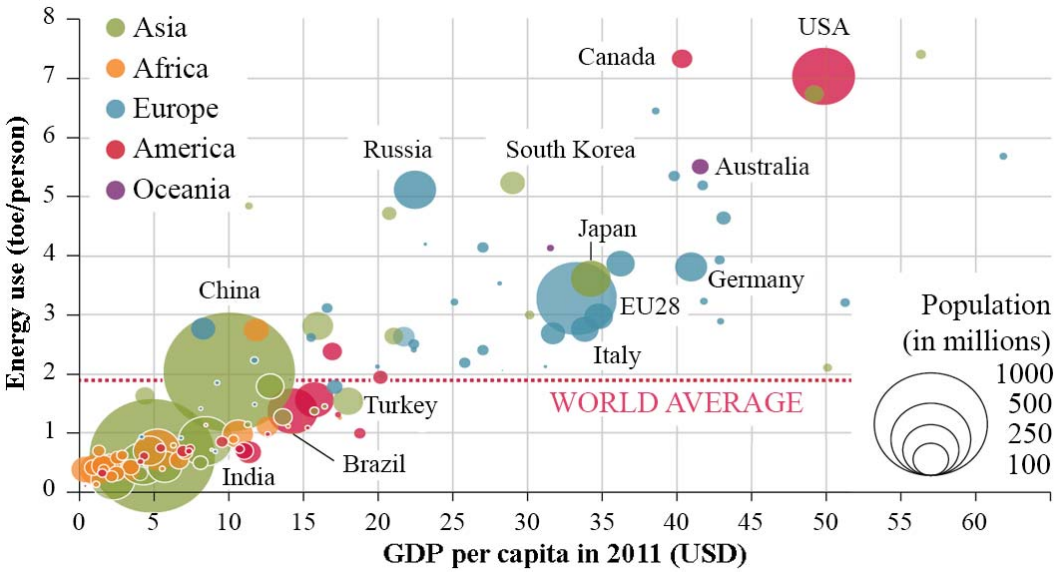

Figure 4. Energy consumption and GDP of different countries.

Source: modified from Priddle (2016).

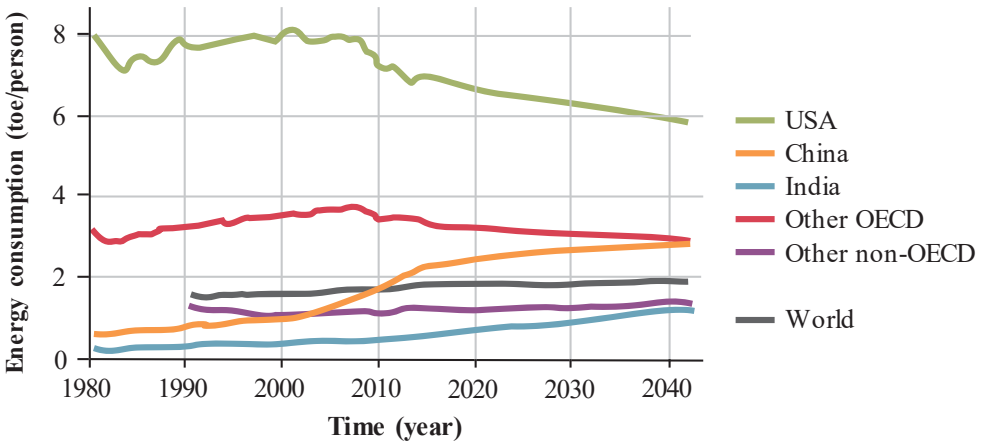

Figure 5. Total final energy consumption per capita by region.

Source: modified from Belotskaia et al. (2016).

Despite the increasing energy efficiency, the energy consumption continues increasing. Figure 6 presents the total final energy consumption from 1970 to 2016. Focusing on the increase observed since the early century, the energy consumption of the OECD countries remains constant and they are the major consumers. China and the non-OECD countries in Asia influence the increase with their contribution to the total consumption.

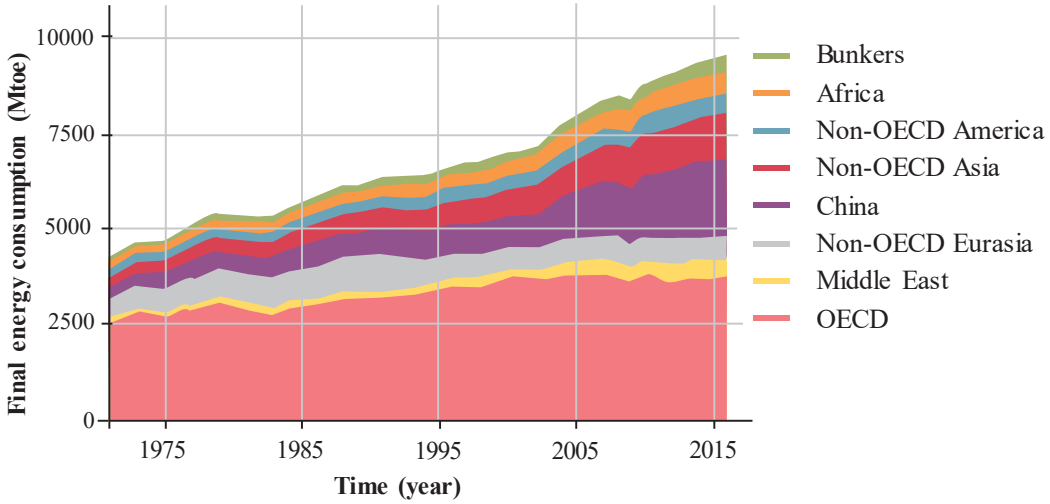

Figure 6. Total final energy consumption evolution by region.

Source: IEA (2018).

Figure 7 shows the evolution of energy balances of traded fuels in 1990 and 2017 as well as the predictions to 2040. These energy balances not only show the information about the energy import needs but it can be also understood as an indicator of the energy self-sufficiency degree of different world regions. The highly oil dependent energy system of the European Union (EU) was maintained between 1990 and 2017 while a slight decrease is observed to 2040. By that time, China, India and South-east Asia together with Oceania will top the negative energy balance of the energy foreign incoming ranking needs. Increases in the energy surplus to 2040 can be observed in Africa and the rest of Asia, while a big change stands out in America. In this case, the energy balance changed from the imports in 1990 to an energy exporter region in 2040.

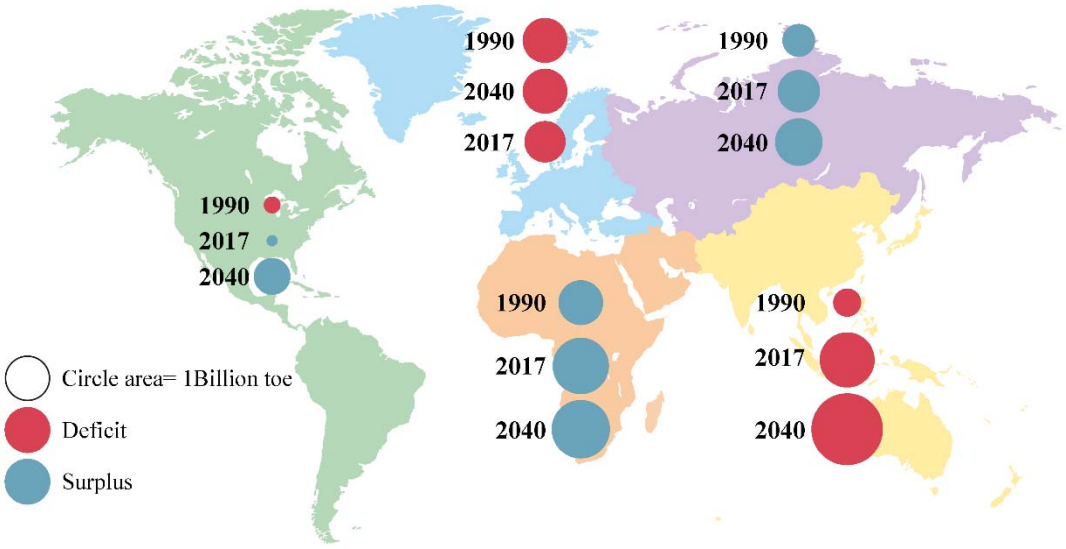

Figure 7. Energy balances of traded fuels by world regions and predictions to 2040.

Source: modified from BP (2019).

Despite the social, geographic or demographic differences, humans are making the greatest modification and exploitation of the environment, and this fact implies direct consequences to life and biodiversity. Current energy needs, raw materials availability and its incorrect use are producing resource depletion, loss of biodiversity and pollution, and consequently this is making sustainability and environmental protection getting more and more important for all the social actors.

1.2 Environmental impacts

The environment is the necessary scenario where life happens. In it, humans have developed their diverse cultures and societies, and because of that, they have produced changes in the environment which have direct impacts on the life in Earth, both positive or negative (Gaston and Spicer 2009). Different classifications of impacts are possible based on the size of the affected territory, the harm produced or the type of the affected environment, among others. Depending on the size of the

affected territory, local and global impacts can be distinguished and a general classification is here presented.

Local impacts:

- Effluents reaching soils or water bodies can harm human health but also a potential loss of biodiversity.
- Emissions. Different gas emissions (CO_2, CH_4, NO_x, SO_x or CFCs among others) and suspended particles stand out as pollutants responsible of a wide range of specific negative effects.
- Residues. The difficulty to treat different solid wastes implies their deposition under specific conditions depending on the inherent nature of the substance
- Resource depletion. The massive utilization of raw materials not considering the non-renewable characteristics of resources are a future developing constrain, with several associated problems.
- Land use changes. The change or even loss of any kind of natural ecosystem derives into the modification, or even loss, of natural functions of this ecosystem.
- Visual impact.
- Sound/noise impact.
- Electromagnetic fields.

Global impacts:

- Loss of biodiversity. This fact implies the reduction of the affected ecosystem resilience. Uncertainties derived from the ecological equilibrium appear and even cultural problems can appear in societies as a consequence of this (Gaston and Spicer 2009).
- Acid rain. The formation of sulfur and/or nitrogen acids in the atmosphere is favored by specific anthropogenic emissions (NO_x and SO_x). These acids are dispersed and fall as precipitation affecting ecosystems.
- Ozone layer depletion. The emission of different CFCs, among other substances with typically long atmospheric residence times, generates the

reaction of the stratospheric ozone with these compounds, reducing the ozone concentration in this atmospheric layer.

- Ocean acidification. CO_2 emissions to the atmosphere increase the CO_2 flows to the ocean (carbon sink) and in this way modifying oceans acidity with negative consequences on biodiversity.
- Climate change. Different substances emitted by human activities affect the natural greenhouse effect increasing it. This modification increases the global average temperature of the planet surface producing the sea level rise and the climate change.

1.2.1 The greenhouse effect modification

The greenhouse effect is the natural process whereby the earth's atmosphere maintains a thermal inertia. It is mainly produced by some gases known as greenhouse gases (GHG), capable of absorbing the infrared radiation reflected by earth surface after reaching it the solar radiation. It was pointed for the very first time by Fourier in 1824 based on his knowledge of heat transfer and ancient observations (Fourier 1824). In 1856, Foote enunciated the different heat absorption capacity of gases, thanks to the experiments with different gases inside glass closed cylinders (Jackson 2019). Nevertheless, the proper name of greenhouse effect was not used before 1896, when Arrhenius proposed the first climate model including the theoretical study of CO_2 concentration influence (Rodhe et al. (1997).

The average of the Earth surface temperature was between 13.9 and 14.2 °C during the 1981–2010 period while a temperature about -18 ºC would be achieved if no atmospheric effects would affect the Earth energy balance (Kump 2004). Figure 8 presents a scheme of the Earth radiative balance. The scheme assumes 100 arbitrary radiation units of incident solar radiation. About 30% of the total Earth high frequency energy input is reflected by surfaces, clouds and suspended particles by a process known as albedo effect. About 45% is absorbed by the Earth and about 25% is absorbed by the atmosphere. As it was mentioned in the previous section, part of this solar energy input has been accumulated by biomass through the photosynthesis

for thousands of years. Furthermore, the energy absorbed by the Earth surface and the atmosphere is dispersed as low frequency radiation. The greenhouse effect is presented in the right part of Figure 8 as 88 more arbitrary radiation units of infrared radiation. This radiation interacts with the GHG maintaining being emitted and absorbed multiple times, making internal fluxes higher than the Earth net energy balance and maintaining the Earth average temperature.

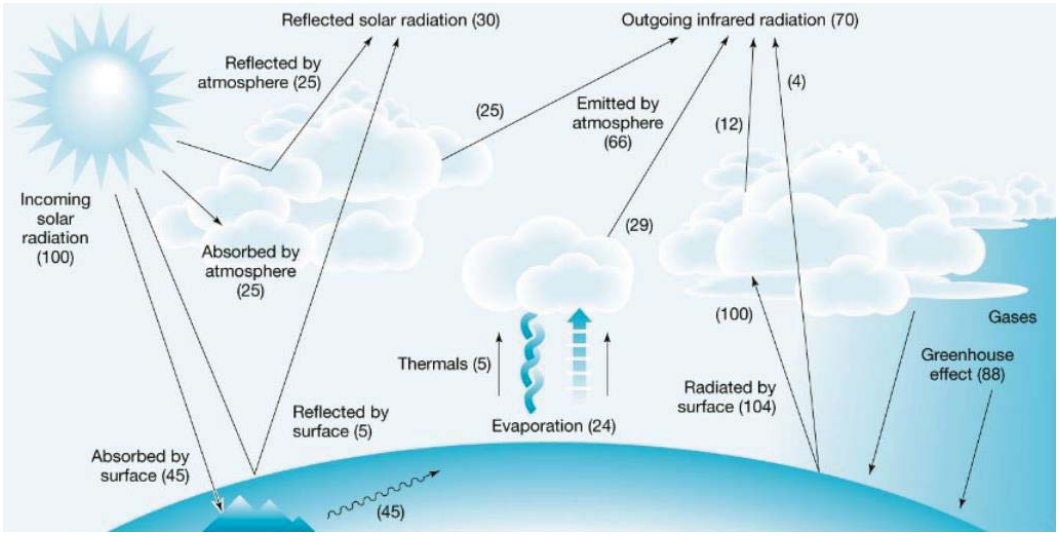

Figure 8. Radiative Earth balance, fluxes expressed as percentages.

Source: modified from Kump (2004).

1.2.2 The global warming

Table 1 presents the concentration of the main gases forming part of the atmosphere in the preindustrial period until the anthropogenic emissions began to modify the atmospheric composition. The preindustrial atmospheric gas composition establishes the needed data for comparison with anthropogenic atmospheric modifications. Earth climate models have considered slightly different variables to simulate the climate behavior with similar relevant and coherent results. As an example, the NASA's model E2 includes separately both natural and anthropogenic variables that influence the climate showing the results as temperature anomalies. This variation represents the difference between the temperature baseline distance and the predicted temperature, a more accurate than the absolute temperature because

of the intrinsic Earth's surface temperature heterogeneity. The natural effect considers variables such as Earth's orbital variations, the Sun's radiation changes (based on the Sun temperature evolution) and the escaping volcanic emissions. Among anthropogenic variables, the model considers deforestation, tropospheric ozone pollution, aerosols pollution and obviously, the GHG emissions. Figure 9 represents the observed and the simulated Earth temperature according to the Goddard Institute for Space Studies (GISS) Model E2 (Schmidt et al. 2014). As it can be seen, while no relation can be observed between the comparison of the observed temperature and the isolated effect of natural factors in the simulated temperature, the addition of all the natural and human variables approaches the observed values.

Table 1. Clean air composition.

Gas (-)	**Concentration (%)**
N_2	78.08
O_2	20.95
Ar	0.94
CO_2	0.028
Ne	$1.82 \cdot 10^{-3}$
He	$5.2 \cdot 10^{-4}$
Kr	$1.1 \cdot 10^{-4}$
Xe	$0.09 \cdot 10^{-4}$

The atmospheric composition continues changing because of human activities. The Intergovernmental Panel on Climate Change (IPCC) certified the relationship between the increase of Earth's average temperature and the increase of the atmospheric GHG concentrations because of the reinforcement of the natural greenhouse effect (IPCC 2014). In this way, the average surface temperature of the Earth was between 13.7 and 14.0°C for the 1961–1990 period, increasing to 13.9-

14.2 °C for the period 1981–2010 (Jones and Harpham 2013). Table 2 shows the main GHG together with their most important global warming characteristics, their atmospheric residence time, the contribution of each GHG to the total GHG emissions and the Global Warming Potential (GWP). This GWP represents the warming caused by the release of 1 kg of any GHG with respect to the warming caused by the release of 1 kg of CO_2 during a time horizon. Despite the large amount of H_2O emitted, the vapor-liquid equilibrium of this substance maintains a constant H_2O concentration for the constant pressure and temperature ranges, reducing the impact of H_2O emissions compared with any other GHG. The CO_2 stands out here as the world's largest contributor to the warming because of the large amount emitted along with the long atmospheric residence time of this gas in the atmosphere.

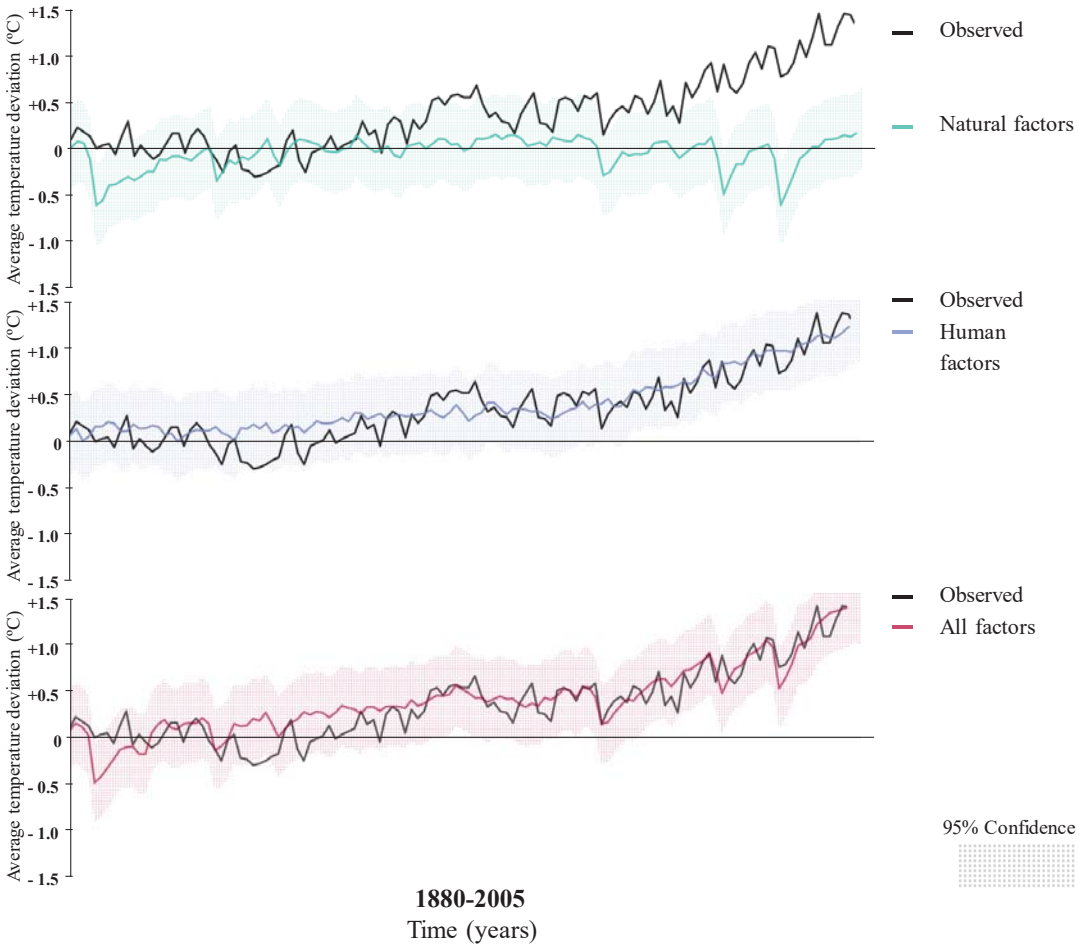

Figure 9. Observed and simulated Earth temperature according to the GISS Model E2. (Dotted area represents the 95% confidence).

Source: modified from Miller et al. (2014).

Table 2. Greenhouse gases and their atmospheric residence time together with the anthropogenic GHG emission contribution percentage and GWP.

Source: IPCC (2013).

	Residence time (years)	Contribution (%)	GWP (kg_{CO2eq})		
			20 years	100 years	500 years
H_2O	0.04	66	-	-	-
CO_2	300	20	1	1	1
CH_4	15	4	56	21	6.5
N_2O	120	1	280	310	170
CFC	$10 - 5 \cdot 10^4$	1.5	4800	7000	10100
SF_6	$10 - 5 \cdot 10^4$	1.5	16300	23900	34900

Apart from the proper increase in the temperature of the atmosphere and the hydrosphere, the main impact derived from global warming are the unpredictable consequences on global climate, producing more extreme weather phenomena, and environmental destruction, among others.

The CO_2 balance

The study of the major carbon sources and sinks contributes to the global warming understanding. The Carbon Budget analyzes the major carbon deposits to stablish an annually carbon flow study that takes into account the Fossil fuel CO_2, the land use change CO_2, the atmospheric CO_2, the ocean CO_2 sink and the terrestrial CO_2 sink, all systematically estimated for the period of 1959–2017 (Le Quéré et al. 2018). The carbon amount in the planet is constant and, from this point of view, the carbon cycle is the carbonaceous exchange process among the biosphere, geosphere, hydrosphere and atmosphere. Figure 10 shows the carbon cycle anthropogenic perturbation scheme averaged for the period 2008-2017. As it can be seen, during the decade 2008-2017 the atmospheric carbon deposit increased by 4.7 Gt_{CO2} per year, while a total amount of approximately 250 Gt_{CO2} was moved to the atmosphere from

1870 to 2017. Fossil fuel combustion since Industrial Revolution and land-use change are highlighted as the major responsible of the disruption in the natural equilibrium. According to the National Oceanic and Atmospheric Administration Earth System Research Laboratory, the CO_2 atmospheric concentration increased from the approximately 280 ppm of CO_2 in the preindustrial atmosphere to the 416 ppm on May 15, 2019 (Keeling et al. 2015).

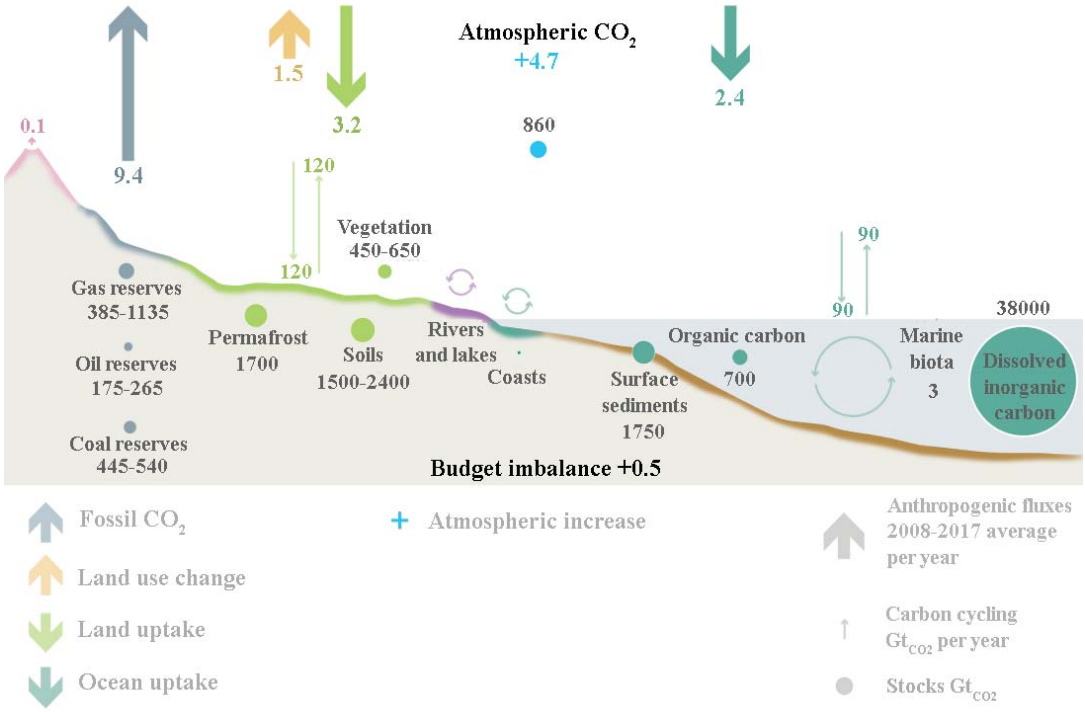

Figure 10. Carbon cycle anthropogenic perturbation scheme annually averaged for the period 2008–2017.

Source: Le Quéré et al. (2018).

Figure 11 shows the evolution of the CO_2 emissions from 1960 to 2017: (a) global emissions, (b) by fuel/process, (c) by regions and (d) per capita by region. In Figure 11 (a), a slight stabilization in CO_2 global emissions can be observed during the first years of the 2010 decade. The growth rate in the GHG emissions decreased from 4.5 % per year in the period 1960–1969 to a period of no or low growth during 2014–2016 (Le Quéré et al. 2018). Focusing in the CO_2 emitters by fuel or process, in Figure 11 (b), fossil fuels highlight as the responsible of the GHG emissions

followed by cement production. A maintained increase growth rate is observed for natural gas use, comparable with oil utilization. Since approximately the year 2000, coal combustion regained the first fuel position by CO_2 emissions, coinciding with the China CO_2 emissions increasing that made China the main GHG emitter, almost doubling USA emissions. The coal stabilization observed after the year 2010 contributed to the stabilization of the global CO_2 emissions in the same line than what can be seen with China emissions during this period (Figure 11 b). In addition, a high increase is also observed in India's emissions in contrast with USA and EU countries. Big differences can be observed in Figure 11 (d) between regions in the CO_2 emissions. The high increase of China during the 2000 decade set their CO_2 emissions per capita to EU28 comparable values. A stable increase was maintained in the CO_2 emissions per capita of India from 1960 to 2020. Moreover, the USA remains as the major contributor per capita to global CO_2 emissions.

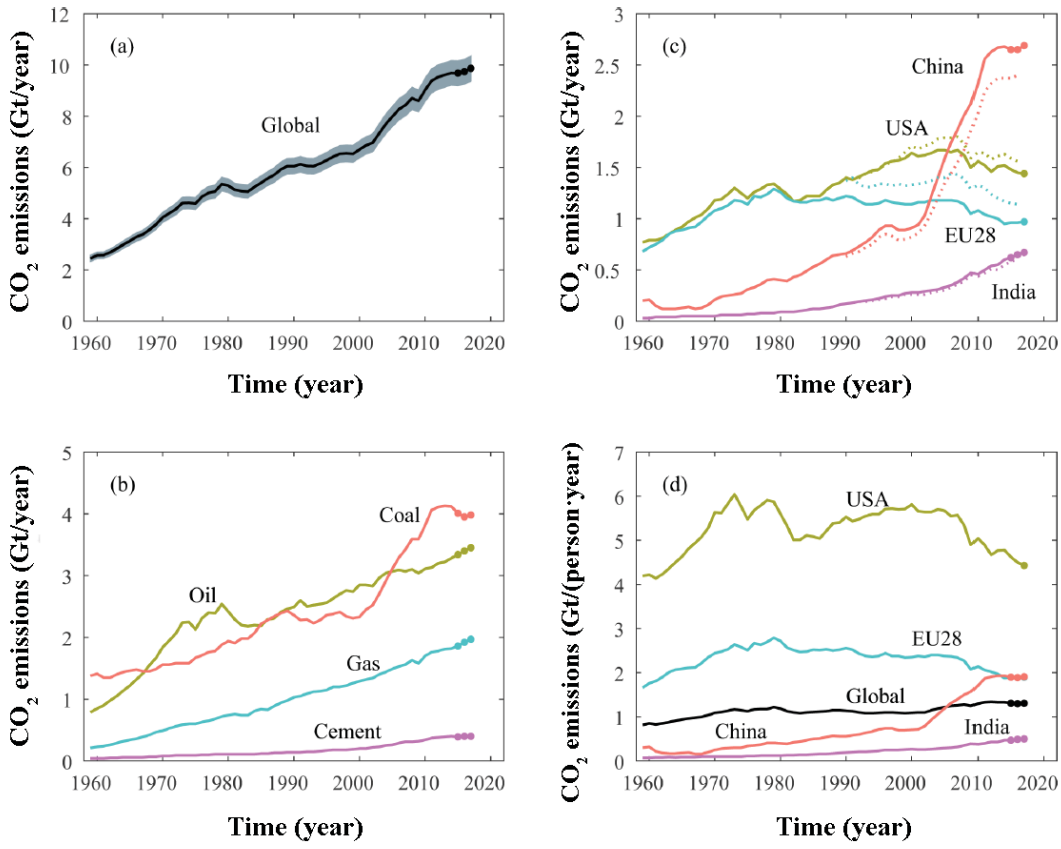

Figure 11. Evolution from 1960 to 2017 of the CO_2 emissions (a) global, (b) by fuel/process, (c) by regions, (d) per capita by region.

Source: Le Quéré et al. (2018).

1.3 The climate change

Arrhenius proposed in 1896 the first climate model including the greenhouse effect and the theoretical study of atmospheric CO_2 concentration influence (Rodhe et al. 1997). In 1972, the first environmental United Nations (UN) conference overlooked the climate change topic focusing on problems like chemical pollution or the atomic bomb consequences. The successive climate simulations reinforced the debate about the climate crisis promoting the IPCC creation in 1988 as a part of the United Nations Environmental Program (UNEP). In this way, in 1998 the Kyoto Protocol attempted to combine international efforts to reduce different GHG emissions, being the first time that GHG emission limits were stablished. In 2014, the fifth Assessment Report (AR5) presented by the IPCC highlighted the anthropogenic responsibility on the global warming and the unpredictable consequences that climate change will produce if GHG emissions continue as usual. The AR5 confirms previous evidences about extreme temperatures, increased precipitations or rising sea levels, among others, and how humans will be affected. Figure 12 shows different impacts already attributable to climate change in 2014. As it can be seen, impacts were produced all around the world affecting physical, biological and human systems. The increase of wildfires in many world areas, the decreasing food production in South-East Asia and Sub-Saharan Africa and impacts on water bodies must be highlighted. In this way, the AR5 made a call to join actions for a necessary clean development, limiting the GHG emissions combined with adaptation strategies to limit the risks of the climate crisis over sustainable and equity development.

Figure 13 shows the IPCC climate change scenarios predicted from 2014 to 2100, (a) annual global GHG emissions and (b) the temperature change for the cumulative CO_2 equivalent atmospheric concentrations. The historical data (dark line) and the Representative Concentration Pathways (RCP) are plotted in Figure 13 (a) by the different colored lines. As an example, the RCP2.6 (blue line) shows the GHG emissions mitigation trend to 2100 that corresponds with the most probable trend into the scenario area of GHG atmospheric concentrations between

430 and 530 ppm of CO_2 equivalent (blue colored areas). Looking at Figure 13 (b), the temperature increase of nearly 2 ºC produced by these cumulative GHG concentrations can be compared with the observed values for the period 2000-2009, showing the necessary reduction of GHG emissions for the coming years. The GHG emissions should be neutral during the last quarter of the 21st century and even negative GHG emissions over the end of the century for the RCP 2.6 (Figure 13 a). The RCP4.5 and RCP6.0 scenarios also presented in Figure 13 (a) show the expected intermediate GHG emissions that would cause the average temperature of 1861-1980 to be exceeded by more than 2 ºC. Finally, the RCP8.5 scenario shows a high GHG emissions that would be achieved considering the current trend of GHG emissions, without mitigation strategies, producing unpredicted consequences of the climate crisis (IPCC 2014).

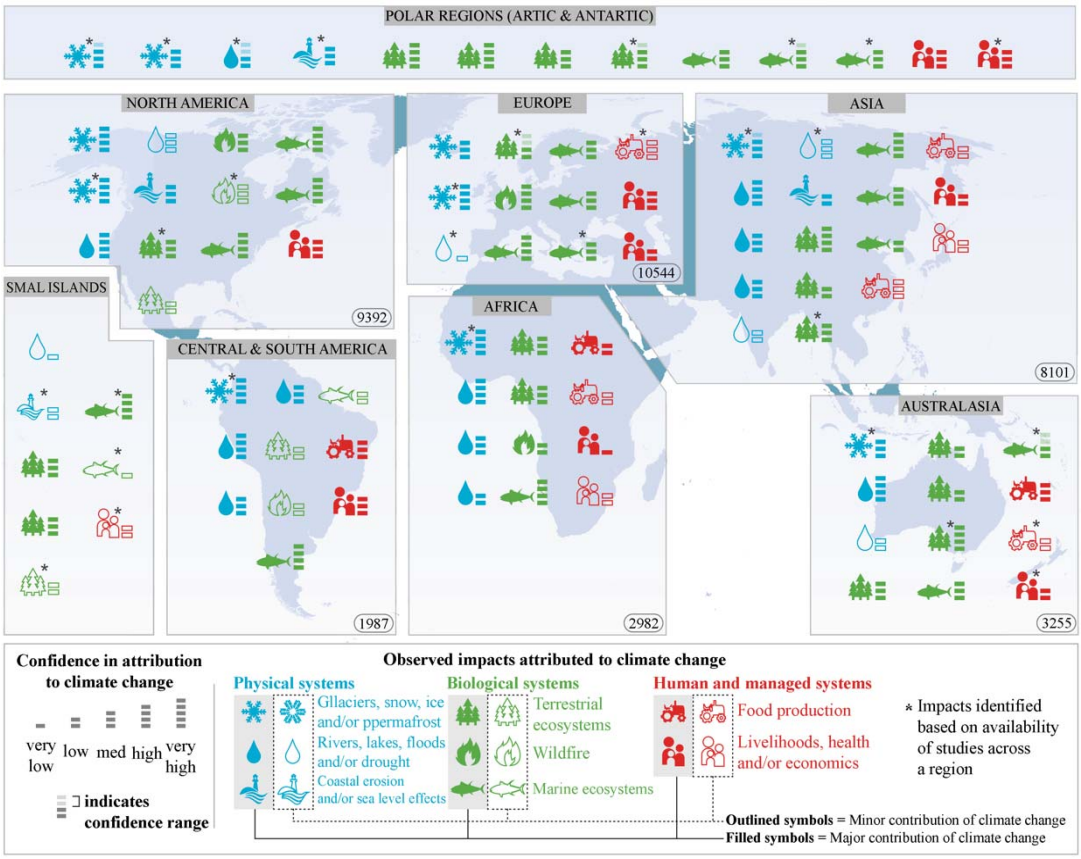

Figure 12. Climate change attributable impacts to 2014 by regions.

Source: modified from IPCC (2014).

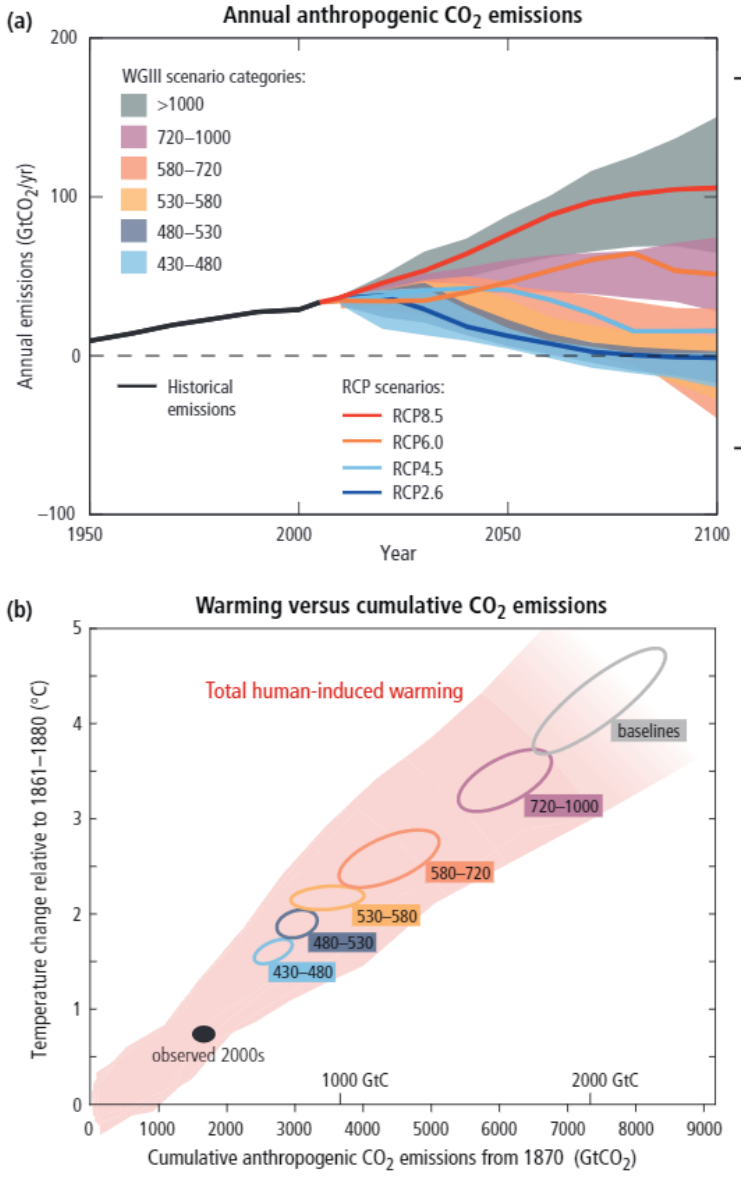

Figure 13. IPCC climate change scenarios predictions 2014-2100 (a) Annual global GHG emissions, (b) temperature change for the cumulative CO_2 atmospheric concentrations.

Source: IPCC (2014).

The social debate continued increasing meanwhile the implication of different actors also increased. The Paris Agreement set the international objective of holding the increase in the global average temperature to well below 2 ºC above preindustrial levels and pursuing efforts to limit the temperature increase to 1.5 ºC above preindustrial level. It would enter into force when at least 55% of the parties with at least 55% of global GHG emissions signed it. In November of 2016, 185 countries

representing more than 87% of global GHG emissions signed it entering into a force. In this agreement, each country independently decides their Nationally Determined Contributions (NDC) of GHG emissions reduction. These NDC are analyzed and revised every five years but they are not mandatory, what increases the uncertainties associated with the climate crisis mitigation. The 24th Conference of the Parties (COP24) to the United Nations Framework Convention on Climate Change (UNFCCC) celebrated in Katowice in 2018 reinforced the Paris Agreement objectives set in 2015, insisting on the emergency and the unprecedented actions needed (UNFCCC 2015). It is clear that no single solution is able to achieve the GHG necessary reduction. Furthermore, the real GHG emissions reduction will depend on the climate policies adopted by the parties, however, recent studies confirm the alarm (UNEP 2018). Figure 14 shows the number of countries achieving the GHG emission peak per decade between 1990 and 2030 as well as the percentage of global emissions covered by these countries at that time. This emissions peak could be already observed in Figure 13 (a) in the RCP 2.6 scenario. The differences among countries and climate policies are here reflected in the 40 years of difference to achieve the GHG emission peak. However, the global GHG emissions peak is expected to 2020, remaining 57 countries with about 60% of GHG emissions to 2030.

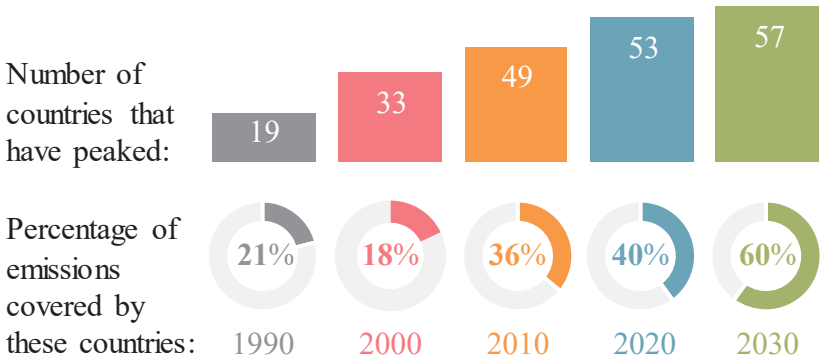

Figure 14. Global CO_2 emissions from fossil fuel combustion.

Source: UNEP (2018).

Differences between the GHG reduction compromise and the achieved GHG reduction have been identified in several studies. According to these studies the commitment of the countries already stablished is not enough to limit the Earth's

average temperature increase to 2 ºC. The UN Gap Report in 2018 shed light on the GHG reduction level by 2030. To this end, several scenarios were considered:

- No policy baseline. It represents the scenario without climate policies implementation since 2005.
- Current policy scenario. It shows the GHG emissions continuing the real data until 2017.
- Unconditional NDC. Contribution on the global GHG reduction objectives of each country to comply with the Paris Agreement.
- Conditional NDC. Additional efforts on the GHG reduction objectives of some countries constrained by a wide range of uncertain variables.
- 2 ºC range. Global GHG reduction objectives to achieve about 2 ºC of global temperature increase and to comply with the Paris Agreement.
- 1.5 ºC range. Global GHG reduction objectives to comply with the Paris Agreement with about 1.5 ºC of global temperature increase.

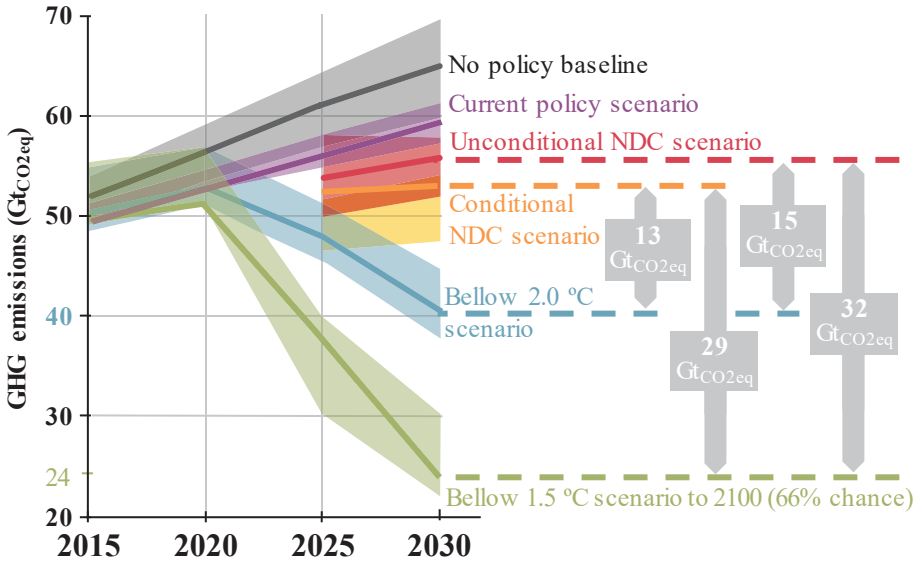

Figure 15. Global GHG emissions in different scenarios and the expected emissions gap in 2030.

Source: modified from UNEP (2018).

Figure 15 shows the global GHG emissions in different scenarios and the expected emissions gap in 2030. According to Figure 15 a large difference, of about

30 Gt_{CO2eq}, is observed among the objectives to comply with the Paris Agreement and any of the represented NDC scenarios. In this way, a major change should initiate the GHG emissions reduction. Otherwise, the climate crisis will produce more and more destructive and irreversible consequences on Earth's life.

1.3.1 Geoengineering

There is a clear scientific consensus on the anthropogenic influence in the modification of atmospheric GHG composition, and therefore, the climate crisis. The GHG emission reduction targets appear to be insufficient and a real compromise must be made effective. The Royal Society defines geoengineering as the climate modification to counter the anthropogenic global warming (Schäfer et al. 2015). The implementation of geoengineering acts on a wide range of climate variables, but also social, political, economic and technical among others (Rayner et al. 2013). Oxford University analyzed the complex context and enounced five principles that try to provide the basis for a correct deployment of climate engineering. These conclusions claim to a conscientious regulation before the implementation of geoengineering techniques (Rayner et al. 2013). The European Commission participates in the European Transdisciplinary Assessment of Climate Engineering Project (EUTRACE) analyzing the state of knowledge and deployment of geoengineering projects. It made a division of available technologies into two different main types.

- Albedo effect modifications. Solar radiation management techniques that increase solar radiation directly reflected by the deployment of reflective surfaces or specific particles injection that favor the overall temperature reduction.
- Atmospheric GHG modifications. Negative emission technologies (NET) are technologies able to remove GHG from the atmosphere.

Atmospheric GHG reduction

The GHG reduction includes a wide range of possibilities that increase natural CO_2 sinks or store the CO_2 for a long period. The NETs should be responsibly analyzed and managed to contribute to reduce the global warming and to mitigate the climate crisis effects. The main NETs are:

- Afforestation. Increasing natural CO_2 sink in forests by afforestation, as well as protecting critical forest environments and reforesting deforested areas.
- Bio char. It is a stable product for hundreds of years obtained by biomass pyrolysis or gasification. Used in soils, it contributes to their fertility while increasing the carbon sink of the earth's soil.
- Ocean fertilization. Favoring the plankton formation, the biological carbon sink would increase its contribution in the carbon cycle, contributing to the reduction of the atmospheric GHG concentration.
- Enhanced weathering. Industrial chemical methods to imitate natural mineralization of atmospheric CO_2.
- Direct air capture (DAC). An important difference must be highlighted here between technologies to absorb into solids and DAC linked with CO_2 capture and storage (CCS). CCS technologies were pointed to play an important role in carbon removal during the next century according to the IPCC AR5 report. (IPCC 2005).
- Bioenergy with CO_2 capture and storage (BECCS). This group of technologies was also highlighted in the IPCC AR5 report because of their capacity to produce energy while the negative CO_2 emissions are guaranteed. The CO_2 is captured in the sustainable managed biomass, which is transformed usually by thermochemical reactions to produce an energy gain. The CO_2 obtained is stored into safe places for a long period. A wide deployment of these technologies during the present century will be necessary (IPCC 2014). For more information about BECCS, see section 1.4.
- Other biomass-based processes: The correct management of land uses can increase the carbon soil sink. Furthermore, the use of biomass-based materials on a wide range of industries, such as buildings or new materials, should contribute to the GHG atmospheric concentration reduction.

1.3.2 The mitigation path

The first effects of the climate crisis are already evidenced in global changes in the planet's behavior. Decisions including all the social actors during coming decades lead the implementation of measures to adapt societies to these changes. Following the objectives in the Paris Agreement, if 2900 Gt_{CO2eq} were emitted by anthropogenic sources to 2011, no more than 1000 Gt_{CO2eq} should be emitted to 2100 to achieve the mitigation pathway with the goal of no more than 2 ºC of global temperature increase. Analyzing the GHG emissions reduction estimated by the IPCC's Synthesis Report (IPCC 2014) for the different sectors, power generation, industry and transportation stand out as the world's leading contributors up to date. However, different GHG emissions reduction capacities are estimated in each sector. Figure 16 shows the annual GHG emissions by sectors and predicted to 2050. A slight reduction is estimated for the period 2020-2050 in industry and transportation in the same line as what happens with buildings, transformation and agriculture. Meanwhile, the power generation sector highlights with an estimated GHG reduction of about 87% in 2050, being the sector with the highest potential of reduction.

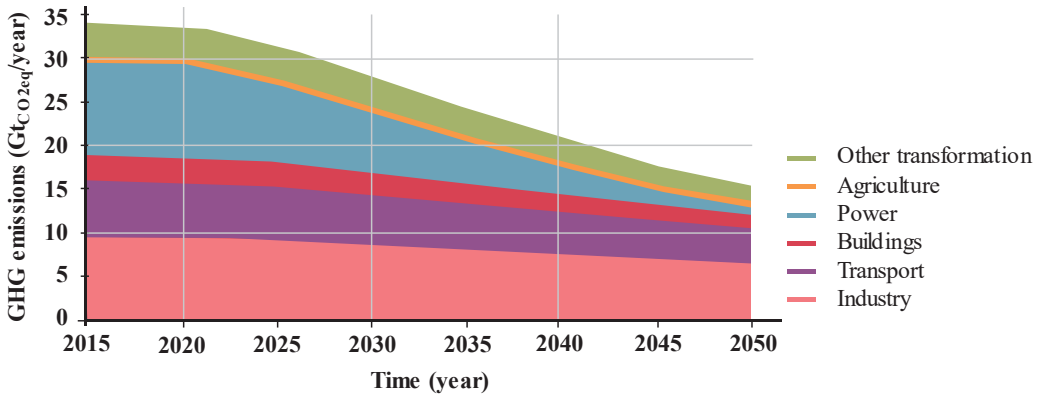

Figure 16. Annual CO_2 emissions by sectors predicted to 2050

Source: IPCC (2016).

Figure 17 shows the energy related emissions evolution and perspectives to 2100 following the trend observed to 2013, as well as the mitigation path objectives according to the IPCC's Synthesis Report (IPCC 2014). All these considerations suggest a GHG emissions reduction of about 100 Gt_{CO2eq} during the present century

and no single solution can achieve the reduction needed. The Mitigation path should include different cost-effective technologies and also a big effort on research about climate mitigation technologies. As it can be seen, the energy save together with an increase in energy efficiency should contribute about a 33% of total energy related GHG emissions reduction at the end of the century. The renewable energies deployment should contribute with about 17%, also the change to sustainable fuels (10%) and nuclear energy (6%) must be mentioned. The deployment of fossil fuel powered plants linked with CCS technologies can reduce nowadays emissions, however, a large deployment of BECCS technologies is expected after 2030. A contribution of 32% is expected for CCS associated technologies at the end of the century. In this way, a zero-emissions energy sector would be achievable about the end of the century, contributing to ensure a 22nd century with a GHG negative emission sector. The mitigation path combines strategies and measures to reduce GHG concentrations in the atmosphere by several techniques. The increase of natural carbon sinks, together with GHG emissions reduction will contribute on the climate crisis mitigation, and the decarbonization of energy sector should make special efforts while the energy supply is guaranteed.

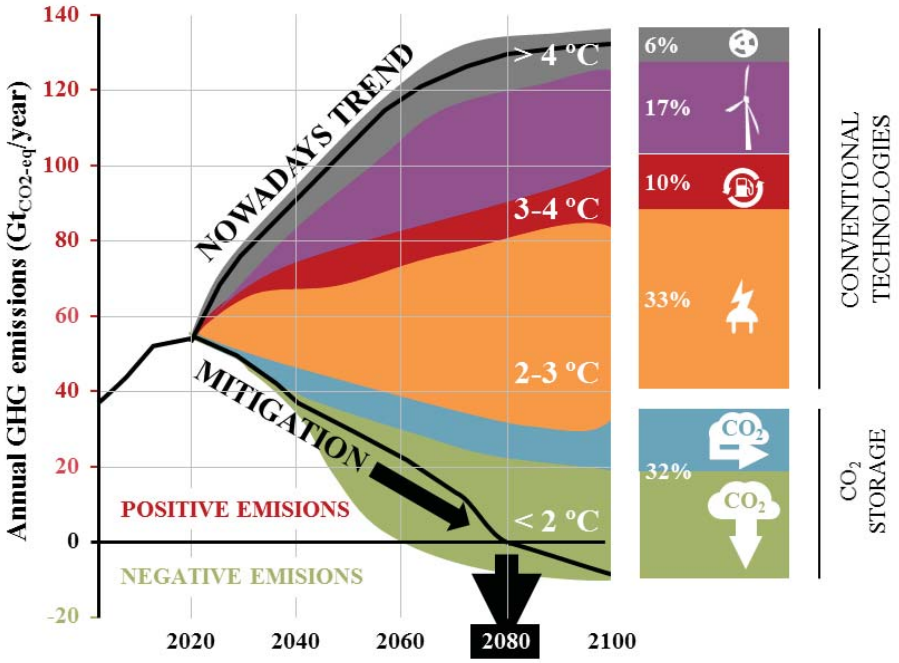

Figure 17. Energy related emissions evolution and perspectives to 2100 following nowadays trend and the mitigation path objectives.

Source: modified from IPCC (2014).

1.3.3 Other energy considerations

Air pollution includes all the emissions of gaseous, liquid and solid particles that locally or globally modify the natural atmospheric properties. Air pollution has been pointed as the fourth major factor producing premature deaths with huge estimated global derived costs. A difference between primary and secondary pollutants should be made. The first ones are those directly emitted in a process while the secondary are those formed by the primary by chemical reactions that also produce undesirable effects. In addition to CO_2, some substances among the various air pollutants derived from human activities should be especially highlighted because of their impacts (Priddle 2016). All these pollutants should also be considered when analyzing power generation processes:

- Carbon monoxide. CO_2 has been already pointed as the main contributor to anthropogenic global warming, but also CO produced by uncompleted combustion is important because of its toxicity.
- Nitrogen oxides. Both NO and NO_2 as well as ammonia favors the formation of tropospheric ozone and particulate matter. N_2O is also a GHG.
- Particulate matter. Suspended particles, usually solids with diameters lower than 10 μm, and also liquids are considered pollutants because of their impact in human health.
- Sulfur oxides. Substances related with human health undesirable effects. These compounds also favor the suspended particles formation and contribute to acid rain.
- Volatile organic compounds. Hydrocarbon vapors with a negative impact on human health and the biodiversity maintenance.

Figure 18 shows the main primary air pollutants together with the main sources where they were produced in the year 2015. As it can be seen, not only power generation, but also all energy related processes are responsible for major of the main air pollutants in all sectors, except non-energy agricultural processes.

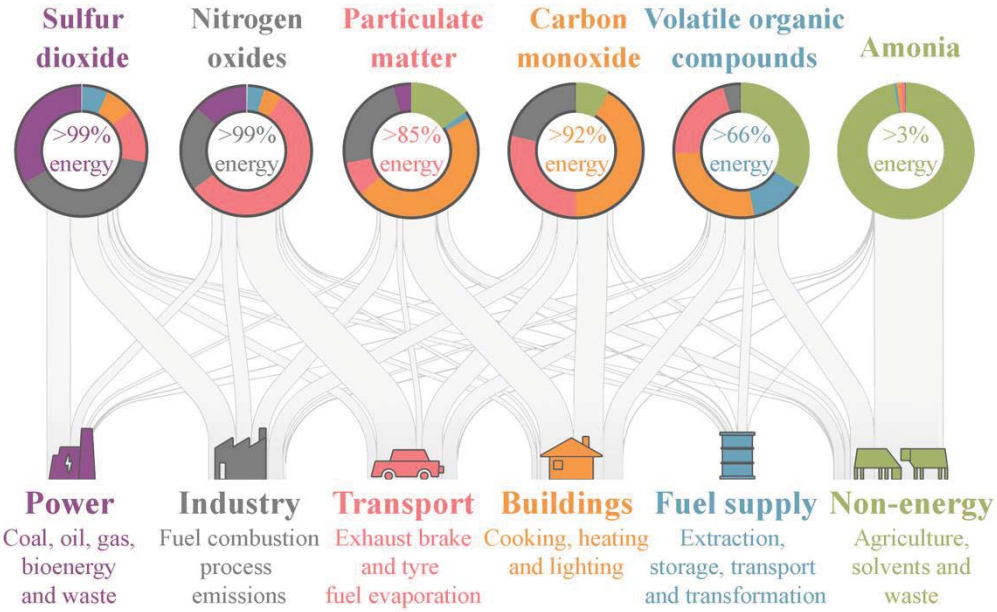

Figure 18. Main primary air pollutants and their sources in 2015.

Source: Priddle (2016).

1.4 BECCS

Social and economic growth is mainly based on energy use producing different impacts on the environment, human health and biodiversity. The generalized unsustainable way to generate energy involves a great effort in research for the correct deployment of different technologies. The whole Life Cycle Analysis (LCA) of the CO_2 emissions from various existing energy technologies, compared per unit of energy produced, is presented in Figure 19. The LCA involves the complete analysis of the process including the emissions derived from every stage from the raw materials extraction to the waste management (generation, transportation, end use, …). Almost all the technologies generate positive CO_2 emissions, and fossil fuel technologies stand out as the major contributors. The combination of traditional coal-fired power plants with CCS achieves a significant reduction in CO_2 emissions, and it is expected to play an important role prior to the deployment of BECCS. CO_2 emissions from the most common renewable energy sources are also shown. Despite their near zero emissions during operation, the CO_2

emissions are mainly emitted during their production. BECCS technologies stand out as the only group of technologies able to produce energy while GHG are removed from the atmosphere because of the CO_2 consumed during the biomass growth. Quantitatively, the reduction of atmospheric CO_2 concentrations per unit of produced energy achieves values that counteract the carbon intensity of traditional fossil fuel energy technologies.

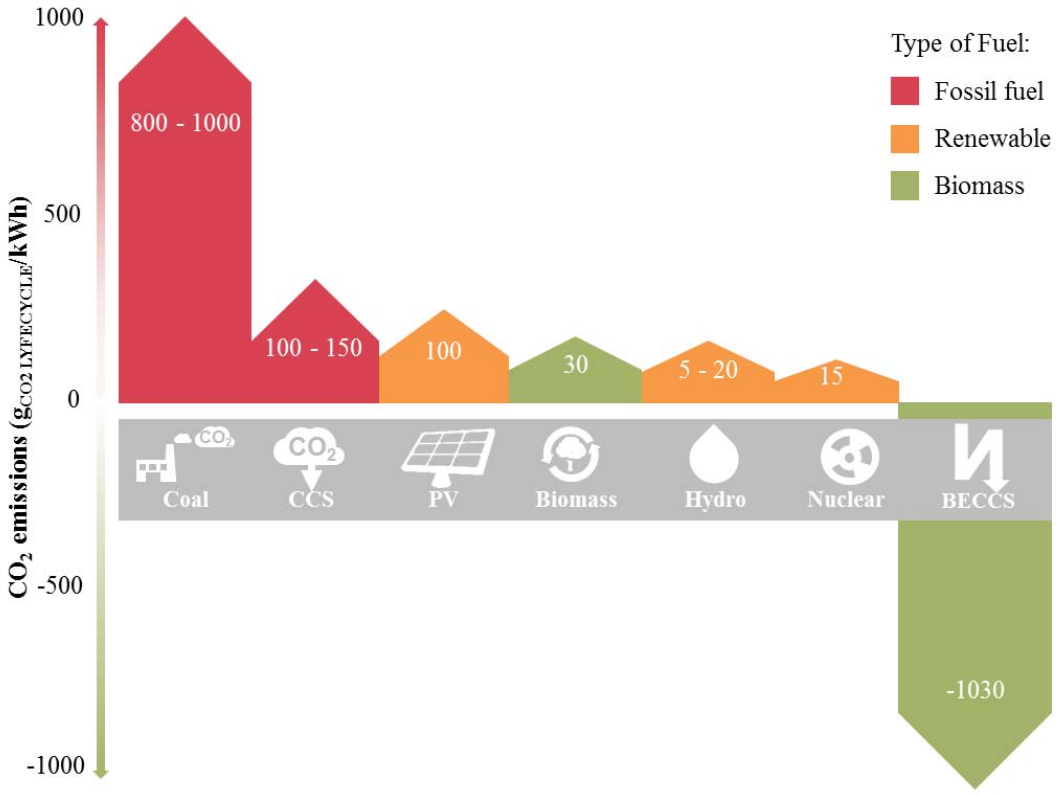

Figure 19. CO_2 emissions in different power generation systems.

Source: modified from IPCC (2014).

Regarding the expected deployment of BECCS during next decades, Figure 20 shows the necessary BECCS deployment from 2020 to 2060 by type of technology to meet the climate targets. In addition, the atmospheric CO_2 cumulative reduction is included (right axis). Biofuel sector will start a great growth around 2030, thanks to the current stage of development of these technologies. About 2040 the biomass power sector will continue growing, achieving almost half of the annual CO_2 stored associated with BECCS technologies about 2060.

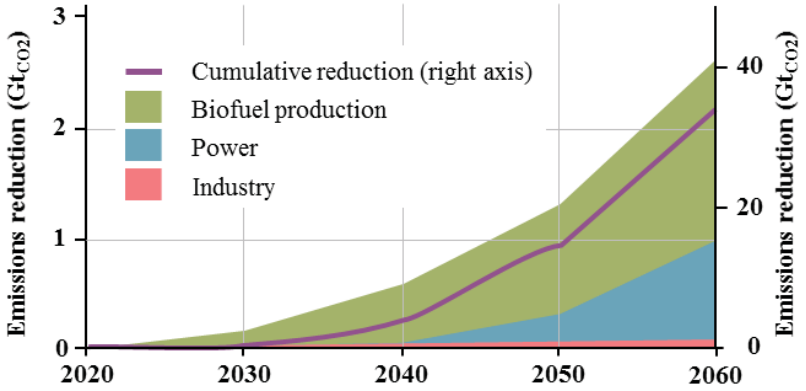

Figure 20. BECCS necessary CO_2 stored perspectives to 2060 for the B2DS scenario.

Source: Brown and Le Feuvre (2017).

Biomass has been used for thousands of years for energy purposes. Biomass fuels are usually considered CO_2 neutral, however, a sustainable management of this resource must ensure that the amount of CO_2 emitted during cultivation, harvesting, pretreatments, transportation and processing is less than the amount of CO_2 captured by the biomass during its growing. The use of CCS processes linked to bioenergy changes the CO_2 balance achieving a NET. Figure 21 presents the different BECCS potential possibilities from biomass feedstock.

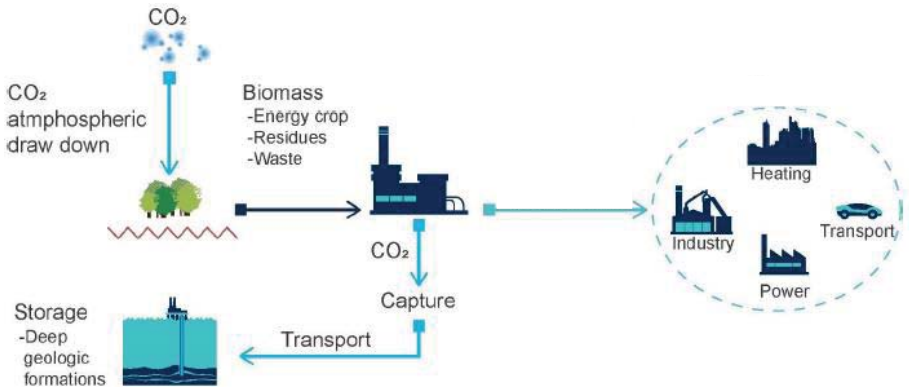

Figure 21. Scheme of different BECCS general possibilities.

Source: Consoli (2019).

As it can be seen, the scheme shows the reduction of the atmospheric CO_2 captured by the biomass. The use of different biomass-based materials, biofuels and/or bioenergy linked with CO_2 storage would contribute on the reduction of GHG emissions in the energy sector and also several industries. The general stages of BECCS processes, biomass production, CO_2 capture, transportation and storing are explained below.

- Biomass. Lignocellulose biomass supply may include starches, energy crops, algae or biomass residues. Figure 22 shows the scheme of a circular bioeconomy. Depending on the biomass origin and the characteristics, different pretreatments and processes can transform it adequately guaranteeing negative CO_2 emissions. However, environmental considerations caused by changes in land use and transportation as well as food-fuel competition must be balanced. For further information about biomass see section 1.4.1.

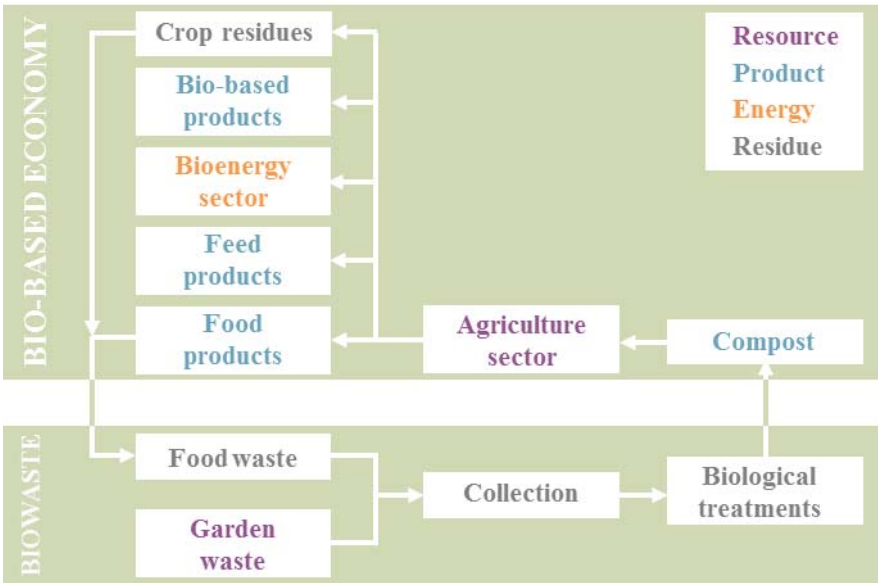

Figure 22. Scheme of a circular biomass based economy.

Source: European Commission (2018).

- CO_2 capture technology. The CO_2 capture process consists basically in the CO_2 separation process from other gases. To this, a high concentrated CO_2

stream is preferable, as the energy lost is reduced and, consequently, the cost of capture, transportation and storage processes. For further information about CO_2 capture technologies, see Consoli (2019).

- Transportation. The knowledge of international transport of natural gas and oil derived fuels is used for the transportation of CO_2. In this way, a dehydration and a compression stage are needed for the different cost-effective options such as maritime transportation or pipes. The quality of the CO_2 to be captured can be affected by the presence of different compounds in the outlet stream. Steam, N_2, O_2, CO, H_2, CH_4 and other hydrocarbons, SO_2, particles and also NO_x levels should be controlled in order to ensure that the captured CO_2 stream can be properly transported and safely stored. To date, there are no legal requirements on the quality of CO_2 transported and only recommendations have been outlined (de Visser et al. 2008). The limit set in the project Dynamis recommendations regarding the contents of these substances in the CO_2 stream is shown in Table 4.

Table 3. Dynamis limit recommended for different substances for CO_2 CCS.

Source: de Visser et al. (2008).

	Dynamis recommended limit
H_2O	500 ppm
H_2S	200 ppm
CO	2000 ppm
O_2	< 4%vol
CH_4	< 4%vol
N_2	< 4%vol
Ar	< 4%vol
H_2	< 4%vol
SO_x	100 ppm
NO_x	100 ppm
CO_2	> 95.5%

Table 4. Large scale and notable BECCS facilities with their main characteristics.

Source: Consoli (2019).

Name	CO_2 capture	Industry	Location	Status	Storage	Operation (year)	Capacity (tpa)
Large scale							
Illinois Industrial CCS	ADM corn to etanol	Ethanol production	US	Operating	Dedicated	2017	1,000,000
Norway full chain CCS	Brevik (Norcem AS)	Cement production and bioenergy	Norway	Completed Advanced Completed	Dedicated	2011-2014 2023 2013	300,000 800,000 Variable
Occidental White Energy	Hereford and Plainview bioenergy	Ethanol production	US	Evaluation		-	650,000
Notable facilities							
Russel CO_2 injection plant	ICM ethanol plant	Ethanol production	US	Completed		2003-2005	7,700 (total)
Arkalon CO_2 compression facility	Bioernergy ethanol plant	Ethanol production	US	Operating	EOR	2009	290,000
Bonanza Bioenergy CCUS EOR	Bioernergy ethanol plant	Ethanol production	US	Operating	EOR	2012	100,000
Husky Energy Lashburn	Lloydminter ethanol plant	Power generation	Canada	Operating	EOR	2012	90,000
Mikawa Post combustion 49 MW_{th}	Mikawa cofired thermal power plant	Power generation	Japan	Advanced Completed		2020 2009	180,000 3,000
Drax bioenergy BECCS	North Yorkshire power station	Ethanol production	England	Operating		2018	330
CPER Artenay	Sugar refinery in the Loiret	Ethanol production	France	Advanced		-	45,000
Biorecro/EERC	Biomass gasification plant	Biomass gasification	US	Advanced		-	1,000-5,000
OCAP	Abengoa's ethanol plant	Ethanol production and oil refinery	Netherland	Planned Operating	Dedicated CCU	2025 2011	100,000 100,000
Lantmannen etanol purification	Lantmannen agroetanol plant	Ethanol production	Sweden	Operating		2015	200,000
Calgren renewable fuels CO_2 recovery	Calgren renewable ethanol plant	Ethanol production	US	Operating		2015	150,000
ABF biorefinery CO_2 recovery	Biorefinery	Ethanol production	Belgium	Operating		2016	100,000
Cargill wheat processing CO_2 purification	Wheat processing plant	Ethanol production	England	Operating		2016	100,000
Saga city waste incineration plant	Municipal waste incineration plant	Waste to energy	Japan	Operating		2016	3,000
Saint-Felicien pulp mill and greenhouse carbon capture	Resolute softwood kraft pulp mill	Pulp and papers	Canada	Operating		2018	11,000

- Storage. After the capture and transport of CO_2, the last stage of BECCS processes is the permanent and safe storage in geological deposits. Three different types of deposits are proposed: depleted oil or natural gas deposits, coal deposits or mines that cannot be exploited and salt aquifers. Figure 25 shows the CCS potential capacity by countries. The growing interest on CCS has led more and more studies to analyze the storage capacity, increasing the accurately of CCS global potential capacity. The CO_2 storage values projected to meet the climate targets quantify about 100 billion tons of accumulated CO_2 to 2060 and about 3.3 Gt per year by the end of the century. In this sense, CCS potential capacity will not constrain the BECCS deployment.

A wide range of industries and sectors can be combined with the use of biomass-based materials or bioenergy. Biomass can be used for the production of bioenergy power or power and heat. The main technologies are based in thermochemical conversion processes. There is a high variability in the maturity of the different technologies used, with technologies that are in the research phase to large-scale commercial facilities. Figure 23 shows the operating BECCS facilities in 2019. As it can be seen, all the operating BECCS plants are installed in OECD countries, mainly North America and Europe, and mostly associated to fossil fuel deposits. Ethanol facilities at different scales were installed during the early years of the 21st century as the first dedicated BECCS plants. The largest BECCS scale operating plant, placed in USA, captures 1 Mt of CO_2 per year during the fermentation process for the ethanol production and the CO_2 generated is stored in dedicated geological formations. Also, some facilities are linked to enhancing oil recovery (EOR), where the CO_2 is injected into fossil fuel deposits for a more efficient oil extraction and the proper CO_2 storage. A large deployment of BECCS processes is expected for the next decades. Further information about these facilities is presented in Table 3. Also, biomass can be used for biofuel production. Figure 24 shows the scheme of the production of different biofuels from various biomass feedstock with chemical or biological processes. A wide range of usable biofuels can be produced for road transportation or aviation, among other sectors that produce diffuse emissions that are difficult to storage.

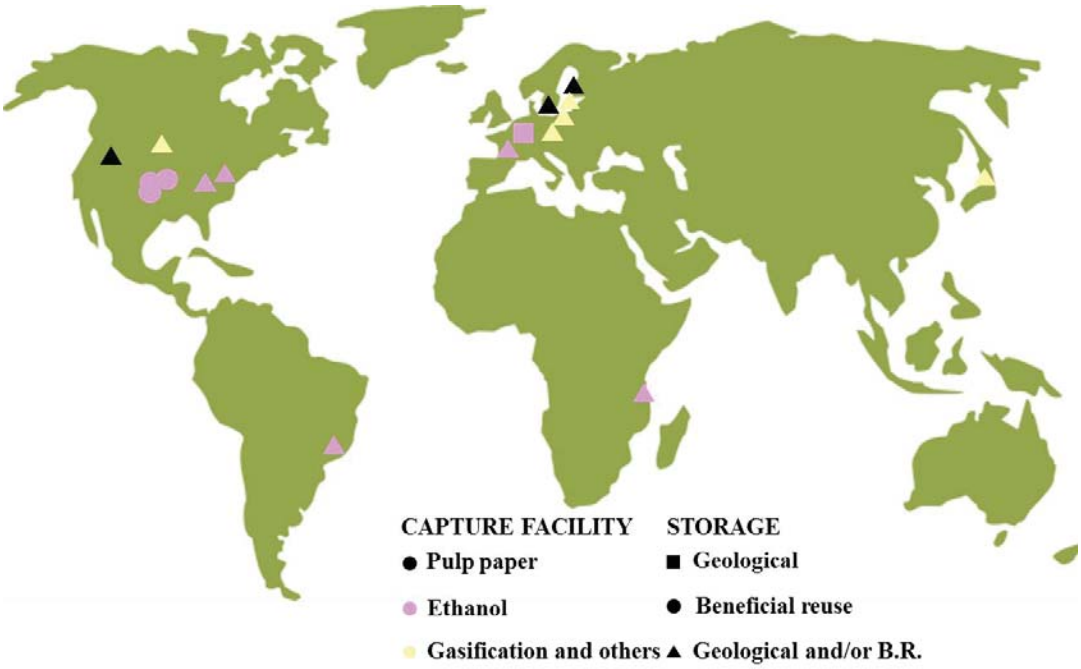

Figure 23. BECCS operating facilities in 2019.

Source: Consoli (2019).

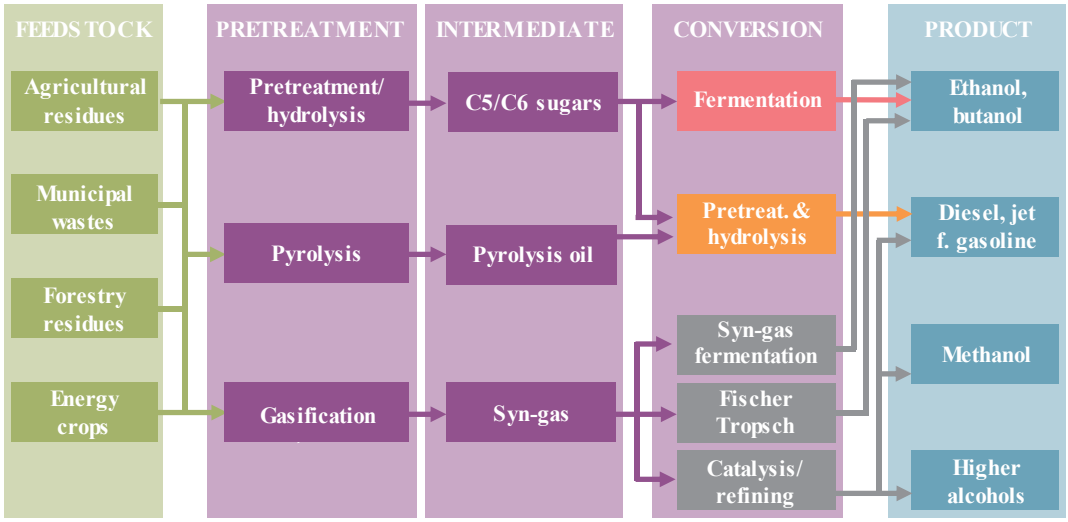

Figure 24. Scheme of different biofuels production possibilities from various biomass feedstock.

Source: modified from Consoli (2019).

Fuss et al. (2018) have analyzed the perspectives of each BECCS technology focusing in the 2100 horizon. The CCS deployment together with the correct

management of the biomass feedstock have been identified as critical variables for the BECCS deployment. Furthermore, the necessary BECCS implementation will require cost-effective technologies.

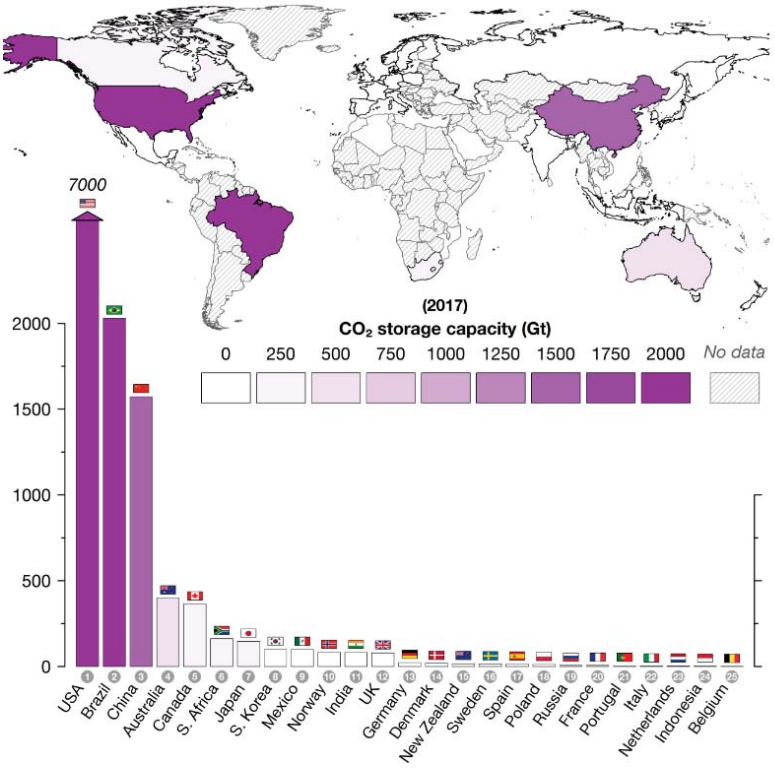

Figure 25. CCS global potential capacity by countries in 2017.

Source: Staffell et al. (2018).

1.4.1 Biomass

Biofuels represent an important fuel sources to guarantee environmental and economic sustainability. They are considered a carbon neutral (CO_2 is captured from the atmosphere and stored by biomass through photosynthesis and then emitted again into the atmosphere during biofuel combustion), renewable and abundant energy resource. Biofuels are generally classified as primary and secondary biofuels (Nigam and Singh 2011). Primary biofuels are used in an unprocessed form (woody biomass, biomass coming from forestry and agriculture, fishery products, municipal wastes, ...). Secondary biofuels are derived from primary biofuels by chemical,

biological or thermal processes to yield a fuel with suitable characteristics for a determined use (ethanol, biodiesel, dimethyl ether) (Sikarwar et al. 2017). Biofuels can be also classified according to their physical characteristics such as solid (woody biomass, …), liquid (ethanol, pyrolysis oils, …), and gaseous (biogas, pyrolysis gases, …). Gaseous and solid biofuels are normally used for heat and power production, whereas liquid biofuels are generally employed in the transport sector.

Among the solid biofuels, biomass has the greatest potential as an energy source. Biomass describes the natural tridimensional polymeric networks formed mainly by cellulose, hemicellulose and lignin of biological origin. The natural origin confers biomass a wide variability of composition. This renewable fuel source can be divided generally into three primary classes: 1. wood and woody materials, 2. herbaceous and other annual growth materials such as straws, grasses, leaves, and 3. agricultural by-products and residues including shells, hulls, pits, and animal manures. The general advantages of using biomass as fuel are: low ash, sulfur and mercury contents and high reactivity for conversion process.

Currently, some economically underdeveloped countries (mainly in sub-Saharan Africa) obtain about 90% of their energy from wood, among other biofuels, and are estimated at around 30% in Asia, Africa and Latin America. However, due to low levels of development and poor technological advances in many of these areas, biofuel consumption can contribute to deforestation rather than sustainable use. Globally, traditional energy sources worldwide declined from 98% in 1800 to 50% in 1900 and by approximately 14% in 2000 (Kander et al. 2014). Figure 26 shows the evolution from 1800 to 2017 of the consumption of various energy resources. Despite the decrease in the contribution of traditional energy uses of biomass, biomass has always remained at a steady consumption rate, while fossil fuels were constantly increasing.

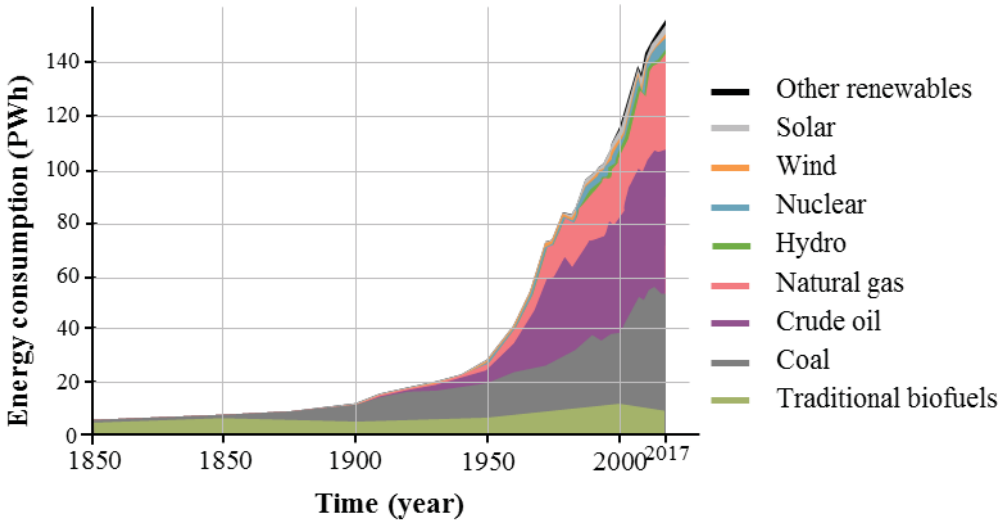

Figure 26. Energy consumption evolution from 1800 to 2017 by sources.

Source: Brown and Le Feuvre (2017).

Figure 27 shows the distribution of solid biofuels consumption by end use in 2015. As it can be seen, traditional uses remain the major consumer of biomass, accounting for more than half of the use of biomass that was around 51 EJ in 2015. Heat in the industry follows the list that continues with power generation and modern bioenergy processes. The use of biomass is maintained and new uses should be deployed with sustainable management of this resource.

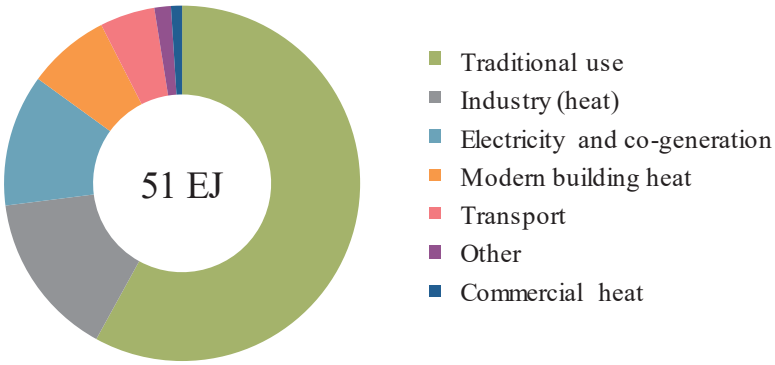

Figure 27. Biomass and waste resources by end use in 2015.

Source: modified from Brown and Le Feuvre (2017).

The use of biomass in the energy mix is nowadays limited compared to fossil fuels. However, the use of biomass in bioenergy could be increased to reduce dependence on fossil fuels. The renewable potential of this resource contrasts with the depletion of other energy resources. Fossil fuels and other energy-related raw materials are being used unsustainably, thus approaching its limit. However, biomass production will require fields with a water supply, so that it could go into competition with food production. Therefore, for sustainable development, the supply of energy from biomass should ensure environmental protection with responsible and sustainable use of water, while food production is guaranteed. In this way, the biomass supply chain would not produce impacts affecting the sustainability of resources.

Figure 28 shows the potential biomass production range of the main biomass sources. As it can be seen, according to Brown and Le Feuvre (2017), agriculture and residual biomass clearly show greater potential for sustainable biomass production than forestry operations or municipal solid waste (MSW). The minimum and maximum values of potential sustainable biomass showed in Figure 28 also include different minor biomass sources. Comparing the total sustainable biomass deployment required to achieve climate targets, the necessary value of sustainable biomass deployment enters in the range of the global potential of sustainable biomass production.

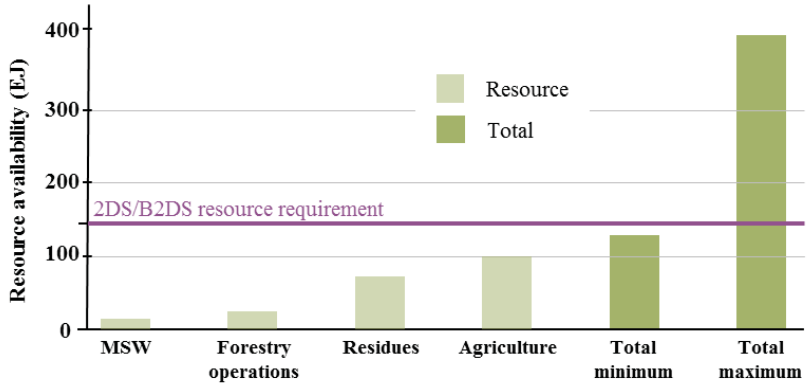

Figure 28. Main biomass sources potential, minimum and maximum potential of sustainable biomass.

Source: modified from Brown and Le Feuvre (2017).

1.4.2 Resources for BECCS in Spain

Different types of biomass can be used for bioenergy purposes. However, the sustainability of the biomass production should be considered in order to guarantee the global process sustainability. An increase in the european sustainable biomass production was pointed by the European Environmental Agency from about 190 Mtoe in 2010 to about 293 Mtoe in 2030. Figure 29 presents the environmentally compatible primary bioenergy potential in the EU-25. Various biomass types were considered and, furthermore, an additional agricultural potential was estimated by Wiesenthal et al. (2006) for Germany and France consequence of the posible rising prices paid for bioenergy. As it can be seen, a general increase in sustainable biomass potential is showed from 2010 to 2030 and basically corresponds to the agricultural potential increase. Meanwhile, maintained waste and forestry sustainable biomass production are shown.

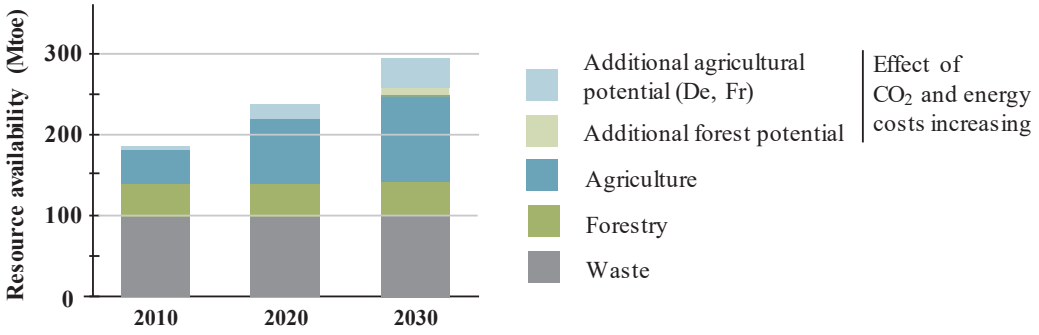

Figure 29. EU primary bioenergy potential environmentally compatible.

Source: Wiesenthal et al. (2006).

Focusing in Spain, an increment from about 17 Mtoe in 2010 to about 25 Mtoe in 2030 (Wiesenthal et al. 2006) was reported. The Spanish Renewable Energy Plan (PER) 2011-2020 shows that about 18066 kt/year of non industrial biomass are available in Spain, covering the objectives of biomass production needed for bioenergy and energy demand set in the plan IDAE (2011), and about 9639 kt/year of biomass from forestry and 5908 kt/year of agricultural waste should be used for energy uses in 2020.

Olive stones (*Olea europaea*) and almond shells (*Prunus dulcis*) are two agricultural residues with high annual production. In 2016 world olive production reached 3.3 million tons and Spanish production represented about 38% of the total production (IOOC 2018). Almond production in the world increased about 43% during the period 2007-2017, achieving at the end of the period about 1.2 million tons. Spanish almond production represented about the 5% of total production (INC 2018).

Biomass production covers the expected biomass demand increase for energy purposes, however, the deployment of NET processes associated to energy generation will need the deployment of transport and storage facilities for the CO_2 produced. In fact, all the considered strategies to mitigate the climate change effects include CCS technologies. The Geocapacity project estimated the CO_2 storage capacity of most of the European countries about 356500 Mt including saline aquifers as well as hydrocarbon and coalfields. In this study, the potential locations for a long and safe CO_2 storage are considered together with the main CO_2 emitters that guarantee the cost-effective implementation. In this sense, sources with emissions higher than 0.1 Mt of CO_2 per year were considered as well as existing natural gas pipelines were taken into account because of the transport similarities (Vangkilde-Pedersen et al. 2009). Spanish CO_2 storage capacity was estimated about 14179 Mt, analyzing 103 geological formations (Zapatero et al. 2008). No large CCS projects are installed in Spain, however, the various small projects will store about 6.5 Mt of CO_2 at the end of the period 2015-2020. Moreover, 20.2 Mt/year are expected to be stored in Spain during the period 2021-2030 (ALINNE 2019). These expected numbers point to the good perspectives for a large-scale deployment of BECCS technologies.

1.5 Chemical Looping Combustion

The CLC concept was developed for pure CO_2 production in 1954 by Lewis and Gilliland (Lewis and Gilliland 1954). Decades later, in 1980s, the CLC process was proposed as a highly efficient technology for power generation (Richter and Knoche 1983; Ishida et al. 1987) and later it was also recognized the possibility of being used as a combustion process with inherent CO_2 capture (Ishida et al. 1996).

The good perspectives of CLC brought attention on these technologies. Initially the process was developed for gaseous fuels, due to its easy handling and high energy density, but in the last years its use has spread to liquid and solid fuels. Moreover, Chemical Looping (CL) processes open up a wide range of biofuels utilization through different processes. Figure 30 presents the general scheme of Chemical Looping Processes showing the different biofuels and products. Depending on the type of biofuel used and the product obtained, different CL processes can be distinguished:

- Chemical Looping Combustion (CLC) implies the combustion of gaseous, liquid or solid fuels obtaining heat and/or power. If the biofuel is solid, two reaction mechanisms are possible: In situ gasification Chemical Looping Combustion (*i*G-CLC) and Chemical Looping with Oxygen Uncoupling (CLOU). Both mechanisms will be described in section 1.5.1.
- Chemical Looping Reforming (CLR) implies partial oxidation reforming of gas or liquid biofuels to produce syngas (H_2 + CO).
- Chemical Looping Gasification (CLG) allows obtaining syngas using solid biofuels.

In these processes, a solid oxygen carrier, usually a metal oxide, provides the oxygen needed for the fuel oxidation or partial oxidation. A wide range of reactor configurations has been proposed for solid, liquid and gaseous biofuels also depending on the oxygen carrier reactivity and the scale of the CL prototype. For

further information about different CL process configurations see Adánez and Abad (2019). Interconnected fluidized bed reactors are commonly the preferred option for CL processes thanks to the good and homogeneous contact between solids and gases (Kramp 2014). Fluidized bed reactors are known because of the good gas/solid contact and the homogeneous temperature distribution.

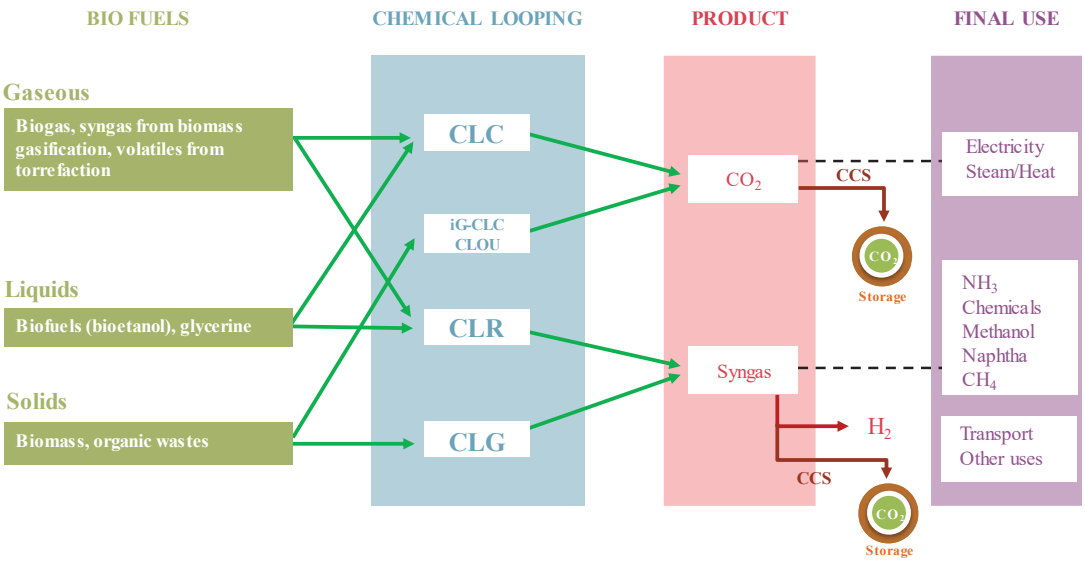

Figure 30. General scheme of Chemical Looping Processes.

Source: modified from Mendiara et al. (2018a).

The CLC process is mainly based in two interconnected fluidized bed reactors, the fuel and air reactors. A simple scheme of the process is shown in Figure 31. The solid oxygen carrier circulates between the fuel and air reactors without gas mixing. In the fuel reactor, the oxygen carrier is reduced providing the oxygen needed for the fuel oxidation to CO_2 and H_2O. After H_2O condensation, an almost pure CO_2 stream is produced during fuel conversion, ready for transportation and storage. Meanwhile, in the air reactor, the oxygen carrier is oxidized again in air to start a new cycle. Loop seals are placed between both reactors to prevent the mixing of fuel and air reactor atmospheres.

The energy balance of CLC process can be calculated as the combination of the reduction and oxidation reactions (R1 and R2), obtaining the traditional

combustion equivalent reaction (R3). The oxygen carrier oxidation in the air reactor is always an exothermic reaction, however, the oxygen carrier reduction in the fuel reactor can be exothermic or endothermic reaction depending on the redox system of the oxygen carrier and the fuel used. In this sense, under endothermic reduction reactions, the oxygen carrier also acts as energy vector by transporting heat from the air reactor to the fuel reactor to maintain constant the temperature in the fuel reactor. Regarding the kinetics of CLC process, the oxygen carrier reduction is usually slower than the oxygen carrier oxidation, however, each reaction can be affected by several variables such as the reactor temperatures, the oxygen carrier used and the gas concentrations.

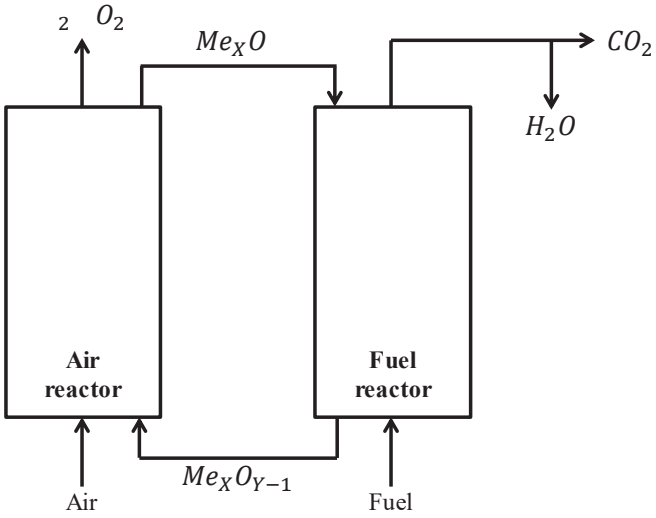

Figure 31. Simplified scheme of a CLC process.

Reduction reaction $\Delta H^0_{Red} < 0 \; or > 0 \; kJ/mol$ (R1)

$$(2n + m - p)Me_xO_y + C_nH_{2m}O_p \rightarrow (2n + m - p)Me_xO_{y-1} + nCO_2 + mH_2O$$

Oxidation reaction $\Delta H^0_{Oxi} < 0 \; kJ/mol$ (R2)

$$(2n + m - p)Me_xO_{y-1} + \left(n + \frac{m}{2} - \frac{p}{2}\right)O_2 \rightarrow (2n + m - p)Me_xO_y$$

Global combustion reaction $\Delta H^0_T < 0 \; kJ/mol$ (R3)

$$C_nH_{2m}O_p + \left(n + \frac{m}{2} - \frac{p}{2}\right)O_2 \rightarrow nCO_2 + mH_2O$$

Guandalini et al. (2019) used a simplified method of costs sequential approach over different CO_2 capture technologies. The results were validated using the results of a coal-fired plant and among various pre-combustion, oxy-fuel, post combustion or absorption processes, CLC stood out with the lowest cost of avoided CO_2. Using biofuels, CLC was pointed as one of the most suitable CO_2 capture technologies to obtain bioenergy (heat and/or electricity) from energetic and economic points of view, producing a negative CO_2 balance (Lyngfelt and Leckner 2015). The inherent CO_2 capture, thanks to the two-stage reaction, makes any separation step unnecessary.

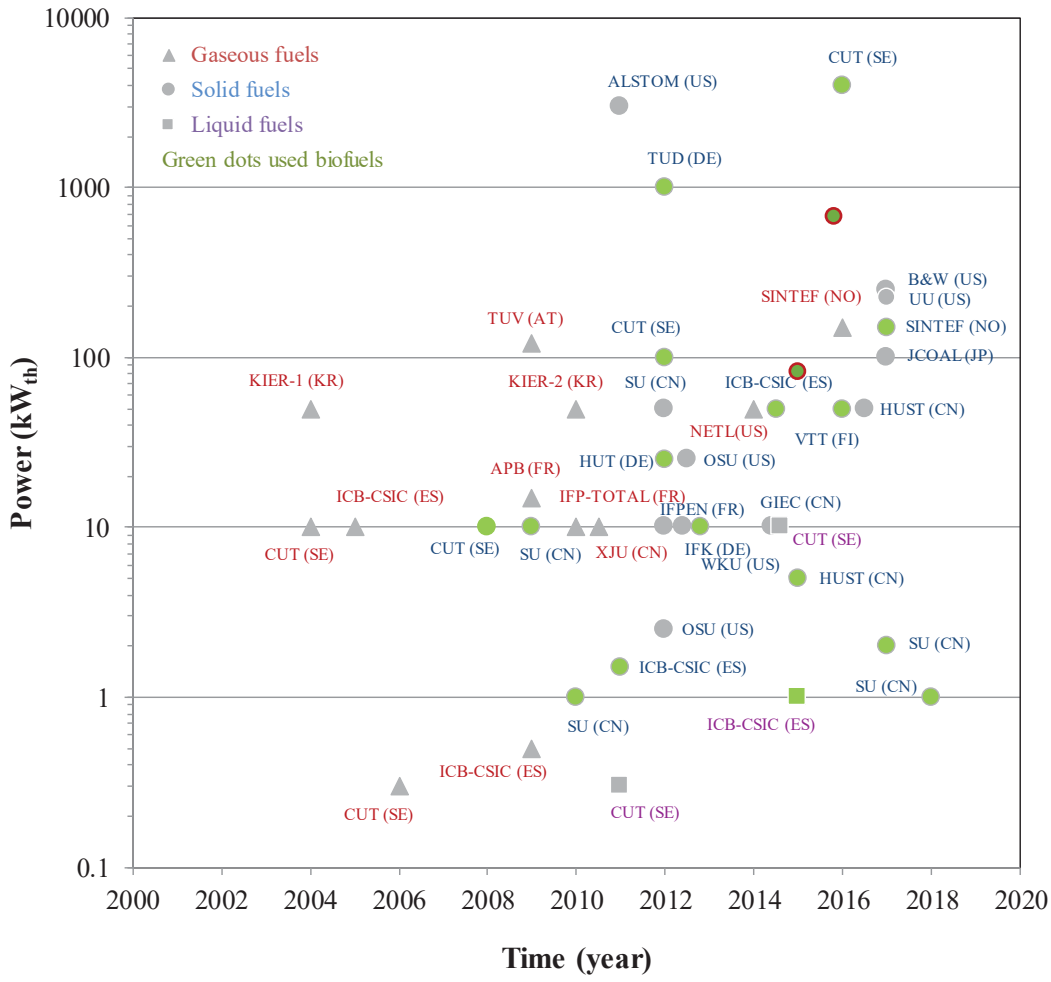

Figure 32. CLC units by power and operation date.

Source: Mendiara et al. (2018a).

Figure 32 presents the CLC units operated since year 2000 to date by power and the type of fuel used. As it can be seen, different CLC sizes were implemented from bench scale to 4 MW_{th}. Bio fueled units to achieve a considered as NET (specially powered by solid biomass), highlighted in green, began to be operated around 2008 and have shown great development in recent years.

1.5.1 Chemical Looping Combustion of solid fuels

Figure 33 shows the scheme of a typical CLC unit for solid fuels. The reactor system used has large similarities with conventional circulating fluidized bed (CFB) boiler. Fuel is introduced into the fuel reactor where it is converted by the oxygen carrier to produce CO_2 and H_2O. The spent oxygen carrier is transported to the air reactor to be oxidized by air in order to start a new cycle. H_2O or CO_2 can be used to fluidize the fuel reactor and air is used in the air reactor as fluidizing gas producing a depleted air.

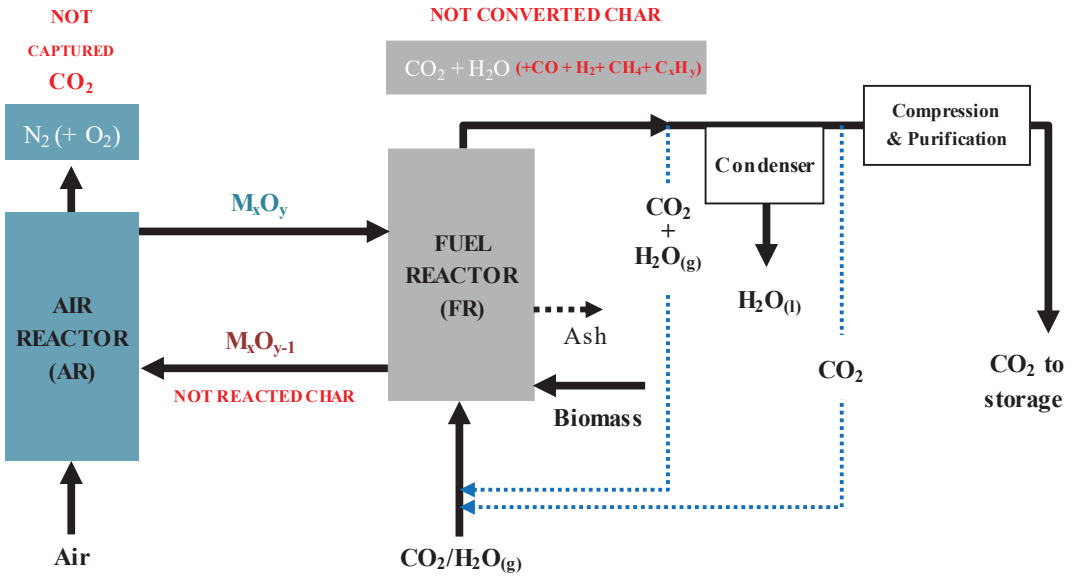

Figure 33. General scheme of a CLC process for solids fuels.

When the solid fuel is introduced into the fuel reactor, the high temperature produces the fuel drying followed by the devolatilization, generating the volatile

matter and the char. This char is mainly formed by carbon. Two options have been proposed depending on how the solid fuel is converted to CO_2 and H_2O: in situ Gasification CLC (*i*G-CLC) and Chemical Looping with Oxygen Uncoupling (CLOU). Figure 34 shows the *i*G-CLC and CLOU reaction schemes.

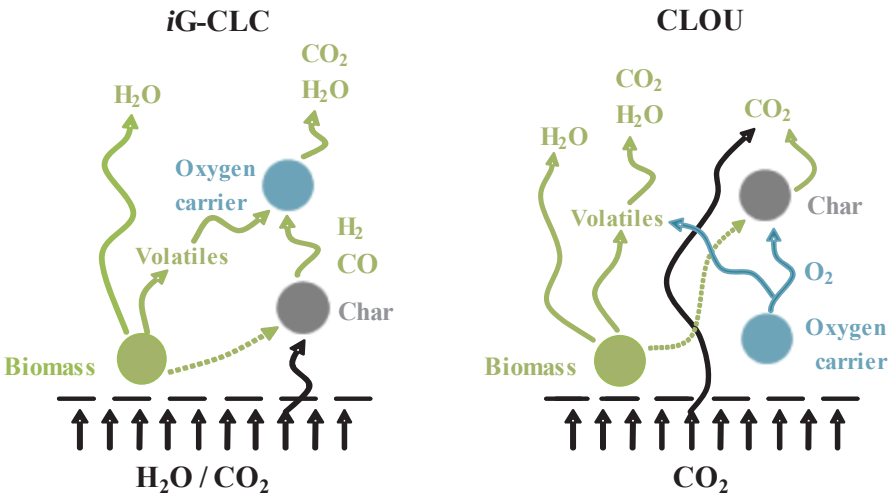

Figure 34. In-situ Gasification CLC (iG-CLC) and Chemical Looping with Oxygen Uncoupling (CLOU) reaction schemes.

Under *i*G-CLC, the steam or CO_2 supplied to the fuel reactor as fluidizing agent also acts as char gasifying agent producing combustible gases according to the following reaction scheme, reactions (R4) to (R6).

$$Solid\ fuel \rightarrow char + volatile\ matter \quad \text{(R4)}$$

$$Char + x\ H_2O \rightarrow x\ H_2 + x\ CO + ash \quad \text{(R5)}$$

$$Char + y\ CO_2 \rightarrow 2y\ CO + ash \quad \text{(R6)}$$

The lattice oxygen in the solid oxygen carrier reacts with the volatile matter and the gasification products of the char to produce CO_2 and H_2O as final products. The prevailing reaction between the oxygen carrier and the fuel is a solid-gas reaction. In this process the CO_2 capture efficiency is reduced by char particles by-

passed to the air reactor together oxygen carrier when these particles are burnt. Char gasification has been identified as the limiting step of this process (Adánez et al. 2018). Thus, char particles need high residence time in the fuel reactor to be gasified. Also the fluidizing agent (H_2O or CO_2) used in the fuel reactor plays an important role in the reactivity, enhancing the char gasification rate. Other characteristic of *i*G-CLC process is that unburnt compounds can be found in the gas stream from the fuel reactor (Adánez et al. 2018). These unburnt compounds should be burnt by using pure O_2 (oxygen demand). Finally, because of the ashes present in the solid fuels it is necessary the drainage of ashes from the system to avoid its accumulation in the reactors. Most of the experience gained in biomass combustion was under this mechanism.

CLOU process is based on the capacity of some specific oxygen carriers to release molecular oxygen at the common operating temperatures in the fuel reactor (about 800-1000 ºC). The O_2 generated reacts with volatiles and char as in conventional combustion with air. In CLOU, the prevailing reaction became a gas-gas reaction. This process was proposed in 2009 by Mattisson, et al. (2009a) and the proof of concept was demonstrated with coal in a 1.5 kW_{th} unit located at ICB-CSIC (Abad et al. 2012). The materials used as oxygen carriers in this process must have suitable thermodynamic properties for oxygen uncoupling at temperatures of interest. The suitable materials that have the property of release oxygen are limited. Three metal oxide systems have so far been identified (Mattisson et al. 2009): CuO/Cu_2O, Mn_2O_3/Mn_3O_4, Co_3O_4/CoO and mixed oxides (Fe-Mn, Mn-Cu, Cu-Fe or Perovskites).

The CLC technology for solid fuels was initially developed for coal use. In this sense, the biomass has significant differences with respect to coal that will affect to its performance in CLC: Firstly, a high fraction of volatile matter is released during devolatilization, which contains 70-80% of the biomass heating value. Thus, a good conversion of the generated volatile matter during biomass devolatilization is a key point for a good process performance. On the other hand, a low fraction of char is produced, which has high gasification reactivity with steam and CO_2. Moreover, the

sulfur content is low and also the ash fraction present in biomass is usually lower than that of coal.

The higher fraction of volatiles, compared to coal, could be a disadvantage due to unburnt volatile matter can increase the amount of unburned compounds in the outlet of the fuel reactor, increasing the total oxygen demand. The lower fraction and much higher reactivity of biomass char in steam and CO_2 gasification is a great advantage because a much smaller fraction of char would be by-passed to the air reactor. Its low ash content is a great advantage because the impact of ash-removal on oxygen-carrier lifetime and thus oxygen-carrier cost will be much less. However, biomass ash components, such as alkali metals and chlorine, are problematic in normal biomass combustion, mainly due to corrosion and agglomeration issues. In CLC, biomass ash could be problematic as several components, alone or together, could cause deactivation of the oxygen carrier particles and, in the worst case, cause agglomeration in the fluidized bed system due to the interaction of oxygen carrier materials and fuel ashes.

Tar compounds can be also produced during the biomass oxidation in the fuel reactor, reducing the biomass conversion efficiency and causing operational problems as fouling (Kobayashi and Fan 2011). However, the use of different oxygen carriers and the operating conditions should be analyzed because of the different tar formation and/or cracking (Virginie et al. 2012; Ge et al. 2016). Other aspect to be considered during biomass processing is the NO_x emissions. Although there is no gas-phase N_2 present during the CLC in the fuel reactor, biomass could contain certain amounts of organically bound nitrogen. This nitrogen may form harmful species, like NO, N_2O, HCN, and NH_3, that can be released in the fuel reactor, affecting the quality of the CO_2 stream produced. In addition, NO_x emissions can be released in the air reactor due to the combustion of the char coming from the fuel reactor. These emissions must be lower than those indicated by the EU regulations.

Compared to gaseous fuels or coal, the direct conversion of biomass in CLC processes is a relatively new subject. At the time of beginning this thesis, the

experience that existed related to CLC processes with biomass combustion was very limited. Works published under CLC conditions using biomass had been carried out on laboratory-scale discontinuous reactors with small amounts of oxygen carriers and fuel fed. Mainly wood char or pine sawdust were used in these experiments, showing the combustion efficiency a great dependence on the reduction temperature (Leion et al. 2009a; Leion et al. 2011). Subsequently, progress has been made in this technology by conducting experiments on continuous prototypes. As a summary, Table 5 presents an overview of the experience accumulated in different bioCLC facilities, indicating the specific fuel and oxygen carrier used among other operating variables. As can be seen, most correspond to work carried out in the framework of this thesis or works published during the period of realization of this thesis.

In any case, to date, most of the biomass fueled CLC studies used mineral oxygen carriers for *i*G-CLC. The natural origin of this type of materials, typically iron or manganese oxides, confers them a low cost. Synthetic oxygen carriers based on Cu and/or Mn have been used for the CLOU process. Different biofuels have been tested at the different pilot plants from 0.5 kW_{th} to 4 MW_{th}. Pine sawdust and pine wood pellets have been usually used as reference materials thanks to the large world production and world distribution. Among other biofuels, agricultural wastes or sewage sludge have also been considered. In general, high carbon capture efficiencies were obtained but also high oxygen demands.

Table 5. Summary of the experience accumulated in bioCLC continuous units. Results highlighted in grey were obtained prior to the beginning of the research carried out in this Ph.D. Thesis.

Research group	Year of publication	Nominal power (kW)	Oxygen carrier	Fuel	FR design	FR Temperature (ºC)	Carbon capture (%)	Oxygen demand (%)	Operation (h)	Ref.
					iG-CLC					
SU	2009	10	Iron oxide	Pine sawdust	SB	740-920	*n.a*	*n.a*	30	(Shen et al. 2009)
SU	2011	1	Australian iron ore	Shenhua bituminous coal/ Sawdust	SB	720-930	95.5-98.5	*n.a.*	-	(Haiming et al. 2011)
SU	2015	1	Hematite	Sewage sludge	SB	800-900	~ 100	8.5-23.5	10	(Jiang et al. 2016)
ICB-CSIC	2013	0.5	Tierga iron ore	Pine sawdust	BFB	880-980	90-100	3.8-14.1	37	(Mendiara et al. 2013a)
CUT	2014	100	Ilmenite	Wood char	CFB	929-973	91-97	4.7-15.5	31	(Linderholm et al. 2014)
SU	2016	1	Hematite	Sewage sludge (SS) / Zhundong (ZD) coal	SB	800-930	94-96	13.5-35	5	(Jiang et al. 2016)
SU	2017	2	Hematite	Sewage sludge	2-stage SB	800-900	~ 100	*n.a.*	8	(Yan et al. 2017)
SU	2018	1	Australian hematite	Sawdust	5-stage BFB	840-920	> 95	*n.a.*	*n.a.*	(Jiang et al. 2018)
SU	2018	1	Australian hematite	Rice husk	5-stage BFB	840-920	> 95	*n.a.*	*n.a.*	(Jiang et al. 2018)
ICB-CSIC	2018	0.5	Tierga iron ore	Pine sawdust	BFB	880-980	90-100	7-34.6	14	(Mendiara et al. 2018b)
ICB-CSIC	2018	0.5	Tierga iron ore	Olive stones	BFB	905-980	90-100	20-30	13.4	(Mendiara et al. 2018b)
ICB-CSIC	2018	0.5	Tierga iron ore	Almond shells	BFB	905-985	90-100	18-28	10.8	(Mendiara et al. 2018b)
ICB-CSIC	2019	0.5	Manganese minerals	Pine sawdust	BFB	891-966	~ 100	9.1-34.8	65	(Pérez-Astray et al. 2019a)
ICB-CSIC	2019	0.5	Manganese-iron mixed oxide	Pine sawdust	BFB	887-951	~ 100	5-21.8	41	(Pérez-Astray et al. 2019b)
ICB-CSIC	2018	20	Tierga iron ore	Olive stones	CFB	900	95-99.9	15-20	20	(García-Labiano et al. 2018)
CUT	2016	10	Manganese ores	Wood char	BFB	887-1000	76.0-96.4	5.8-11.4	32	(Schmitz et al. 2016)
CUT	2016	100	Tierga iron ore	Wood char	CFB	880-960	> 96	7.4-8.5	26	(Linderholm and Schmitz 2016)
CUT	2018	10	Sintered manganese ore	Biochar and black wood pellets	BFB	900-970	92.8-99	6.5-30	20	(Schmitz and Linderholm 2018)

CUT	2018	100	Sintered manganese ore	Biochar and black wood pellets	CFB	940-981	99-100	10-35	28	(Schmitz and Linderholm 2018)
CUT	2019	10	Steel converter slag	Wood char, biochar and black pellets	BFB	920-985	~ 99	*n.a.*	28	(Moldenhauer et al. 2019)
CUT	2019	100	$CaMn_{0.775}Ti_{0.125}Mg_{0.1}O_{3-\delta}$ + Ilmenite (10-20 /80-90 wt%)	Wood char and black wood pellets	CFB	933-954	99.3-99.5	10.5-20.2	3	(Gogolev et al. 2019)
CUT	2017	4000*	Australian ilmenite or Brazilian manganese ore	Spruce tree wood pellets	CFB	~830	n.a.	~ 40	>1000	(Berdugo Vilches et al. 2017)
VTT	2016	50	Ilmenite	White and black pellets	BFB	~850	83-96	29-41	16+20	(Pikkarainen et al. 2016)
VTT	2017	50	Braunite	White and black pellets, Wood char	BFB	838-897	72-96	11-31	20	(Pikkarainen and Hiltunen 2017)
HUT	2018	25	CuO/Al_2O_3	Hard wood	Two-step BFB	850	93	1.6	*n.a.*	(Haus et al. 2018)
SINTEF	2018	150	Ilmenite	Black wood pellets	CFB	960-980	94-97	23-28	3	(Langørgen and Saanum 2018)
TUD	2017	1000	Tierga iron ore	Hard coal and torrefied biomass	CFB	900-950	Up to 66	38-45	6	(Ohlemüller et al. 2017)
					CLOU					
ICB-CSIC	2014	1.5	$CuO/MgAl_2O_4$	Pine sawdust	BFB	900-935	98-100	0	10	(Adánez-Rubio et al. 2014)
ICB-CSIC	2018	1.5	$Cu_{1.5}Mn_{1.5}O_4$	Pine sawdust	BFB	775-850	86-100	0	20	(Adánez-Rubio et al. 2018)
ICB-CSIC	2018	1.5	$Cu_{1.5}Mn_{1.5}O_4$	Olive stones	BFB	775-850	78-91	0	10	(Adánez-Rubio et al. 2018)
ICB-CSIC	2018	1.5	$Cu_{1.5}Mn_{1.5}O_4$	Almond shells	BFB	775-850	73-93	0	10	(Adánez-Rubio et al. 2018)
CUT	2016	10	$CaMn_{0.9}Mg_{0.1}O_{3-\delta}$	Biochar	BFB	917-970	82-95.2	2.1-4.9	37	(Schmitz and Linderholm 2016)
CUT	2018	10	MnSiTi mixed oxide	Wood char	BFB	900-970	81.3-95.5	3.4-6.7	7.5	(Schmitz et al. 2018)
CUT	2019	100	$CaMn_{0.775}Ti_{0.125}Mg_{0.1}O_{3-\delta}$ + Ilmenite (80-90/10-20 wt%)	Black wood pellets	CFB	946-957	> 99.5	3-5	3	(Gogolev et al. 2019)

* Corresponds to the gasifier acting as fuel reactor in the Chalmers boiler/gasifier loop (with inputs of 12 MW_{th} and 2–4 MW_{th}, respectively)

(SB= Spouted bed, BFB= Bubbling fluidized bed, CFB= Circulating fluidized bed)

1.5.2 Oxygen Carriers

The oxygen carrier particles are responsible of the oxygen exchange from the air in the air reactor to the fuel in the fuel reactor. Furthermore, depending on the thermodynamics of the process, the oxygen carrier acts as heat vector between the reactors. Several properties of the oxygen carriers should be considered for a suitable CLC performance: 1. A correct fluidization behavior should be guaranteed (no agglomeration problems). 2. The oxygen transport capacity of the oxygen carrier (R_{oc}) must be enough to allow the complete combustion of the fuel. 3. A high reactivity and its maintenance over a high number of redox cycles. 4. High selectivity to CO_2 and H_2O during combustion. 5. High mechanical resistance of the particles and its maintenance over a high number of redox cycles. In general, the lower chemical stress affects the of oxygen carrier particles, the longer their lifetime should be (Adánez et al. 2012). 6. Low price of the materials. Oxygen carrier origin (synthetic or natural) will affect the oxygen carrier cost. 7. The low toxicity of the oxygen carrier and residues generated must be taken into account (Mendiara et al. 2012).

Figure 35 presents the oxygen transport capacity of the most important redox pairs used in CLC. Different colors were used to classify the oxygen carriers depending on their capacity to release molecular oxygen under specific conditions. Hundreds of oxygen carriers (natural or synthetic) have been tested for years in CLC, most of them using gaseous fuels (Adánez et al. 2012). Minerals, or ores, usually are low cost oxygen carriers. Even some mining residues have been used as oxygen carriers with good results. On the contrary, synthetic oxygen carriers, usually more reactive carriers than ores, need a preparation processes that increases the cost. Synthetic oxygen carriers are normally formed by an active phase, actually able to react with the fuel, and an inert support that increases resistance. The variability in the price of the oxygen carrier feedstock can greatly influence the total cost. Different oxygen carrier preparation methods can be used. Among them, spray drying, impregnation and granulation processes are the most commonly used. Cobalt based and nickel based oxygen carriers present high costs as well as toxicity effects, what

disregard their use in CLC units. Meanwhile, iron, manganese, and copper oxygen carriers generate inert residues that can be disposed as nonhazardous materials.

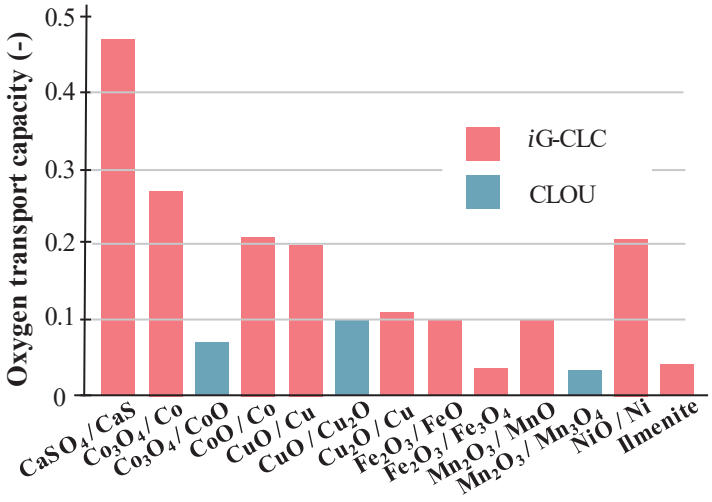

Figure 35. Oxygen transport capacity (R_{OC}) of various redox pairs.

The majority of the CLC units for combustion of solid fuels, including biomass, have been operated under the *i*G-CLC mode using minerals or residues. Despite the lower ash content of solid bio fuels compared with coal, the necessary ash removal associated with the use of solid fuels implies the oxygen carrier drainage. Because of this oxygen carrier purge, the oxygen carrier price can greatly affect the total costs, being low-cost oxygen carriers the preferable option for the CLC of biomass. In this sense, the natural origin of ores, typically iron or manganese oxides, confers them a low-cost appropriate for this use. Moreover, synthetic oxygen carriers based on Cu and/or Mn have been used for the CLOU process.

First results using biomass (pine sawdust) and iron ore as oxygen carrier were obtained by Shen et al. (2009) in a 10 kW_{th} unit during about 30 h of operation. They evaluated the influence of the fuel reactor temperature on the gas products of the fuel reactor and they found a higher influence of the temperature on the CO formation than the observed on the CO oxidation. Pine sawdust was also used in the experiments performed at *Instituto de Carboquímica* by Mendiara et al. (2013a) with a Fe-based iron ore (Tierga ore) as oxygen carrier. The influence of the fuel reactor

temperature on the CO_2 capture and combustion efficiencies and the oxygen demand was assessed. In the interval 880–915 ºC, high carbon captures (> 95%) were achieved using both steam and CO_2 as gasifying agents and the total oxygen demand decreased by increasing the fuel reactor temperature. Moreover, no interaction of biomass ashes with the oxygen carrier was observed after 78 h of continuous operation. The same oxygen carrier was also used by Linderholm and Schmitz (2016) in a 100 kW_{th} CLC plant located at Chalmers University of Technology (CUT) using wood char as fuel. The highest combustion efficiency observed in these experiments was 93% (Linderholm and Schmitz 2016). Gogolev et al. (2019) used a mixture of synthetic calcium manganite (10 - 20%) and natural ilmenite (80 - 90%) as oxygen carrier in a 100 kW_{th} during an experimental campaign with black pellets of steam-exploded stem wood, straw pellets and wood char. Close to 100% of CO_2 capture efficiency and about 95% gas conversion was achieved for black pellets. Pikkarainen et al. (2016), at the VTT Technical Research Centre in Finland, built a 10-50 kW_{th} CLC plant for biomass combustion, which was operated with ilmenite during 16 h. They found high oxygen demands during the combustion of wood pellets due to an insufficient bed temperature of the fuel reactor, as the unit was originally designed for gasification. Ohlemüller et al. (2017) presented the results with hard coal mixed with biomass in their 1 MW_{th} pilot plant. High total oxygen demands were obtained using the Tierga ore as oxygen carrier. Low CO_2 capture efficiencies were reached, however, no carbon stripper was used. Langørgen and Saanum (2018) used black pellets with ilmenite in a 150 kW_{th} CLC pilot unit. CO_2 capture efficiencies over 90% were achieved while a minimum total oxygen demand about 23% was reached.

More recently, Mn-ores are being considered as an alternative to Fe-based materials due to its relatively high reactivity and its positive effect on the char conversion rate (Abad et al. 2018). A wide number of manganese ores with different origins all around the world and different characteristics have been studied during recent years for their use as oxygen carriers at various laboratory scales. The researcher group from Chalmers University of Technology (Schmitz el al. 2016; Schmitz and Linderholm 2018) has used several manganese ores as oxygen carriers in two different 10 and 100 kW_{th} CLC units with wood pellets and wood char. The influence of several operating conditions was studied and, in general, high carbon

capture and combustion efficiencies (> 90%) and low oxygen demands were obtained. However, the lifetime of the oxygen carrier was not very high.

A major step in the scale-up of the biomass CLC process was recently presented by Berdugo-Vilches et al. (2017). Several experimental campaigns were carried out in a semi-commercial dual fluidized bed unit at Chalmers University consisting of a 12 MW_{th} boiler coupled to a 2-4 MW_{th} bubbling bed gasifier. The gasifier can be assimilated to a fuel reactor of a conventional CLC unit and the boiler to the air reactor. More than 1000 hours of combustion were reported using commercial wood pellets as fuel and ilmenite and a manganese ore as oxygen carriers. Combustion efficiencies up to 60% were achieved although the temperature in the gasifier was not high, about 830 ºC (Berdugo Vilches et al. 2017). Despite this pilot plant represents a non-optimized reactor design for CLC applications, these results highlight the strong potential of the CLC technology for biomass combustion and reinforce its possibilities as BECCS technology.

Current experience in biomass combustion under CLOU mode is quite limited. As it is shown in Figure 36, few metal oxides present adequate partial pressure of oxygen at conditions relevant for combustion processes (CuO/Cu_2O, Mn_2O_3/Mn_3O_4 and Co_3O_4/CoO) (Mattisson et al. 2009). Assuming similar oxygen excess (about 20%) to those used in traditional biomass boilers, about 4% of oxygen would be preferable at the air reactor outlet for a CLOU process, and therefore different temperatures in the air reactor would be needed depending on the redox pair used. Regarding the fuel reactor temperature, the increase of the fuel reactor temperature favours the oxygen release.

Table 6 shows the temperature operating window for CuO/Cu_2O and Mn_2O_3/Mn_3O_4 redox pairs. The difference between the fuel reactor and the air reactor temperatures can difficult CLC energy integration, however the low differences on the operating windows for each reaction of the considered oxygen carriers can be easily managed. Despite the CLOU capacity of Co_3O_4/CoO, the energy balance of this redox reaction difficulties the integration of reduction and oxidation reactors

(Leion et al. 2009a) since the reduction reactions are endothermic. In addition, Co-based materials are toxic.

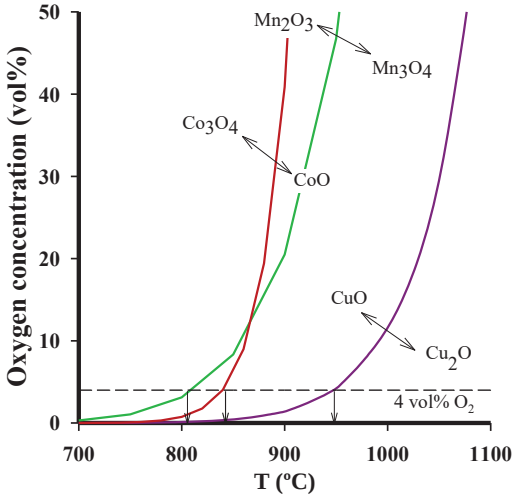

Figure 36. O_2 equilibrium concentration of CuO/Cu_2O, Mn_2O_3/Mn_3O_4 and Co_3O_4/CoO redox pairs.

Source: Abad et al. (2012).

Table 6. Operating window for the CuO/Cu_2O and Mn_2O_3/Mn_3O_4 redox pairs.

	Fuel reactor temperature (ºC)	**Air reactor temperature (ºC)**
CuO/Cu_2O	900-950	900-950
Mn_2O_3/Mn_3O_4	850-900	800-825

Among them, Cu-based materials have been the focus of research as their oxygen release is greater and faster than that of Mn-based oxides, and their temperature window for oxygen release is higher than in the case of Mn oxides. Adánez-Rubio et al. (2014) demonstrated the feasibility of CLOU with biomass using a Cu-based oxygen carrier in a 1.5 kW_{th} continuous unit. In this work, almost 100% CO_2 capture and combustion efficiencies were achieved at 935 °C.

In order to improve the thermodynamic restrictions associated with manganese, mixed oxides (Mn-Si, Mn-Mg, Mn-Fe, Mn-Cu) have been proposed

(Azimi et al. 2013; Jing et al. 2014). Adding another metal to manganese oxide enables oxidation of the material to be used at higher temperatures (Shulman et al. 2009, 2011; Pour et al. 2013; Adánez-Rubio et al. 2016; Hosseini et al. 2015; Rydén et al. 2014; Sajen et al. 2016). Hanning et al. (2016) studied the combustion of wood char in a batch fluidized with Mn-Si and Mn-Si-Ti oxygen carriers. They found the *i*G-CLC reaction to be more important than CLOU with these oxygen carriers. On the contrary, a natural mixed oxide based on Cu-Mn (Hopcalite) has shown high oxygen uncoupling capability (Adánez-Rubio et al. 2016). Also, a synthetic Cu-Mn mixed oxide material was tested by Adánez-Rubio et al. (2017a, 2018) in a 1.5 kW_{th} continuous unit using coal as fuel. With this oxygen carrier, combustion efficiencies close to 100% were reached, which qualified this oxygen carrier as a potential material for testing in experiments with biomass. Schmitz and Linderholm (2016) tested in a 10 kW_{th} unit a perovskite ($CaMn_{0.9}Mg_{0.1}O_{3-\delta}$) during about 37 h using as fuel a bio char with a very low sulfur content. They achieved high combustion efficiencies and CO_2 capture efficiencies of up to 98%. These results confirmed, for the first time, the utilization of non-copper oxygen carriers for CLOU combustion using a biomass based fuel.

1.5.3 Next challenges on biomass fueled CLC

Next challenges on biomass fueled CLC involves both operational and design solutions to improve the performance of this technology, reducing the unburnt matter at the outlet of the fuel reactor and the char reaching the air reactor. Some of the operational and design improvements proposed for solid fuel CLC are briefly discussed below.

Operational improvements:

- Temperature. An increase in the fuel reactor temperature favors the gasification rate of the char and the combustion kinetics of the gases generated during the gasification.

- Oxygen availability. For each oxygen carrier, the oxygen availability in the fuel reactor depends on the solids circulation rate. Increasing the solids circulation rate, the oxygen availability is increased. However, the increase of the solids circulation rate can reduce the residence time of solids in the reactor and counteract the desired effect.
- Oxygen carrier. The use of an oxygen carrier appropriate for their oxygen transport capacity, molecular oxygen releasing capacity, reactivity or even the selectivity should be considered to improve the CLC process (Lyngfelt and Leckner 2015; Gayán et al. 2013).

Design improvements:

- Carbon stripper. Implementation of a solid particles separator (carbon stripper) to recirculate char particles in the fuel reactor and in this way avoid the char combustion in the air reactor (Gayán et al. 2013).
- Distributors. Introduction of internals (Figure 37-1a) or distributor plates (Figure 37-1b) can improve the homogeneity of the fluidized bed increasing the contact among reactants. Also different fuel reactor designs were suggested to increase the contact of the oxygen carrier and the biomass products (Gayán et al. 2013).
- Secondary fuel reactor (Figure 37-2). Implementation of a secondary fuel reactor was pointed as a potential solution for typically high volatile matter content of the fuel reactor outlet (Gayán et al. 2013). Some technological alternatives have been already tested and results published in literature (Yan et al., 2017; Haus et al. 2018; Jiang et al. 2018).
- Recycling of the fuel reactor outlet steam. The recycling of the fuel reactor outlet stream to the fuel reactor (Figure 37-3) or even to the carbon stripper increases the contact time between biomass gasification products and the oxygen carrier particles. This would reduce the unburnt compounds and therefore would increase the combustion efficiency (Lyngfelt and Leckner 2015; Gayán et al. 2013).
- Unburnt compounds separation during the CO_2 purification and compression steps can be recycled to the fuel reactor (Figure 37-4).

- Change of the fuel feeding to the carbon stripper (Figure 37-5), which will act as a first fuel reactor, or to the entrance of the fuel reactor (Figure 37-6). Both options would increase the contact time between biomass gasification products and the oxygen carrier.

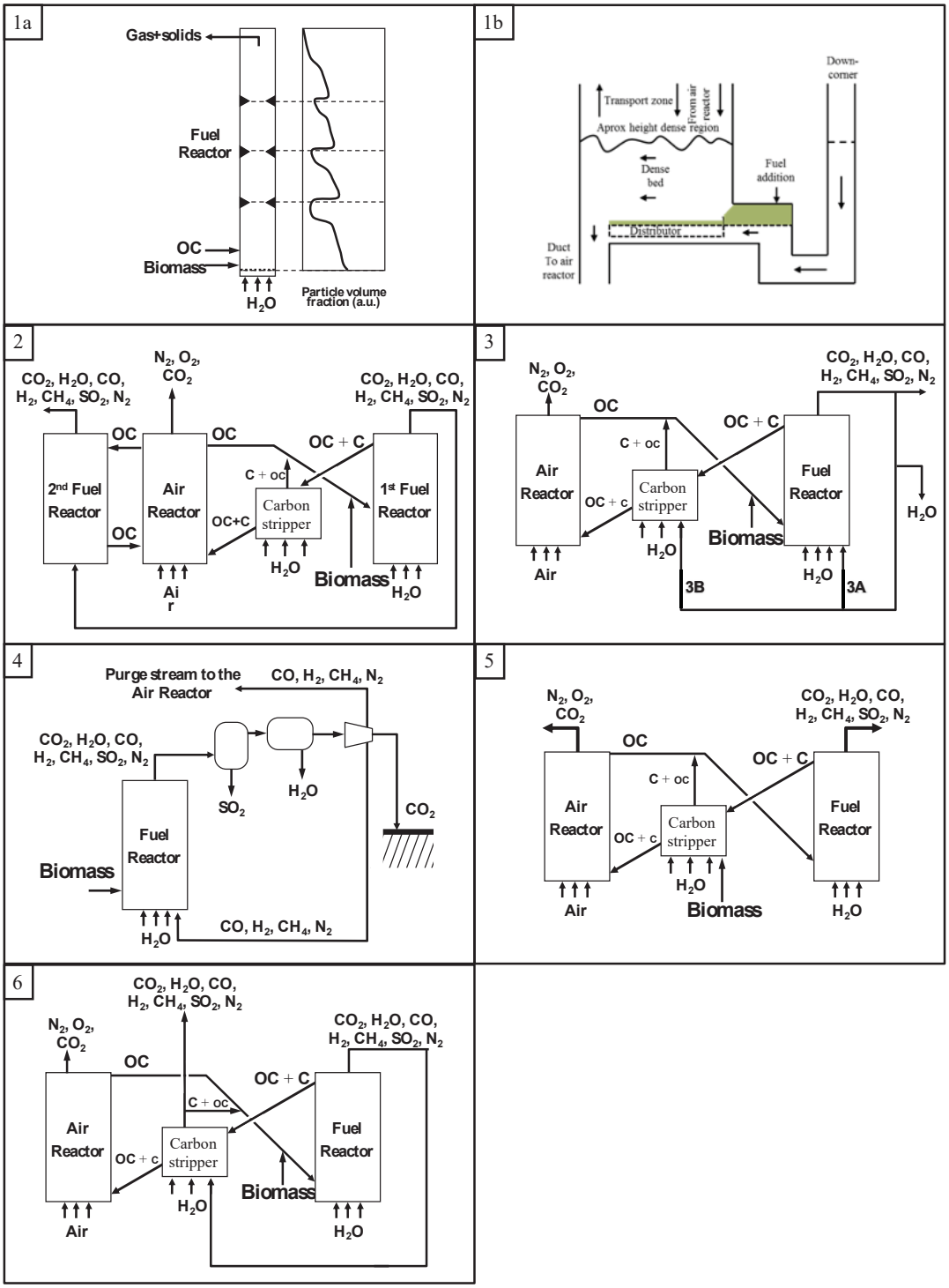

Figure 37. Main technical CLC proposed improvements.

Source: Adánez et al. (2018).

1.6 Scope of study

Biomass is considered a carbon neutral fuel since the CO_2 released in biomass combustion has previously been removed from the atmosphere during its growth. For this reason, biomass is being used for partial replacement of fossil fuels in many thermo-chemical processes. Moreover, if the CO_2 generated during biomass combustion is captured, this would lead to negative CO_2 emissions. A power plant that integrates both biomass and Carbon Capture and Storage (CCS) technologies will receive carbon credits, potentially making this process economically attractive.

The main objective of this Thesis was to evaluate the integration of solid biofuels in the Chemical Looping Combustion technology (bioCLC). The whole combustion process can then be considered as Bioenergy with CCS (BECCS) technology allowing to achieve negative CO_2 emissions while energy is produced. The Thesis was carried out at the *Instituto de Carboquímica* in Zaragoza (Spain), including a four-month stay at the Institute of Solids Process Engineering and Particle Technology in the *Technische Universität Hamburg* (TUHH) in Hamburg (Germany).

The specific objectives defined for this Thesis were:

1. To identify suitable oxygen carriers for the biomass-fueled CLC process and to validate their performance under relevant operating conditions.
2. To investigate the influence of operating conditions on the overall process performance for different types of biomass.
3. To demonstrate the technology performance at scale of 20 kW_{th}.
4. To assess the effect of biomass ash constituents on the oxygen carrier behavior (deactivation and agglomeration).
5. To evaluate the presence of different pollutants (tar and NO_x) generated during combustion in the CLC system

The investigation performed during the Thesis covered from basic research at particle level to continuous operation in 1 kW_{th} and 20 kW_{th} units to demonstrate the

process concepts. Focus was made on the analysis of the effect of the operating conditions on the performance of the bioCLC process as well as on the determination of a window of suitable operating conditions for different oxygen carriers.

Results obtained throughout this Thesis were presented in six papers. **Paper I and II** summarize the results reached with low-cost oxygen carriers based on iron and manganese oxides named as Tierga ore, MnGBHNE and MnSA. All were tested in the 1 kW_{th} CLC unit working under the so-called *i*G-CLC mode. The influence of operating conditions such as gasifying agent, temperature in the fuel reactor, solids inventory in the fuel reactor and solids circulation rate between reactors was assessed. Moreover, the influence of the type of biomass used as biofuel was included. Pine sawdust, olive stones and almond shells were chosen based on their wide use for energy purposes as well as large availability. **Paper III** shows the evaluation as oxygen carrier for the bioCLC process of a synthetic mixed manganese and iron-based oxygen carrier (Mn66FeTi7). This oxygen carrier shows the ability to release molecular oxygen under specific conditions, what could improve the combustion efficiency of the bioCLC process. The influence of the operating conditions on the oxygen release capability of the material and therefore on the performance of the bioCLC process was studied in the 1 kW_{th} CLC unit using pine sawdust as fuel. **Paper IV and V** continue the analysis of different types of oxygen carriers for the bioCLC process and evaluate the performance of a synthetic Cu-based CLOU oxygen carrier (Cu34Mn66) characterized by its higher and faster oxygen release capability. The effect of different operating conditions on the performance of the process was studied and the operating window for the biomass combustion was determined in the 1 kW_{th}. Another aspect to be considered in the combustion of biomass is the NO_x formation and the possible existence of tar in the gaseous product stream. **Paper VI** presents a comparison between the *i*G-CLC and CLOU operating modes regarding the NO_x and tar formation when different types of biomass are considered. Finally, results concerning the demonstration of the bioCLC process at higher scale in 20 kW_{th} CLC unit are shown (**Conference paper J**) (García-Labiano et al. 2018) using olive stones as biofuel and the Tierga ore as oxygen carrier.

1.7 List of papers

I. Mendiara, T., A. Pérez-Astray, M. T. Izquierdo, A. Abad, L. F. de Diego, F. García-Labiano, P. Gayán, J. Adánez. Chemical Looping Combustion of different types of biomass in a 0.5 kW_{th} unit. *Fuel* 2018, 211, 868-875.

II. Pérez-Astray A, T. Mendiara, L. F. de Diego, A. Abad, F. García-Labiano, M. T. Izquierdo, J. Adánez (2019) Manganese ores as low-cost oxygen carriers for biomass chemical looping combustion in a 0.5 kW_{th} unit. *Submitted to Fuel Processing Technology.*

III. Pérez-Astray A, T. Mendiara, L. F. de Diego, A. Abad, F. García-Labiano, M. T. Izquierdo, J. Adánez. (2019a) CLC of biomass as a BECCS technology using a manganese-iron mixed oxide. *Submitted to Separation and Purification Technology.*

IV. Adánez-Rubio, I., A. Pérez-Astray, T. Mendiara, M. T. Izquierdo, A. Abad, P. Gayán, L. F. de Diego, F. García-Labiano, J. Adánez. Chemical Looping Combustion of biomass: CLOU experiments with a Cu-Mn mixed oxide. *Fuel Processing Technology* 2018, 172, 179-186.

V. Adánez-Rubio, I., A. Pérez-Astray, A. Abad, P. Gayán, L. F. de Diego, J. Adánez. Chemical Looping with oxygen uncoupling: an advanced biomass combustion technology to avoid CO_2 emissions. *Mitigation and Adaptation Strategies for Climate Change* 2019. (In press). doi: 10.1007/s11027-019-9840-5.

VI. Pérez-Astray, A., I. Adánez-Rubio, T. Mendiara, M. T. Izquierdo, A. Abad, P. Gayán, L. F. de Diego, F. García-Labiano, J. Adánez. Comparative study of fuel-N and tar evolution in chemical looping combustion of biomass under both *i*G-CLC and CLOU modes. *Fuel* 2019, 236, 598-607.

Conference papers:

A. Mendiara, T., P. Gayán, F. García-Labiano, L. F. de Diego, A. Pérez-Astray, M. T. Izquierdo, A. Abad, J. Adánez.

Chemical looping combustion of biomass: an approach to BECCS.

13th Conference on Greenhouse Gas Control Technologies (GHGT), 14-18 November 2016, Lausanne, Suisse.

B. Mendiara, T., M. T. Izquierdo, A. Pérez-Astray, A. Abad, L. F. de Diego, F. García-Labiano, P. Gayán, J. Adánez.

Biomass with CO_2 capture using CLC: results in a 500 W_{th} unit.

4th International Conference on Chemical Looping, 26-28 September 2016, Nanjing, China.

C. Mendiara, T., P. Gayán, F. García-Labiano, L. F. de Diego, A. Pérez-Astray, M. T. Izquierdo, A. Abad, J. Adánez.

Combustión de biomasa con captura de CO_2.

7ª Jornada de Jóvenes Investigadores (Física y Química) de Aragón, 24 November 2016, Zaragoza, Spain.

D. Mendiara, T., I. Adánez-Rubio, A. Pérez-Astray, M. T. Izquierdo, A. Abad, P. Gayán, L. F. de Diego, F. García-Labiano, J. Adánez.

Chemical Looping Combustion of biomass: CLOU experiments with a Cu-Mn mixed oxide.

10th conference on Sustainable Energy and Environmental Protection (SEEP) 2017, 27-30 June 2017, Bled, Slovenia.

E. Pérez-Astray, A., T. Mendiara, M. T. Izquierdo, L. F. de Diego, F. García-Labiano.

Combustión de diferentes tipos de biomasa mediante transportadores de oxígeno.

XIV Reunión del Grupo Español del Carbón. 22-25 October 2017, Malaga, Spain.

F. Pérez-Astray, A., T. Mendiara, M.T. Izquierdo, A. Abad, L. F. de Diego, F. García-Labiano, P. Gayán, J. Adánez.

In Situ Gasification Chemical Looping Combustion of different biomass types.

10th World congress of Chemical Engineering. 1-5 October 2017, Barcelona. Spain.

G. Abad, A., R. Pérez-Vega, A. Pérez-Astray, T. Mendiara, L. F. de Diego, F. García-Labiano, P. Gayán, M. T. Izquierdo, J. Adánez.

Biomass Combustion with CO_2 Capture by Chemical Looping: Experimental results in a 50 kW_{th} Pilot plant.

I International Conference on CO_2 Negative Emissions. 22-24 May 2018, Goteborg, Sweeden.

H. Adánez-Rubio, I., A. Pérez-Astray, A. Abad, P. Gayán, L. F. de Diego, J. Adánez.

Biomass combustion by Chemical Looping with Oxygen Uncoupling process: experiments with Cu-based and Cu-Mn mixed oxide as oxygen carriers.

I International Conference on CO_2 Negative Emissions. 22-24 May 2018, Goteborg, Sweeden.

I. Adánez-Rubio, I., R. Pérez-Vega, A. Pérez-Astray, T. Mendiara, J. Adánez.

Coal and biomass combustion by Chemical Looping with Oxygen Uncoupling (CLOU) with a Cu and Cu-Mn materials.

5th International Conference on Chemical Looping. 24-27 September 2018, Park City, Utah, USA.

J. García-Labiano, F., R. Pérez-Vega, A. Pérez-Astray, T. Mendiara, L. F. de Diego, M. T. Izquierdo.

Chemical Looping Combustion of Biomass in a 50 kW_{th} unit.

5th International Conference on Chemical Looping. 24-27 September 2018, Park City, Utah, USA.

K. Abad, A., R. Pérez-Vega, A. Pérez-Astray, T. Mendiara, L. F. de Diego, F. García-Labiano, P. Gayán, M. T. Izquierdo, J. Adánez.

Biomass combustion with CO_2 capture by CLC: Experimental results in a 50 kW_{th} unit.

XXXVI Jornadas Nacionales de Ingeniería Química, September 2019, Zaragoza, Spain.

EXPERIMENTAL

2.1 Oxygen carriers

Different promising oxygen carriers, both ores and synthetic, were selected for operation in the CLC prototypes. The selection was based on the previous experience reached in CLC by the Combustion and Gasification Group at the *Instituto de Carboquímica* (ICB-CSIC) working with gaseous fuels and especially with coal. All the selected oxygen carriers were physically and chemically characterized and their main properties are shown in Table 7.

Reactivity analyses of the oxygen carriers were performed in a thermogravimetric analyzer (TGA) in sequential redox cycles using different gaseous fuels (H_2, CO or CH_4) for the reduction reaction and air for the oxidation reaction. The TGA was also used to determine the oxygen transport capacity of the oxygen carriers. The identification of crystalline chemical species in each material was carried out by powder X-ray diffraction (XRD) patterns acquired in a Bruker D8 Advance diffractometer equipped with a linear detector. The force needed to fracture a particle of oxygen carrier was measured in a Shimpo FGE-5X dynamometer. Then,

the crushing strength was calculated as the average value of twenty measurements of individual particles randomly chosen. A three-hole air jet attrition tester ATTRI-AS (Ma. Tec. Materials Technologies Snc.) configured according to the ASTM-D-5757 standard was used to determine the Air Jet Index (AJI) of the different samples (Cabello et al. 2016). The oxygen carrier density was determined using a Micrometrics AccuPyc II helium pycnometer. The BET surface area was measured in a Micromeritics Autopore V, whereas a Quantchrome PoreMaster 33 mercury pycnometer was used to measure the porosity of the oxygen carrier particles. Finally, a Hitachi S 3400 N scanning electronic microscopy (SEM) was used to evaluate changes in the microstructure of the oxygen carrier particles.

Table 7.Main physical and chemical properties of the selected oxygen carriers.

	Tierga[a]	**MnGBHNE**[b]	**MnSA**[b]	**Mn66FeTi7**	**Cu34Mn66**
XRD main phases	Fe_2O_3, SiO_2, Al_2O_3, CaO, MgO	Mn_2O_3, Fe_2O_3, SiO_2	Mn_2O_3, Mn_3O_4, Fe_2O_3	$(Mn_xFe_{1-x})_2O_3$, $(Mn_xFe_{1-x})_3O_4$, TiO_2	$Cu_{1.5}Mn_{1.5}O_4$, Mn_3O_4
Redox composition, (wt%)	76.5 (Fe_2O_3)	Mn_3O_4 (67.5) Fe_2O_3 (10.8)	Mn_3O_4 (65.6) Fe_2O_3 (18.6)	$(Mn_xFe_{1-x})_2O_3$ (81.0) $(Mn_xFe_{1-x})_3O_4$ (13.4)	$Cu_{1.5}Mn_{1.5}O_4$ (72.0)
Crushing strength,(N)	5.8	1.8	4.6	2.0	1.9
Oxygen transport capacity, R_{OC} (wt%)	2.5	5.1	4.7	9.4	4.0
Porosity, (%)	26.3	38.7	12.3	9.5	12.1
Skeletal density of particles, (kg/m^3)	4216	2800	3510	2290	4100
Specific surface area, BET (m^2/g)	1.4	12.3	0.6	< 0.5	< 0.5

[a] Calcined at 950 ºC during 12 h. [b] Calcined at 800 ºC during 2 h.

2.1.1 Iron ore

An iron ore obtained from a hematite mine in Tierga (Zaragoza, Spain) was selected to be used as oxygen carrier. This oxygen carrier, named Tierga ore, showed the highest reactivity in the combustion of coal as well as stability and durability, in a comparative study among different Fe-based oxygen carriers, highlighting its low cost (Mendiara et al. 2014a). The ore was crushed and sieved to a particle size of 100-300 μm and subsequently calcined in air atmosphere at 950 ºC during 12 hours to increase its mechanical strength. The ferrite-magnetite (Fe_2O_3-Fe_3O_4) redox pair was considered for the reaction of this material. Reactions (R7) to (R10) show the main iron oxide redox reactions.

$$3Fe_2O_3 + H_2 \Leftrightarrow 2Fe_3O_4 + H_2O \quad \text{(R7)}$$

$$3Fe_2O_3 + CO \Leftrightarrow 2Fe_3O_4 + CO_2 \quad \text{(R8)}$$

$$12Fe_2O_3 + CH_4 \Leftrightarrow 8Fe_3O_4 + CO_2 + 2H_2O \quad \text{(R9)}$$

$$4\,Fe_3O_4 + 0.5\,O_2 \Leftrightarrow 3Fe_2O_3 \quad \text{(R10)}$$

2.1.2 Manganese ores

Tests performed in a batch fluidized bed reactor with different manganese ores showed good fluid dynamics properties as well as an estimated long lifetime (Mei et al. 2015; Mei et al. 2016). Also, a previous study carried out at the *Instituto de Carboquímica* using a manganese based oxygen carrier with coal as fuel showed comparable results to those obtained with a highly reactive iron-based oxygen carrier (Tierga ore) working in a CLC continuous unit under similar operating conditions (Abad et al. 2018). Based on these previous studies, two manganese-based ores have been used in the present work as oxygen carriers. One came from Gabon (hereafter named MnGBHNE) and another one from South Africa (hereafter named MnSA), both supplied by *Hidro Nitro Española S.A.* After received, both materials were crushed and sieved to 100–300 μm. Then, a thermal treatment was carried out in air at 800 °C during 2 h to ensure the complete oxidation of the particles and also to increase the crushing strength of the oxygen carriers. For more information about the oxygen carriers see Mei et al. (2015). The redox pairs considered for the reaction of

these materials, both MnGBHNE and MnSA, were Mn_3O_4-MnO and Fe_2O_3-Fe_3O_4, reactions (R11) to (R14) and (R7) to (R10), respectively.

$$Mn_3O_4 + H_2 \Leftrightarrow 3\,MnO + H_2O \quad \text{(R11)}$$

$$Mn_3O_4 + CO \Leftrightarrow 3\,MnO + CO_2 \quad \text{(R12)}$$

$$4\,Mn_3O_4 + CH_4 \Leftrightarrow 3\,MnO + CO_2 + 2\,H_2O \quad \text{(R13)}$$

$$3\,MnO + 0.5\,O_2 \Leftrightarrow Mn_3O_4 \quad \text{(R14)}$$

2.1.3 Mn66FeTi7

Manganese and iron mixed oxides have received attention because of their relatively low cost and high reactivity. Previous results working with these materials showed high reactivity with H_2, CO and CH_4 thanks to their capacity to release a small amount of molecular oxygen during the reduction phase under specific operating conditions (Pérez-Vega et al. 2020). This ability has been named Chemical Looping assisted by Oxygen Uncoupling (CLaOU). Reactions (R15) to (R18) describe the reduction reactions of the iron-manganese mixed oxides in CLC. The bixbyite phase, $(Mn_xFe_{1-x})_2O_3$, decomposes into a spinel phase, $(Mn_xFe_{1-x})_3O_4$, and molecular oxygen (R15) at specific operating conditions. Furthermore, the spinel phase oxidizes the biomass gasification products with lattice oxygen, (R16) to (R18). The oxygen release capacity of these oxygen carriers is affected by the kinetics and the thermodynamics (Pérez-Vega et al. 2019).

$$3(Mn_xFe_{1-x})_2O_3 \leftrightarrow 2(Mn_xFe_{1-x})_3O_4 + 0.5O_2 \quad \text{(R15)}$$

$$(Mn_xFe_{1-x})_3O_4 + H_2 \rightarrow 3(Mn_xFe_{1-x})O + H_2O \quad \text{(R16)}$$

$$(Mn_xFe_{1-x})_3O_4 + CO \rightarrow 3(Mn_xFe_{1-x})O + CO_2 \quad \text{(R17)}$$

$$4(Mn_xFe_{1-x})_3O_4 + CH_4 \rightarrow 12(Mn_xFe_{1-x})O + CO_2 + 2H_2O \quad \text{(R18)}$$

For this Thesis, a synthetic oxygen carrier, named Mn66FeTi7, based on manganese and iron oxides doped with TiO_2 was selected. The oxygen carrier was prepared at the ICB-CSIC in Zaragoza (Spain) using 60 wt% of Mn_3O_4 (Elkem),

33 wt% of Fe_2O_3 (Chemlab) and 7 wt% of TiO_2 (Panreac), achieving a stoichiometric formula of the particles of $(Mn_{0.66}Fe_{0.34})_2O_3(TiO_2)_{0.15}$. The powder mixture was converted into a solution with suitable viscosity by heating at 80 ºC. The particles were manufactured by spray granulation in a Glatt spouted bed system, model Procell5. After that, particles were thermally processed during 2 h at 1050 ºC and then, sieved to the particle size distribution 100-300 μm. For more information about the oxygen carrier preparation see Pérez-Vega et al. (2020).

2.1.4 Cu34Mn66

In this Thesis, a Cu-Mn mixed oxide was selected as oxygen carrier for the CLOU process. The oxygen carrier was prepared at the ICB-CSIC using 34 wt% of CuO (Chemlab) and 66 wt% of Mn_3O_4 (Micromax®, Elkem). The powder mixture was converted into a solution with an adequate viscosity for the spray granulator and the particles were manufactured by spray granulation in a Glatt spouted bed system, model Procell5. Finally, the particles were calcined for 2 h at 1125 ºC and then sieved to a particle size of 100-300 μm. The active phase in the mixed oxide was $Cu_{1.5}Mn_{1.5}O_4$. The excess of Mn_3O_4 in the particles acted as an inert (Adánez-Rubio et al. 2017b). Reaction (R19) describes the release of gaseous oxygen by the oxygen carrier.

$$2Cu_{1.5}Mn_{1.5}O_4 \Leftrightarrow 3CuMnO_2 + O_2 \qquad \text{(R19)}$$

Figure 38 shows the O_2 equilibrium concentrations as a function of the temperature for the redox systems CuO/Cu_2O and Mn_2O_3/Mn_3O_4 together the O_2 concentrations measured in tests carried out in a batch fluidized bed reactor with the prepared oxygen carrier.

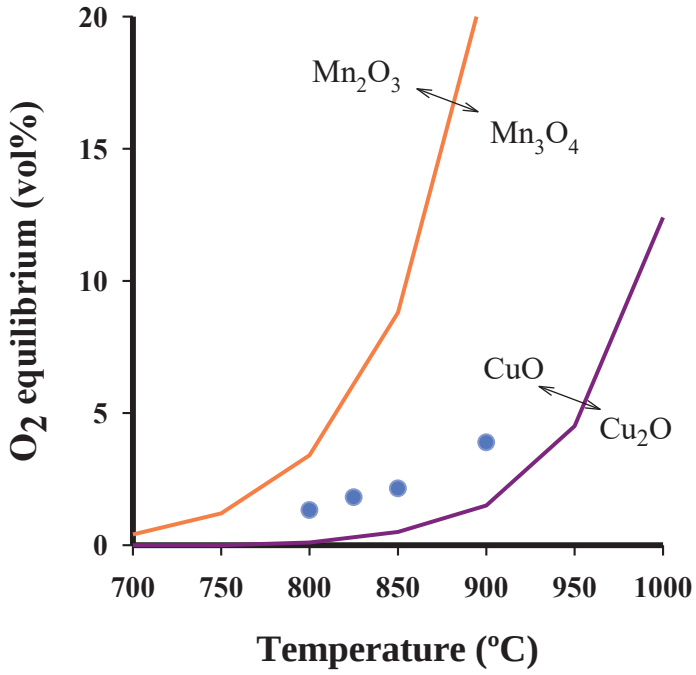

Figure 38. O_2 concentrations at equilibrium as a function of the temperature for the systems: CuO/Cu_2O, Mn_2O_3/Mn_3O_4 and experimental points for (●) $Cu_{1.5}Mn_{1.5}O_4$/$CuMnO_2$.

2.2 Solid biofuels

Three Spanish biomass wastes were used as fuels for the CLC experiments: Pine sawdust (*Pinus sylvestris*), olive stones (*Olea europaea*) and almond shells (*Prunus dulcis*). Pine sawdust was chosen as the reference material because of its large use and wide distribution. Olive stones and almond shells are two agricultural residues used for energy production with high annual production in Spain.

Raw materials were ground and sieved to adequate their size particle distribution between 0.5 - 2 mm. Table 8 shows the proximate and ultimate analyses of the three types of biomass including the low heating value and the value of the oxygen demand of the solid fuel (Ω_{sf}), which represents the amount of oxygen needed to burn the biomass.

Biomass ashes were prepared by controlled combustion in a muffle at 900 ºC. An inductively coupled plasma optical emission spectrometry equipment and a fusibility equipment were used for the ash characterization. Table 9 presents the content on sodium (Na), potassium (K) and calcium (Ca), the three major alkali and alkaline earth metal (AAEM) components, of the three types of biomass. It is worth noting the high potassium content of the almond shells, as well as the high calcium content of the pine sawdust and olive stones. Melting temperatures for biomass ashes in reducing atmosphere were about 1000 ºC for the pine sawdust and about 780 ºC for the olive stones and the almond shells.

Table 8. Proximate and ultimate analyses of the various biomass types used.

	Pine sawdust	**Olive stones**	**Almond shells**
Proximate analysis (wt%)			
Moisture	4.2	9.4	2.3
Ash	0.4	0.8	1.1
Volatile matter	81.0	72.5	76.6
Fixed carbon	14.4	17.3	20.0
Ultimate analysis (wt%)			
C	51.3	46.5	50.2
H	6.0	4.8	5.7
N	0.3	0.2	0.2
S	0.0	0.0	0.0
O	37.8	38.3	40.5
LHV (kJ/kg)	19158	16807	18071
Ω_{sf} (kg oxygen/kg fuel)	1.5	1.2	1.4

Table 9. Na, K y Ca content of the different types of biomass used (mg/kg$_{dry\ fuel}$).

	Pine sawdust	**Olive stones**	**Almond shells**
Na	4	17	12
K	152	1053	2157
Ca	1194	1334	749

2.3 Experimental installations

2.3.1 Thermogravimetric analyzer

The reactivity of the different oxygen carriers, before and after their utilization in the CLC pilot plants, was determined in a TGA CI Electronics. For that, the sample weight variation versus time during reaction with gases under well-defined conditions and during successive redox cycles was measured. About 50 mg of oxygen carrier sample were loaded in a platinum wire mesh basket. The basket design reduced the mass transfer resistance and improved the contact of the oxygen carrier sample with the gaseous reactants. The sample was heated to the operating temperature in air atmosphere with an electric furnace. After stabilization, the sample was successively exposed to reducing and oxidizing reactive atmospheres. For reduction, 25 L/h (STP) of CH_4, CO_2 were used. For oxidation, 25 L/h (STP) of air were used. In order to avoid the mixing of combustible gas and air, nitrogen was introduced for 2 min between the oxidizing and the reducing periods. Figure 39 shows the TGA scheme and a picture of the experimental set-up. For more information about the TGA characteristics and utilization procedure see Adánez et al. (2004).

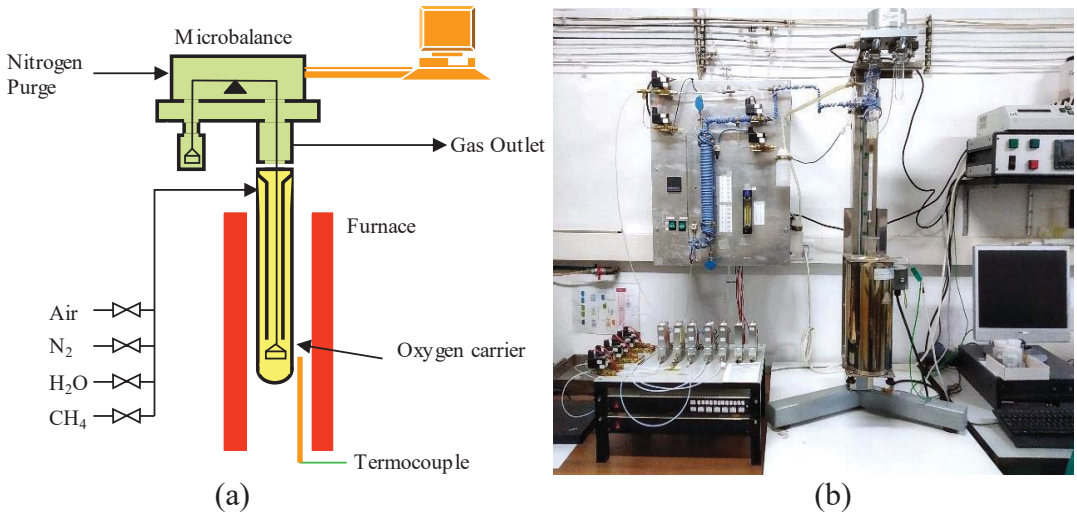

Figure 39. (a) Scheme of the TGA CI Electronics and (b) picture of the experimental set-up.

Data evaluation

Reactivity data were obtained from the oxygen carrier weight evolution measurements in TGA during successive redox cycles as a function of the time. The oxygen carrier conversions during the reduction and oxidation reactions were calculated by Equation (1) and Equation (2), respectively, where *m* is the mass of the sample at any time, m_{Ox} is the mass of the fully oxidized oxygen carrier sample and m_{Red} is the mass of the reduced oxygen carrier sample.

$$X_{Red} = \frac{m_{Ox} - m}{m_{Ox} - m_{Red}} \quad (1)$$

$$X_{Ox} = 1 - \frac{m_{Ox} - m}{m_{Ox} - m_{Red}} \quad (2)$$

The oxygen transport capacity, R_{OC}, which evaluates the total amount of oxygen that the material can exchange in each redox cycle, was obtained by Equation (3).

$$R_{OC} = \frac{m_{Ox} - m_{Red}}{m_{Ox}} \quad (3)$$

2.3.2 Batch fluidized bed reactor

A batch fluidized bed reactor was used for the analysis of agglomeration as well as changes in reactivity of the oxygen carrier samples under successive redox cycles due to the isolated effect of the presence of alkali and alkaline earth metals (AAEM) in the biomass. This experimental work was carried out in the Institute of Solids Process Engineering and Particle Technology at Hamburg (Germany). The experimental set-up consisted of a fluidized bed reactor, a gas feeding system, a solids feeding system, a calibrating system, a sampler and gas analyzers. Figure 40 shows the scheme of the batch fluidized bed reactor and the solids feeding system and the online sampling design. The oxygen carrier sample, used as bed material, was introduced in a 53 mm internal diameter fluidized bed reactor. An electric furnace heated the sample to the operating temperature while air was introduced

through a distributor plate at the bottom part of the reactor. Different mass flow controllers allowed the use of different fluidizing agents. Four thermocouples and five pressure taps allowed the measurement of the temperatures and pressures at the different parts of the reactor. A valve system allowed the AAEM salt introduction into the fluidized bed as well as the online bed sampling. A ceramic filter placed inside the bed material allowed the gas measuring preventing the fine particle. A nondispersive infrared analyzer (NDIR) was used for the CO, CH_4 and CO_2 measurements while a thermal conductivity analyzer was used for the H_2 measurement using a four-channel measurement system TAD GmbH type GME.84-K4. A paramagnetic cell (ABB Magnos 3K) was used for the O_2 measurement.

Experimental procedure

About 250 g of oxygen carrier sample were loaded as bed material in the batch fluidized bed reactor and heated to the desired temperature. An air flow was used for fluidization during the heating up of the bed material. After reaching the operating temperature of 950 ºC, as no biomass was added, the oxygen carrier was partly reduced with 15 vol% of H_2 (N_2 balance) during a specific time to reach the desired oxygen carrier reduction degree (50 and 75%). The reduction degrees were chosen to adapt oxygen carrier characteristics to the normal operation behaviour of a CLC plant. After the reduction of the oxygen carrier, pure nitrogen was fed for fluidization and salt batches of approximately 0.1–0.2 g each, with a separation among them of 5 minutes, were added to bed. The fluidization conditions were maintained at 0.1 m/s, analysing the fluidization properties by using differential pressure measurements. For each salt tested (NaCl, KCl or $CaCl_2$) and for each oxygen carrier, a total of 30 batches of salt were added. Finally, the bed was oxidized in air to start a cycle. In each experiment, oxygen carrier samples, both reduced and oxidized, were extracted after salt additions for characterization.

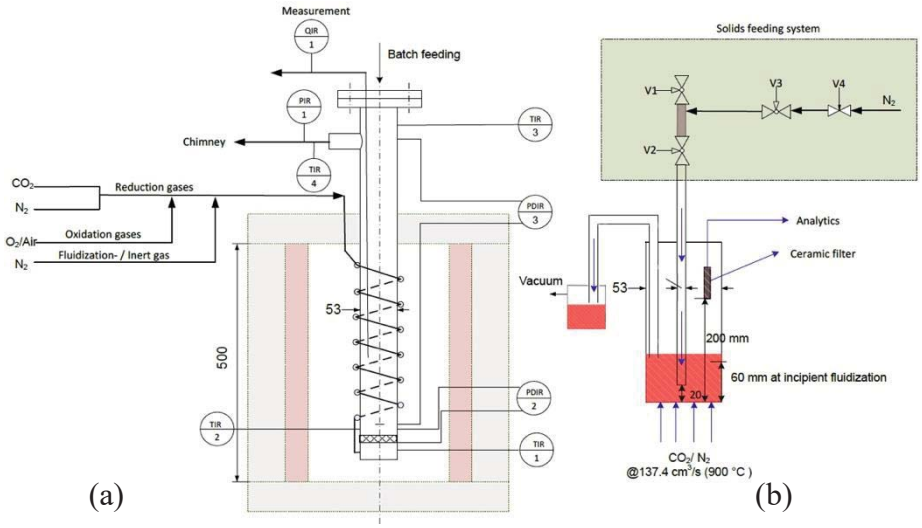

Figure 40. Scheme of (a) the batch fluidized bed reactor and (b) the solids feeding system and the online sampling design.

2.3.3 Continuous pilot plants

2.3.3.1 1 kW_{th} prototype (ICB-CSIC-s1)

A scheme of the ICB-CSIC-s1 experimental unit is shown in Figure 41. It consists of the fuel (1) and the air (3) reactors, both bubbling fluidized bed type. The biomass is fed into the fuel reactor (50 mm ID) at the bottom of the bubbling fluidized bed through a series of two screw feeders (9). It is fed just above the fuel reactor distributor plate in order to maximize the time that the fuel and volatile matter are in contact with the bed material. CO_2 or steam can be used as gasifying agents. Steam is produced by heating up in an evaporator the corresponding water flow supplied by a peristaltic pump. The fuel reactor is connected to the air reactor by a U-shaped bubbling fluidized bed reactor (30 mm ID) placed as loop seal (2) to prevent the mixture of the gases between them. There is no carbon stripper between the fuel and the air reactors. The loop seal is fluidized with nitrogen and, during operation, the percentage of the loop seal fluidizing agent reaching the fuel reactor can be calculated. The reduced oxygen carrier is transferred to the air reactor (80 mm ID). Once re-oxidized, the oxygen carrier leaves the air reactor through a riser (4) helped by a secondary air flow. The oxygen carrier is then collected by a cyclone (5) and

sent to a deposit (7) that keeps both reactor atmospheres separated. A diverting solid valve (6) is used to measure the solids circulation rate between reactors during the experiment. The flow of oxygen carrier fed to the fuel reactor from this deposit is controlled by a solids valve (8). The temperature in both reactors is controlled with electrical furnaces (11). Figure 42 shows a picture of the 1 kW_{th} ICB-CSIC-s1 CLC unit.

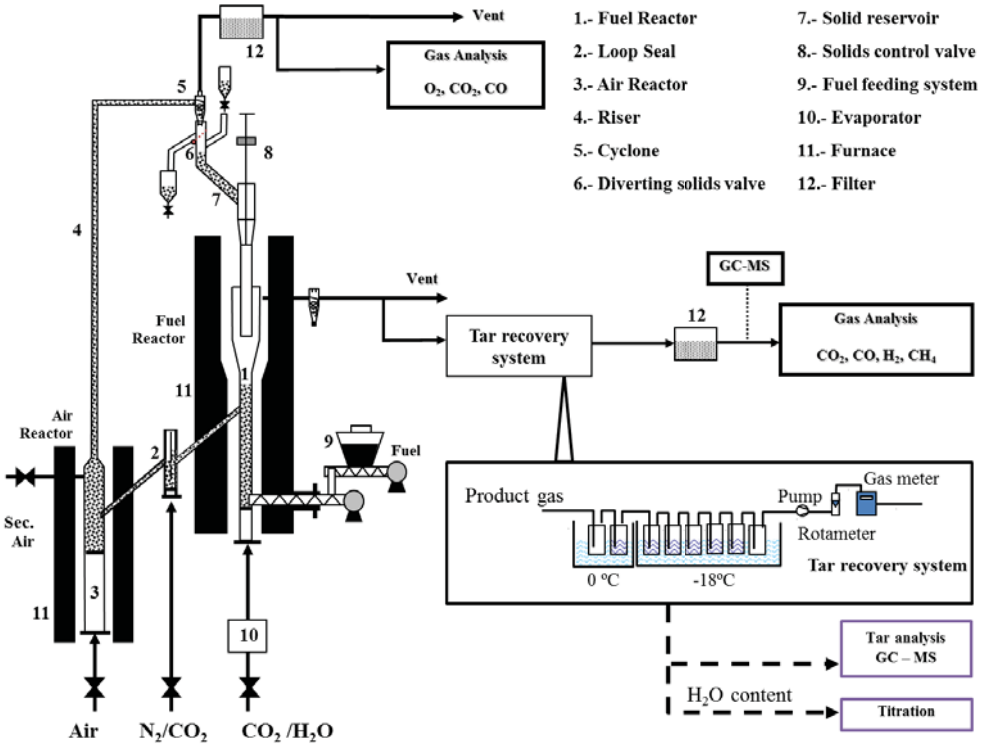

Figure 41. Scheme of the 1 kW (ICB-CSIC-s1) experimental set-up.

Different electronic mass flow controllers allow the use of various fluidizing gases. The fluidization velocities in each reactor were kept constant, about 0.1 m/s for the fuel reactor and 0.5 m/s, for the air reactor during all the experiments. The reactor temperatures, independently controlled thanks to the electric furnaces, and the pressure drops in the reactors were recorded during all the experiments. The gas outlet composition of both reactors was measured and recorded. A non-dispersive infrared analyzer (Siemens Ultramat 23) was used for the CO_2, CO and CH_4 online analysis and a thermal conductivity detector (Siemens Calomat 6) for the H_2. The O_2 concentration was measured with a paramagnetic analyzer (Siemens Ultramat 23 and Oxymat 6). A non-dispersive infrared analyzer Siemens Ultramat 23 was used for

the NO_x determination. Gas samples were taken in order to analyze gaseous C_2-C_4 hydrocarbons at the fuel reactor outlet with an HP 5890 gas chromatograph (GC) coupled with a Thermal Conductivity Detector (TCD). More detailed information about the design and operation of the unit can be found elsewhere (Cuadrat et al. 2011).

Figure 42. Picture of the 1 kW (ICB-CSIC-s1) experimental set-up.

Tar can appear as a biomass gasification byproduct reducing the combustion performance of the process and causing operational problems. Tar compounds at the fuel reactor outlet were collected in impingers filled with isopropanol according to the standard tar protocol (Simell et al. 2000). The quantitative determination of the concentrations of the different tar compounds in the samples was done by a gas chromatograph (Agilent 7890A) fitted with a capillary column (HP-5) and a Flame Ionization Detector (FID). Furthermore, the gas chromatograph was coupled with a mass spectrometer (Agilent 5975C). Naphthalene and phenanthrene were selected for the external calibration procedure. The quantitative values were obtained assuming a similar response factor to naphthalene for tar compounds of 1–2 rings and similar to phenanthrene for 3-rings compounds.

2.3.3.2 20 kW_{th} prototype (ICB-CSIC-s50)

A scheme of the ICB-CSIC-s50 experimental unit is shown in Figure 43. This facility was designed to operate in both *i*G-CLC and CLOU modes. The nominal thermal power was 20 kW_{th} for *i*G-CLC mode and 50 kW_{th} for CLOU mode. In this work, the unit was operated in *i*G-CLC mode by using Tierga ore as oxygen carrier.

The CLC unit mainly consists of two circulating fluidized bed reactors, the fuel and the air reactors, interconnected by different loop seals, and one carbon stripper. The fuel reactor was designed with two parts: bottom bed (0.10 m inner diameter, 1.2 m height) and upper part (0.08 m inner diameter, 2.8 m tall). The gas velocities in both sections of the fuel reactor are fitted to operate in the turbulent regime. The solids circulation rate can be independently controlled by handling the fluidization conditions in each reactor and loop-seals. Furthermore, two different solids diverting valves allow the measurement of the solids circulation rate. The global solids circulation rate evaluates the amount of oxygen carrier leaving the air reactor while the fuel reactor solids circulation rate includes the fraction recycled to the fuel reactor in the double loop seal. A bubbling bed reactor acting as a carbon stripper, installed between the fuel and the air reactors, allows the char and the oxygen carrier particles separation and, in this way, the char particles are recycled to the fuel reactor while the oxygen carrier particles reach the air reactor to be reoxidized. The air reactor, 4.8 m height was also designed with two parts: the bottom bed (0.30 m inner diameter) and the upper part (0.10 m inner diameter). Figure 44 shows a picture of the ICB-CSIC-s50 CLC unit.

The solid fuel is fed into the fuel reactor at the bottom part with two screw feeders. CO_2 or H_2O can be used as gasifying agents. When H_2O is used, an evaporator is installed for the steam production. Different mass flow controllers allow fluidizing gases to be fed in reactors, loop-seals and carbon stripper. The reactor temperatures were independently controlled thanks to the electric furnaces. These temperatures and the pressure drop at the different parts of the unit were recorded during all the experiments. The gas outlet composition of each reactor was measured online and recorded. The same gas analyzers described for the 1 kW_{th} unit

were used. More detailed information about the design and operation of the unit can be found elsewhere (Abad et al. 2015a).

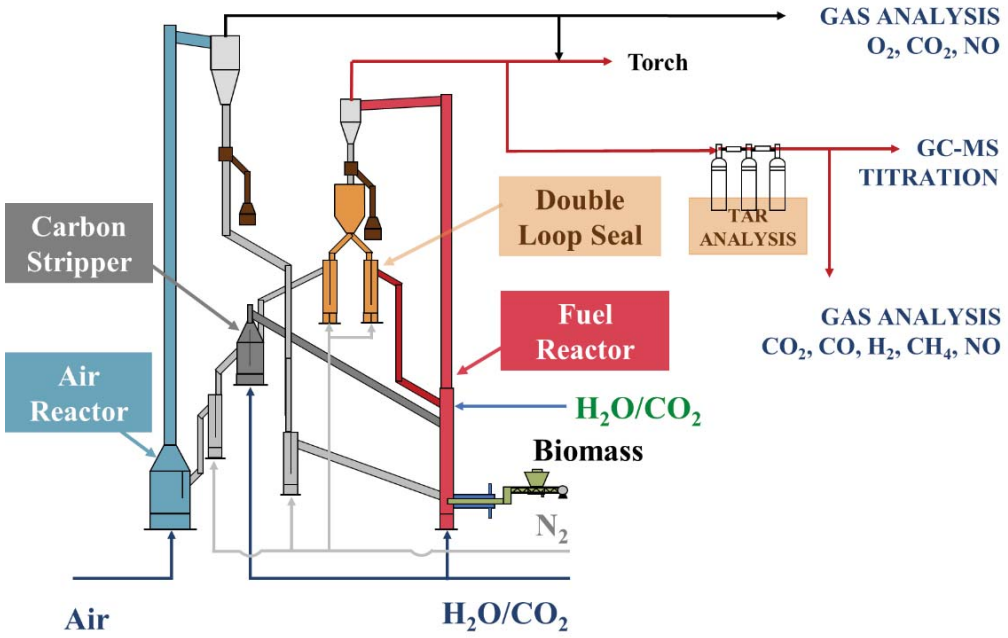

Figure 43. Scheme of the 20 kW_{th} experimental set-up.

Figure 44. Picture of the 20 kW_{th} experimental set-up.

2.3.3.3 Data evaluation

To analyze the performance of the CLC process in the continuous prototypes using different types of biomass and oxygen carriers the main parameters evaluated are the CO_2 capture efficiency, the combustion efficiency, and the oxygen demand. All of them as a function of the oxygen carrier to fuel molar ratio.

The oxygen carrier to fuel molar ratio (ϕ) compares the oxygen that is transported by the oxygen carrier with the oxygen needed for the complete combustion of the fed fuel. A value of ϕ = 1 corresponds to the stoichiometric flow of oxygen carrier needed to fully convert the fuel to CO_2 and H_2O. ϕ was calculated by Equation (4)

$$\phi = \frac{\dot{m}_{OC} \cdot R_{OC}}{\dot{m}_{sf} \cdot \Omega_{sf}} \quad (4)$$

Where $\dot{m}_{OC}$ is the solids circulation flow rate in the completely oxidized state, R_{OC} is the oxygen transport capacity, $\dot{m}_{sf}$ the mass-based flow of fuel fed in to the reactor, and Ω_{sf} the stoichiometric kg of oxygen to convert 1 kg of fuel to CO_2 and H_2O.

The CO_2 capture efficiency (η_{CC}) is defined as the fraction of the carbon introduced in the fuel reactor which was converted to gas in this reactor. The converted carbon was calculated from the concentrations of CH_4, CO and CO_2 measured at the exit of the fuel reactor and the CO_2 concentration measured at the exit of the air reactor. Considering the low amounts of C_2-C_4 detected in the tests, the amounts of hydrocarbons heavier than CH_4 were considered negligible for the calculations. The CO_2 capture efficiency was calculated by Equation (5).

$$\eta_{CC} = \frac{\left[F_{CO_2,FR} + F_{CO,FR} + F_{CH_4,FR}\right]_{out}}{\left[F_{CO_2,FR} + F_{CO,FR} + F_{CH_4,FR} + F_{CO_2,AR}\right]_{out}} \quad (5)$$

The CO_2 capture efficiency calculated according Equation (5) depends on the fraction of char that is gasified in the fuel reactor. The char conversion (X_{char}), defined

as the fraction of carbon in the char which is gasified and released to the fuel-reactor exhaust gas stream, was calculated by Equation (6):

$$X_{char} = \frac{[F_{CO_2,FR}+F_{CO,FR}+F_{CH_4,FR}-F_{C,vol}]_{out}}{[F_{CO_2,FR}+F_{CO,FR}+F_{CH_4,FR}+F_{CO_2,AR}-F_{C,vol}]_{out}} \quad (6)$$

The combustion efficiency in the fuel reactor ($\eta_{comb,FR}$) evaluates the gas conversion in the fuel reactor. It was defined in Equation (7), as the fraction of oxygen demanded by the fuel that is supplied by the oxygen carrier in the fuel reactor, where M_{O_2} represents the molecular weight of O_2 (kg/mol).

$$\eta_{comb,FR} = 1 - \frac{[4F_{CH_4,FR}+F_{CO,FR}+F_{H_2,FR}]_{out}}{\frac{1}{M_{O_2}}2\Omega_{sf}\dot{m}_{sf}-2F_{CO_2,outAR}} \quad (7)$$

The total oxygen demand (Ω_T), Equation (8), was calculated as the quotient between the oxygen required in order to reach complete combustion of the unconverted gases (CH_4, CO and H_2) and the oxygen needed for the complete combustion of the biomass fed.

$$\Omega_T = \frac{4\cdot F_{CH_4,FR}+F_{CO_{FR}}+F_{H_2,FR}}{\frac{1}{M_O}\cdot \dot{m}_{sf}\cdot\Omega_{sf}} \quad (8)$$

Similarly, the tar oxygen demand (Ω_{tar}) was calculated, Equation (9), as the quotient between the oxygen required in order to reach complete combustion of the tar and the oxygen needed for the complete combustion of the biomass fed.

$$\Omega_{tar} = \frac{(j+k/4)\cdot F_{C_jH_{k,FR}}}{\frac{1}{M_O}\cdot \dot{m}_{sf}\cdot\Omega_{sf}} \quad (9)$$

Other parameters that can help to analyze the performance of the CLC process in the continuous prototypes are:

The specific solids inventory in the fuel reactor (m^*_{FR}) allows the comparison of the CLC performance among different oxygen carriers and the used power input. It was calculated by Equation (10), where P_{th} is the power input of the unit, $m_{OC,FR}$ is the mass of oxygen carrier in the fuel reactor, ΔP is the pressure drop in the fuel reactor and S is the reactor surface area.

$$m^*_{FR} = \frac{1}{P_{th}} m_{OC\,FR} = \frac{1}{P_{th}} \left[\left(\frac{\Delta P \cdot S}{g} \right)_{bottom} + \left(\frac{\Delta P \cdot S}{g} \right)_{riser} \right] \quad (10)$$

The carbon mass balance allows an accurate analysis of the CLC performance. It was calculated by Equations (11) and (12), where $F_{C,sf}$ is the carbon flow in the solid fuel, $F_{C,char}$ is the carbon flow as derived char and $F_{C,vol}$ was calculated from the biomass analyses as the difference between the total carbon in the biomass and the fixed carbon.

$$F_{C,sf} = F_{C,char} + F_{C,vol} = \left(F_{C,FR\ out} - F_{CO_2 in} \right) + F_{C,elu} + F_{C,AR_{out}} \quad (11)$$

$$F_{C,FR\ out} = (F_{CO_2} + F_{CO} + F_{CH_4})_{FR,out} \quad (12)$$

The solid fuel conversion (X_{sf}) is a measurement of the amount of solid fuel, biomass in this case, converted in the CLC unit, including both the fuel and air reactors. According to the carbon mass balance showed in Equation (13), this parameter was calculated as:

$$X_{sf} = \frac{(F_{C,FR,out} - F_{CO2,in}) + F_{C,AR,out}}{F_{C,sf}} \quad (13)$$

RESULTS AND DISCUSSION

3.1 Performance of the bioCLC in a 1 kW_{th} continuous unit

The objective of this first section (**Papers I, II, III, IV, V and VI**) was to evaluate the performance of different types of oxygen carriers in the bioCLC process. As it was mentioned in the previous chapter, the evaluation process consisted in the combustion of different types of biomass in a 1 kW_{th} continuous combustion unit and the subsequent analysis of the results obtained following several parameters already defined, mainly the CO_2 capture efficiency (η_{CC}) and the total oxygen demand (Ω_T).

Both natural (minerals/ores) and synthetic materials were considered. First, low-cost oxygen carriers for the *i*G-CLC process were tested (**Papers I, II and III**). The potential of iron and manganese ores as oxygen carriers for the bioCLC process was evaluated and compared.

3.1.1 Combustion under *i*G-CLC: low-cost oxygen carriers

3.1.1.1 Fe-based oxygen carrier

The first tested low-cost oxygen carrier was an iron-based ore denoted as Tierga ore (**Paper I**). Previous experiments with this oxygen carrier had already been performed using pine sawdust as fuel (Mendiara et al. 2013a). The oxygen carrier showed good performance and adequate lifetime. The experimental campaign accomplished in the present work aimed at complementing these results previously published, in which higher specific solids inventories were used (> 1000 kg/MW_{th}). Theoretical studies dedicated to CLC scaling-up (Abad et al. 2015b; Cuadrat et al. 2012) established that specific solids inventories larger than 1000 kg/MW_{th} were not recommended since they would only slightly improve the combustion efficiency while the pressure drop in the fuel reactor would excessively increase. A compromise should be reached between enlarging reactors to allow higher solids inventories and the increase of the combustion efficiency. Thus, in the present study, the specific solids inventories considered were in all cases below 1000 kg/MW_{th}.

Table 10 summarizes the experiments carried out with Tierga iron ore. Three types of forest and agricultural residues (pine sawdust, olive stones and almond shells) were tested at a fuel reactor temperature between 900-980 ºC. A total of 78 h of hot fluidization corresponding to 40 h of biomass combustion were registered.

Figure 45 presents the temporal evolution of the different gas concentrations as well as the temperatures in both fuel and air reactors for a typical experiment during 50 min of steady state operation. Data correspond to pine sawdust combustion experiment at 950 ºC, although similar profiles were obtained for the rest of the types of biomass. CO_2 appeared as the major compound, with about 70% in all cases, followed by the unburnt compounds: H_2 (10-15 vol%), CO (10-12 vol%) and CH_4 (6-8 vol%). The amount of other light hydrocarbons, C2-C4, was negligible.

Table 10. Operating conditions with the Tierga ore in the 1 kW_{th} experimental unit.

Test	FA (-)	T_{FR} (ºC)	T_{AR} (ºC)	ϕ (-)	$\dot{m}_{OC}$ (kg/h)	$\dot{m}_{sf}$ (kg/h)	P_{th} (W_{th})	m^*_{FR} (kg/MW_{th})	$norm.\dot{m}_{OC}$ ((kg/s)/MW_{th})
Pine sawdust									
T1	H_2O	**895**	950	1.1	10.1	0.152	809	475	3.5
T2	H_2O	**910**	950	1.3	9.2	0.113	601	750	4.2
T3	H_2O	**950**	950	1.1	6.7	0.098	522	785	3.6
T4	H_2O	**985**	950	1.1	6.7	0.098	522	780	3.6
Olive stones									
T5	H_2O	**905**	950	1.0	8.8	0.164	766	600	3.2
T6	H_2O	**955**	950	1.0	7.6	0.141	658	600	3.2
T7	H_2O	**980**	950	1.0	7.6	0.141	658	590	3.2
Almond shells									
T8	H_2O	**905**	950	1.2	13.0	0.190	954	370	3.8
T9	H_2O	**955**	950	1.2	7.0	0.102	512	550	3.7
T10	H_2O	**985**	950	1.2	5.9	0.088	442	890	3.7

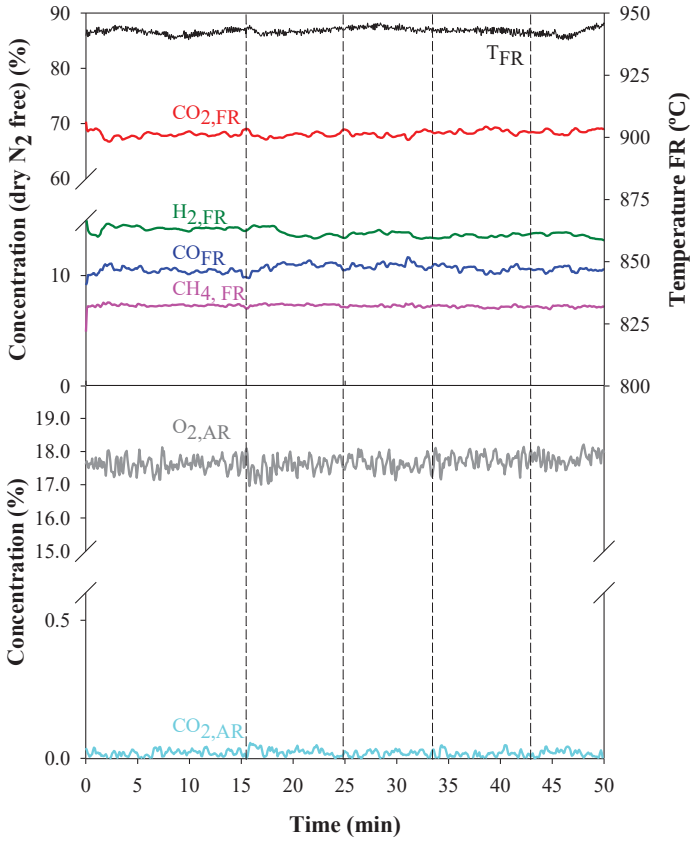

Figure 45. Example of temporal evolution of gas concentrations and temperatures at steady state operation in a normal test in the 1 kW_{th} CLC unit (pine sawdust at 950 ºC, $norm.\dot{m}_{OC}\approx$ 3.6 kg/(s·MW_{th}).

Figure 46 presents the obtained values for the CO_2 capture efficiency and the char conversion for the three types of biomass. Both parameters increased with the

fuel reactor temperature, reaching values of about 100% from 950 ºC in the case of pine sawdust and almond shells and from 985 ºC for the olive stones. This could be due to their higher volatile content of pine sawdust and almond shells compared to olive stones, see Table 8. It is interesting to highlight that 100% CO_2 capture was achieved with the three types of biomass at 980 ºC even in the absence of a carbon stripper between the fuel and the air reactors in this experimental unit.

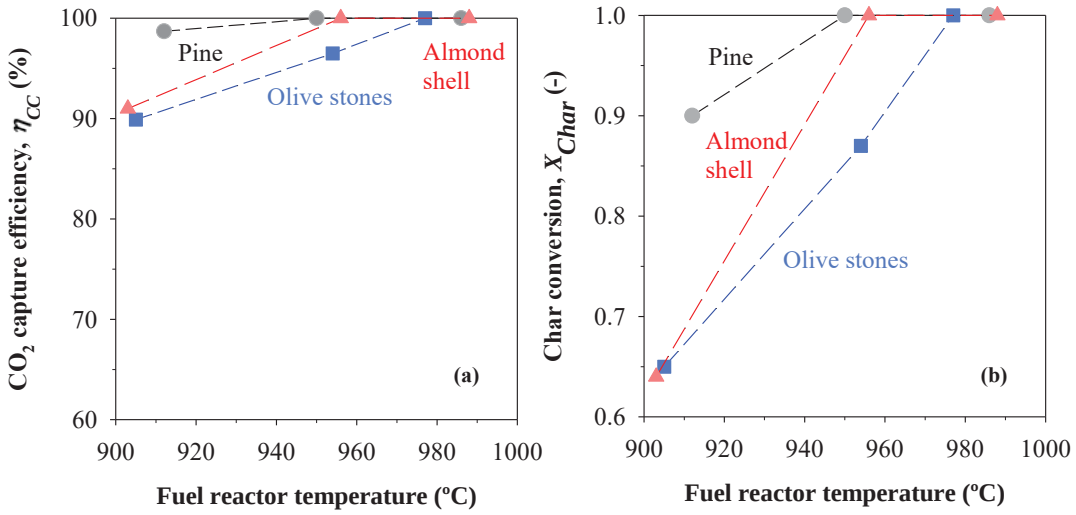

Figure 46. Effect of the fuel reactor temperature on the (a) CO_2 capture efficiency and (b) char conversion for the three types of biomass norm. $\dot{m}_{OC} \approx 3.7$ kg/(s·MW_{th}).

Previous experiments with Tierga ore and different types of coal, such as anthracite, bituminous and lignite, reached lower CO_2 capture efficiencies at temperatures in the range 900-930ºC (Mendiara et al. 2014a). The volatile matter of those coals represented about 7.5% for the anthracite, 33.0% for the bituminous coal and 28.6% for the lignite. Therefore, it can be concluded that the higher volatile content of biomass and the reactivity of biomass char compared to coal makes the use of a carbon stripper not as decisive as in the combustion of coal.

Figure 47 presents the total oxygen demand obtained in the combustion of the three types of biomass with the Tierga ore at different fuel reactor temperatures. No clear trend was observed with the fuel reactor temperature increase. In general, the total oxygen demand for these types of biomass was similar and about 20-30%.

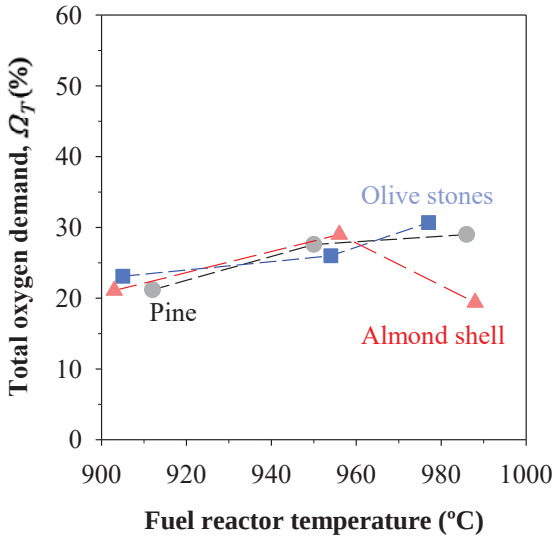

Figure 47. Effect of the fuel reactor temperature on the total oxygen demand for the different types of biomass and norm. $\dot{m}_{OC} \approx 3.7$ *kg/(s·*MW_{th}*).*

It is realistic to assume that most of the oxygen demand is generated by the volatiles that escape the fuel reactor bed without interacting with the oxygen carrier particles. This aspect was more deeply analysed by the estimation of the conversion of the biomass volatiles in this bed. Only CH_4 at the fuel reactor outlet was considered as coming from the volatile matter since both the CO and H_2 in this outlet stream could also come from char gasification.

In order to estimate the volatile conversion, an empirical model by Neves et al. (2011) for the prediction of biomass pyrolysis products was used. The model does not consider the physical-chemical processes occurring within the biomass particles. It is based on mass balances to the overall pyrolysis processes and experimentally-based closing parameters obtained after the compilation of a significant amount of experimental data for different types of biomass and pyrolysis conditions. It should be pointed out that only mass balances to carbon, hydrogen and oxygen were considered. Those corresponding to nitrogen, sulphur and chlorine were not included in the original model.

The input data required by the model were the CHO composition of the parent fuel (dry-ash-free) and the temperature of pyrolysis in ºC. As output, the model calculates the dry-ash-free composition of resulting tar, C_xH_y, CH_4, CO, CO_2, H_2O

and H_2. An extra assumption was herein made in order to adapt this composition to the reacting conditions existing in the CLC process. It must be remarked that steam is used as gasifying agent in the fuel reactor in order to convert the char produced during biomass pyrolysis to CO and H_2. The presence of steam would facilitate the conversion of most of the tar and C_xH_y formed during biomass pyrolysis to CH_4 and carbon. Considering this, the amounts of the different species resulting from biomass pyrolysis predicted by the model were recalculated.

As it was mentioned, CH_4 was used as volatile reference compound to calculate volatile conversion. Thus, the flow of methane at the fuel reactor outlet was compared to that predicted by the model at the corresponding fuel reactor temperature. Table 11 shows the estimated volatile conversion based on CH_4 at 900 ºC for the three types of biomass tested. An average volatile conversion about 70% was estimated for the three types of biomass. These values are in line with the oxygen demand about 20-30% showed in Figure 47.

Table 11. Volatile conversion referred to methane in the experiments with Tierga ore at about 900 ºC in the fuel reactor.

	Pine sawdust	**Olive stones**	**Almond shells**
Fuel reactor	910	905	905
Air reactor	950	950	950
CH_4 conversion (%)	73.5	65.1	71.0

Other studies found in literature also used Tierga ore as oxygen carrier in the combustion of biomass. Linderholm and Schmitz (2016) performed experiments using wood char as fuel in a 100 kW_{th} CLC unit in a temperature interval (880-960 ºC) close to that in the present study and specific solids inventories between 400-600 kg/MW_{th}. High CO_2 capture efficiencies were also attained, although the 100 kW_{th} unit is equipped with a carbon stripper. Besides, values of the total oxygen demand were reported between 7.4-8.5 %. These values were lower than those obtained in the present work, which can be attributed to two reasons. First the used fuel was wood char, with a lower volatile content (16.7 %) compared to pine sawdust. Second, the fuel reactor in the 100 kW_{th} unit is a circulating fluidized bed where a

better contact between volatiles and oxygen carrier particles is expected and therefore lower total oxygen demands.

3.1.1.2 Mn-based oxygen carriers

One of the options to improve the volatile conversion, and this way, to reduce the high values of total oxygen demand found in the experiments with Tierga ore is the use of more reactive low-cost oxygen carriers. This possibility was investigated using different manganese ores (**Paper II**), which had been identified in previous studies of the research group as potential alternatives to Tierga ore considering their high reactivity and their estimated lifetime (Mei et al. 2015; Mei et al. 2016; Abad et al. 2018). Thus, two manganese-based ores were used (MnGBHNE and MnSA) in the combustion of the three different types of biomass.

Table 12 summarizes the experiments carried out with MnGBHNE and MnSA with pine sawdust, olive stones and almond shells under similar conditions to those previously used with Tierga ore. The experimental campaign involved more than 160 h of hot fluidization with more than 63 h of biomass combustion. Neither agglomeration, nor fluidization problems were detected with any of the oxygen carriers and the three types of biomass used during all the experimental campaign.

The first series of experiments (G1-G17) in Table 12 evaluated the performance of MnGBHNE oxygen carrier in a range of specific solids inventories of 520-775 kg/MW_{th}. Tests G1 to G7 corresponded to the evaluation of the effect of the fuel reactor temperature. Tests G8-G11 analyzed the influence of the gasifying agent. Finally, the influence of the variation of the solids circulation rate normalized per MW_{th}, ($norm.\dot{m}_{OC}$) was addressed (G12-G17). The second series of experiments used MnSA as oxygen carrier and pine as fuel at different fuel reactor temperatures (S1-S4). In the discussion of the results obtained with manganese ores, some tests in Table 10 identified as T1-T6 were considered for comparison.

Evaluation of MnGBHNE: Influence of the fuel reactor temperature and the gasifying agent

Figure 48 presents the effect of the fuel reactor temperature (G1 to G7) on both the CO_2 capture efficiency (η_{CC}) and the total oxygen demand (Ω_T) using the different types of biomass (pine sawdust, olive stones and almond shells). These experiments were done using steam as fluidizing agent and values of normalized solids circulation rates ($norm.\dot{m}_{OC}$) close to 3 kg/(s·MW_{th}). Also previous experimental results obtained with the Tierga ore are presented (open symbols) to facilitate the comparison between both oxygen carriers

Table 12. Operating conditions with the manganese ores in the 1 kW_{th} experimental unit.

Test	FA (-)	T_{FR} (ºC)	T_{AR} (ºC)	ϕ (-)	$\dot{m}_{OC}$ (kg/h)	$\dot{m}_{sf}$ (kg/h)	P_{th} (W_{th})	m^*_{FR} (kg/MW_{th})	$norm.\dot{m}_{OC}$ ((kg/s)/MW_{th})
Pine sawdust									
G1	H_2O	**935**	950	2.0	7.2	0.120	639	605	3.1
G2	H_2O	**900**	950	2.0	7.2	0.120	639	625	3.1
G3	H_2O	**855**	950	2.0	7.2	0.120	639	590	3.1
G4	H_2O	**890**	950	1.8	7.2	0.135	718	555	2.8
Olive stones									
G5	H_2O	**900**	950	1.9	6.2	0.132	610	700	2.8
Almond shells									
G6	H_2O	**905**	950	1.9	6.5	0.124	617	675	2.9
G7	H_2O	**940**	950	1.5	5.0	0.124	617	650	2.3
Pine sawdust									
G8	**CO_2**	910	950	2.9	9.8	0.115	612	775	4.5
G9	**CO_2**	915	950	2.7	9.8	0.123	655	715	4.2
G10	**CO_2**	900	950	2.9	9.7	0.115	612	665	4.4
G11	**CO_2**	950	950	3.3	12.4	0.128	681	520	5.0
G12	H_2O	935	950	1.0	3.8	0.128	681	700	**1.6**
G13	H_2O	920	950	3.5	12.0	0.120	639	685	**5.4**
G14	H_2O	925	950	3.5	12.0	0.117	623	675	**5.4**
G15	H_2O	950	950	1.0	3.8	0.117	623	650	**1.6**
G16	H_2O	950	950	3.5	12.0	0.128	681	670	**5.4**
G17	H_2O	965	950	0.7	2.8	0.117	623	530	**1.2**
S1	CO_2	910	950	2.5	9.2	0.116	617	**770**	4.4
S2	CO_2	930	950	2.7	9.6	0.116	617	**730**	4.0
S3	CO_2	900	950	1.9	7.2	0.120	639	**970**	3.1
S4	CO_2	890	950	2.2	8.4	0.120	639	**970**	3.7

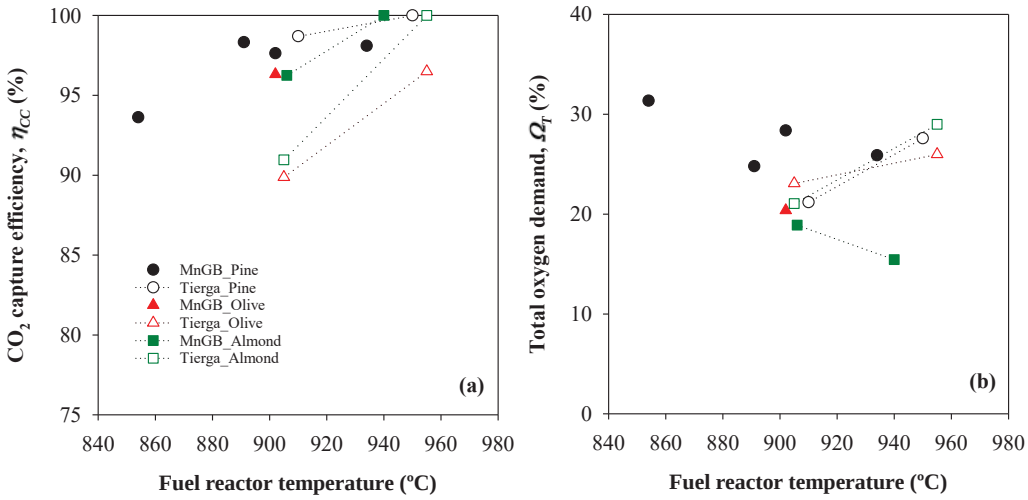

Figure 48. Effect of the fuel reactor temperature on (a) the CO_2 capture efficiency and (b) the total oxygen demand with the three types of biomass $norm.\dot{m}_{OC} \approx 3\ kg/(s{\cdot}MW_{th})$.

Following the trend previously shown in Figure 46 with Tierga ore, the CO_2 capture efficiencies obtained with the MnGBHNE oxygen carrier increased with the increase of the fuel reactor temperature reaching values higher than 90% regardless the biomass used. It should be here again reminded that these results were obtained in the absence of a carbon stripper. Nevertheless, differences can be observed in Figure 48 (a) among oxygen carriers and types of biomass. While similar values of CO_2 capture efficiency were observed for pine, olive stones and almond shells using the MnGBHNE in the temperature range between 855 and 935 ºC (> 95%), in the experiments with the Tierga ore, lower CO_2 capture efficiencies were reached in the experiments with olive stones and almond shells compared to pine. This different behaviour would indicate that the conversion of biomass char would be more favoured using the MnGBHNE as oxygen carrier, as it has been previously reported using coal as fuel (Abad et al. 2018). Figure 48 (b) shows the values obtained for the total oxygen demand with the different types of biomass. The MnGBHNE results showed a clear decrease with the increase of the fuel reactor temperature. Nevertheless, the oxygen demand values reached were in line to those previously obtained for Tierga ore working under similar conditions (**Paper I**). Higher total oxygen demand values were determined for the experiments with pine compared to those obtained with olive stones and almond shells, which may be attributed to the different composition of the volatiles/gasification products depending on the biomass

considered. In order to further investigate the differences between the two oxygen carriers, Figure 49 shows the contribution to the total oxygen demand of the different unburnt compounds measured at the fuel reactor exit (H_2, CO and CH_4) for the experiments performed with pine and Tierga ore and MnGBHNE under similar operating conditions.

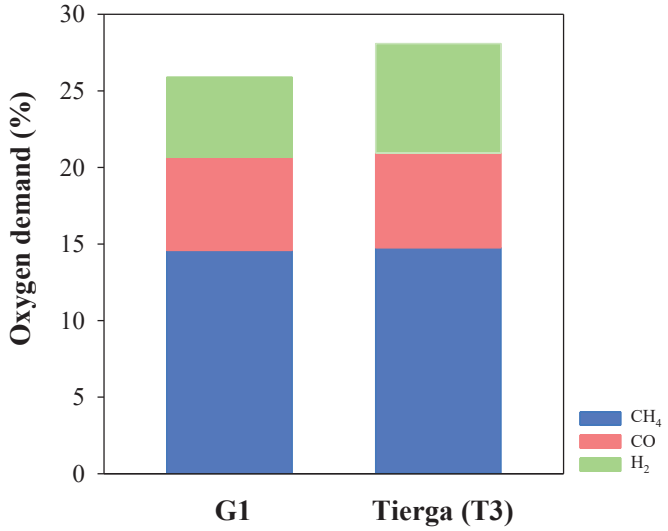

Figure 49. Comparison of partial oxygen demand for H_2, CO and CH_4 at similar conditions using Tierga ore and MnGBHNE as oxygen carriers in experiments with pine sawdust, norm.$\dot{m}_{OC}$≈ 3.4 kg/(s·MW_{th}).

As it can be seen in Figure 49, the partial oxygen demands for CO and CH_4 were similar at comparable specific solids circulation rates for MnGBHNE and Tierga ores in experiments using H_2O as gasifying agent and pine sawdust as biomass. However, a reduced contribution to the total oxygen demand of the H_2 partial demand is observed in the experiments with MnGBHNE in comparison to Tierga.

The influence of the gasifying agent used in the fuel reactor had been previously addressed with Tierga ore (Mendiara et al. 2013a) and no significant differences were found in the performance of the process when CO_2 replaced steam as the gasifying agent. Similar conclusions were obtained with MnGBNHNE, as it is shown in Figure 50. CO_2 capture efficiencies near to 100% were obtained in Figure 50 (a) in all the experiments with CO_2, working at the temperatures higher than 900 ºC in the fuel reactor. The total oxygen demand values obtained with H_2O

and CO_2 as gasifying agents, in Figure 50 (b), follow the same decreasing trend with the fuel reactor temperature increase, reaching a value of 17% at 950ºC. Therefore, it is possible to conclude that it is possible to use dry recirculated CO_2 as feed in the fuel reactor, which is an important advantage since the energy required to produce steam is avoided.

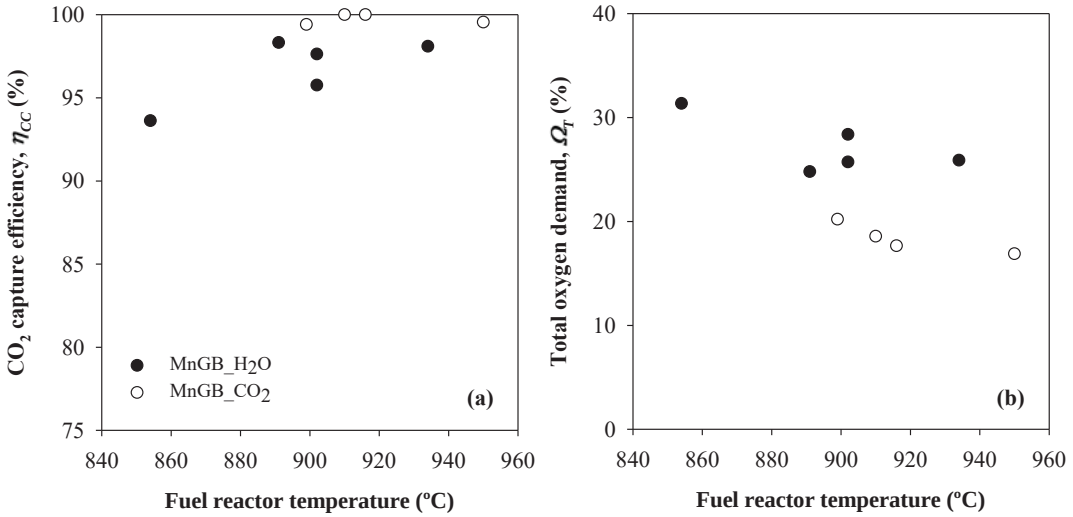

Figure 50. Effect of the gasifying agent at different fuel reactor temperatures on (a) the CO_2 capture efficiency and (b) the total oxygen demand for experiments with MnGBHNE.

Evaluation of MnGBHNE: Influence of the normalized solids circulation rate ($norm.\dot{m}_{OC}$)

The normalized solids circulation rate ($norm.\dot{m}_{OC}$) is defined as the solids circulation rate normalized per MW_{th}. This parameter is related with the amount of oxygen available in the fuel reactor for the combustion, i.e. the oxygen carrier to fuel ratio (ϕ), and can influence the total oxygen demand. Figure 51 shows the CO_2 capture efficiency and the total oxygen demand at various normalized solids circulation rates burning pine sawdust and using H_2O as gasifying agent at temperatures of about 940 ºC in the fuel reactor. Although the CO_2 capture efficiency was not clearly affected by the specific solids circulation rate (> 98% in all cases) the total oxygen demand decreased when the normalized solids circulation rate

increased, reaching a value about 20% at 5.4 kg/(s·MW_{th}). A higher solids circulation rate implies higher oxygen supply in the fuel reactor, increasing the combustion of volatiles and gasification products and, therefore, decreasing the total oxygen demand values.

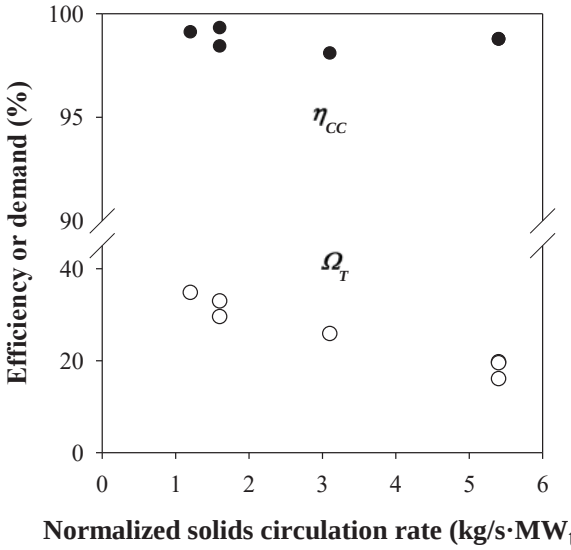

Figure 51. Effect of the normalized solids circulation rate on the CO_2 capture efficiency and the total oxygen demand with the MnGBHNE and pine sawdust, T_{FR}≈ 940 ºC.

The comparison of the results obtained with the MnGBHNE ore and the Tierga ore under similar conditions, showed that both oxygen carriers performed similarly in CLC of biomass and there was no clear advantage of one carrier over the other. For this reason it was evaluated another pre-selected manganese mineral, i.e. MnSA, which had been previously found by the authors as especially reactive to CO (Mei et al. 2015). Moreover, it presented adequate fluidization properties and lifetime.

Evaluation of MnSA

The comparison between MnGBHNE and MnSA was made with the in experiments carried out at different fuel reactor temperatures maintaining almost constant the rest of the operating conditions (tests G8-G11 and S1-S4). Figure 52 presents the CO_2 capture efficiencies and the total oxygen demands obtained with both oxygen carriers under similar conditions.

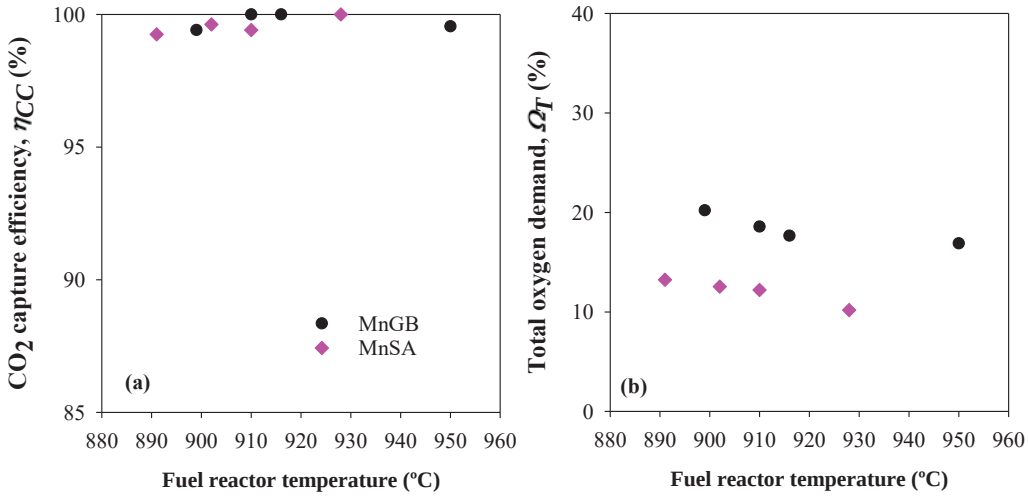

Figure 52. Effect of the fuel reactor temperature on (a) the CO_2 capture efficiency and (b) the total oxygen demand with the MnGBHNE and the MnSA with pine sawdust, norm. $\dot{m}_{OC} \approx$ 4 kg/(s·MW_{th}).

Regarding the CO_2 capture efficiency values showed in Figure 52 (a), no differences were found between oxygen carriers. Despite the different fuel reactor temperatures, CO_2 capture efficiencies higher than 99% were reached with both oxygen carriers in a CLC unit without a carbon stripper. In Figure 52 (b) the total oxygen demand decreased with the fuel reactor temperature increase for both materials. In the comparison between MnGBHNE and MnSA it was observed that total oxygen demands obtained with MnSA were clearly lower than those corresponding to MnGBHNE, reaching a value as low as 10.2% at 930 ºC. Moreover, to obtain oxygen demand values about 10% working with Tierga ore, it was necessary to increase the solids inventory to about 1400 kg/MW_{th} and decrease the normalized solids circulation rate (Mendiara et al. 2013a). Therefore, it can be concluded that the MnSA had a better performance than the other two minerals and it can be considered a better alternative for the bioCLC process. The analysis of the partial contributions to the total oxygen demand made in Figure 53 with the two manganese ores and for two fuel reactor temperatures revealed that the major contribution to the oxygen demand came from unburned methane. However, the contribution of all unburned compounds is clearly diminished in the case of MnSA compared to that found for MnGBHNE since MnSA seems to be more reactive to the combustion of these gases than MnGBHNE. It should be highlighted that complete H_2 combustion at a fuel reactor temperature as low as 910 ºC was reached with the MnSA.

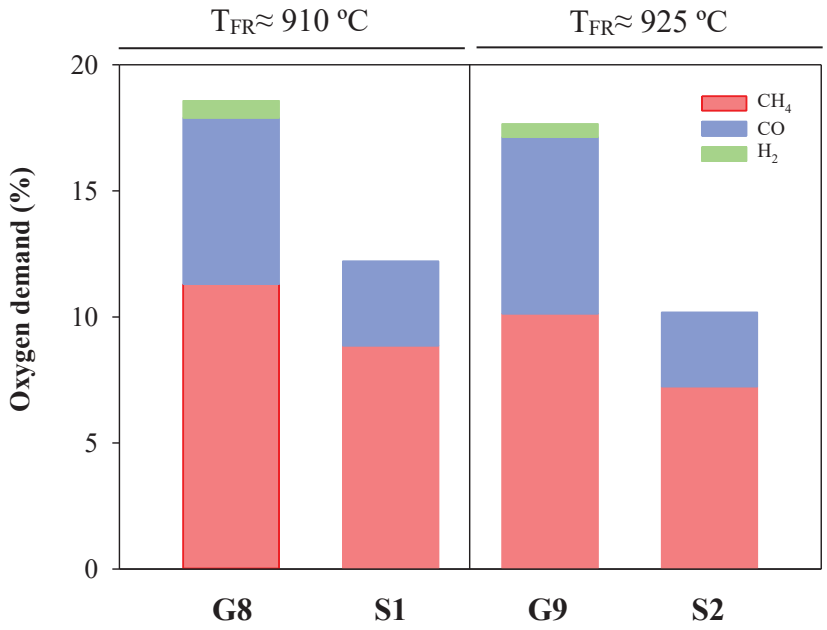

Figure 53. Comparison of partial oxygen demand for H_2, CO and CH_4 using MnGBHNE and MnSA as oxygen carriers in experiments with pine at fuel reactor temperatures between 910 and 925 ºC and norm. $\dot{m}_{OC}$*≈ 4 (kg/s)/*MW_{th}.

The results obtained with MnSA are quite remarkable when they are compared to other results reported in literature with different manganese ores. Recently, Schmitz and Linderholm (2018) reported the results obtained with a sintered manganese ore as oxygen carrier burning different types of biomass: Swedish and German wood char and black pellets. They performed experiments in a 10 kW_{th} and in a 100 kW_{th} continuous CLC units. The fuel reactor in the 10 kW_{th} unit was a bubbling fluidized bed. In this unit and using black pellets as fuel they reported combustion efficiencies between 65 and 70% working at a fuel reactor temperature of 970 ºC and high specific solids inventories (> 1200 kg/MW_{th}), which would correspond to oxygen demands about 30%, higher than those reported in the present work. The same authors reported results using the same sintered manganese ore and black pellets in a 100 kW_{th} unit where the fuel reactor was a circulating fluidized bed. In this case, the fuel reactor temperature varied between 910 and 981 ºC and the specific solids inventories were lower (300-600 kg/MW_{th}). The reached combustion efficiencies oscillated between 81 and 90%, similar to those reached in the present work with MnSA, although in the present work, results were obtained in a bubbling fluidized bed fuel reactor, where volatile combustion may not be as favored as in a circulating fluidized bed. Higher oxygen demand values than those reported here for

MnSA were obtained in experiments with braunite as oxygen carrier and white/black pellets in a 50 kW_{th} unit operating at 900 ºC. (Pikkarainen and Hiltunen 2017).

3.1.1.3 Recycling of the fuel reactor outlet stream

Results obtained in the present work and those reported under similar conditions in literature pointed to one of the main cornerstones in the development of the bioCLC technology: the high values obtained for the total oxygen demand associated to the high volatile content of biomass when compared to other fuels such as coal (Mendiara et al. 2018a). The existence of an elevated amount of unburned products at the fuel reactor outlet makes necessary the incorporation of a polishing step to complete the combustion. This oxygen polishing implies an energy penalization for the CLC process and therefore it should be either minimized or even avoided (Adánez et al. 2018). Several strategies have been proposed in literature to avoid this oxygen polishing step (Gayán et al. 2013), most of them commented in section 1.5.3. One of them is the use of highly reactive oxygen carriers. A higher reactivity of the oxygen carrier would facilitate the combustion of H_2, CO and CH_4 in the fuel reactor and would decrease the total oxygen demand. This strategy was already considered in the present work with the testing of MnSA, searching for an improvement of the results obtained with MnGBHNE or Tierga ore.

Among the technical solutions commented in section 1.5.3 to reduce the total oxygen demand values, the fuel reactor outlet recycling is considered. In the present work, the effect of the recirculation to the fuel reactor of the fuel reactor outlet stream has been evaluated assuming a simulated recycled stream. The methodology used for this purpose was to simulate a recycled stream and to analyze the behavior of the different unburned compounds (i.e. H_2, CO and CH_4), see **Paper II**. For that, tests identified in Table 12 as G8 and S1 were selected and individual flows of each unburned compound corresponding to gas concentrations from 0-10% in the inlet stream were introduced while the total flow at the fuel reactor inlet was kept constant at 130 L/h (STP). Then, the composition of the new gas outlet stream leaving the fuel reactor was analyzed once the steady state was again reached. Knowing the amount of gas introduced and the gas concentrations before and after the gas introduction,

the degree of conversion (χ) in the fuel reactor were estimated for each of the introduced gases in Table 13. Hydrogen was completely converted regardless the molar flow introduced to the fuel reactor. In the case of CO and CH_4, about 80% and 70% conversion, respectively, were reached for the different molar flows of each compound that were tested.

Table 13. Conversion χ (%) for each recycled unburned compound gas in the fuel reactor at 900 ºC

	MnGBHNE	MnSA
H_2	100	100
CO	81	78
CH_4	67	70

After the experimental tests, the behavior of a CLC unit was simulated with different gas recirculation (*R*), see Figure 54.

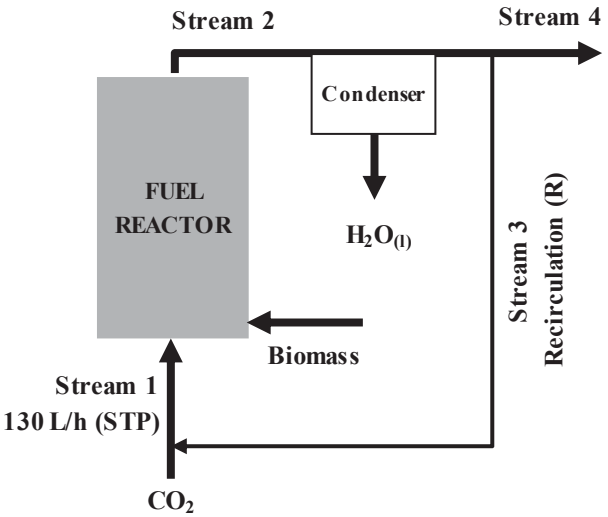

Figure 54. Fuel reactor outlet recycling scheme.

Dry recycling (stream 3) was assumed in the calculations. The recirculation (R) is defined as the percentage of the outlet stream (stream 2) being recycled to the fuel reactor (stream 3). The iterative process started considering the composition of stream 3 which is the same than that in stream 2 when recirculation is R = 0 %. Then, a value of R is assumed and the molar flows of each component calculated. The value

of χ in Table 13 for each gaseous compound was considered in order to recalculate the composition in the new stream 2. These values were compared to those calculated in the previous iteration. If the molar flows are similar, then the iterative process is stopped and the total oxygen demand at the fuel reactor outlet calculated based on these molar flows. If they are not similar, the process is repeated.

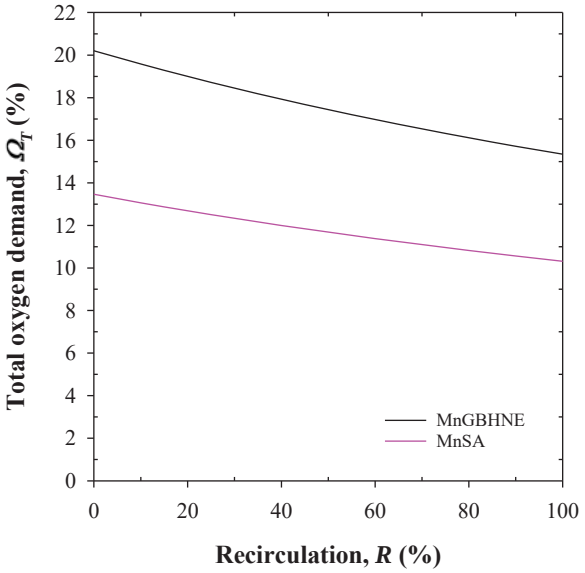

Figure 55. Fuel reactor outlet recycling simulation (data used for the iG-CLC simulation with MnGBHNE and MnSA burning at 900 ºC, about 4 (kg/s)/MW_{th} and about 770 kg/MW_{th}.

The simulation was carried out with a molar $CO_2/C_{biomass}$ ratio ~ 1.2, similar to the ratio in the experiments G8 and S1 and assuming in the first iteration the composition of those tests. Figure 55 represents the total oxygen demand values obtained through the application of the iterative simulation as a function of the recirculation for both MnGBHNE and MnSA oxygen carriers in the combustion of pine sawdust. As it can be observed, the total oxygen demand is reduced when the gas recirculation is increased. In the limit case, that is, when the fuel reactor is fluidized with only recirculated gas (R~50%), values close to 30% of total oxygen demand reduction were observed for both oxygen carriers, pointing to the promising possibilities of this technical improvement.

3.1.1.4 Improved oxygen carrier: Mn66FeTi7

Manganese-iron mixed oxides have received attention because of their ability to release oxygen during the reduction under specific operating conditions. Their use had led to a new process, denoted as Chemical Looping assisted by Oxygen Uncoupling (CLaOU), that allows to obtain better results in the oxygen demand without expensive scheme modifications, such as using distributor plates at the bottom part of the fuel reactor for a better volatile distribution or a second fuel reactor to convert the unburnt matter at the exit of the first fuel reactor. As it was mentioned in the experimental chapter, a synthetic oxygen carrier, named Mn66FeTi7, based on manganese and iron oxides doped with TiO_2 has been used in the present work to test its effect on the oxygen demand reduction (**Paper III**). The bixbyite phase, $(Mn_xFe_{1-x})_2O_3$, present in this oxygen carrier decomposes into a spinel phase, $(Mn_xFe_{1-x})_3O_4$, and molecular oxygen is released at specific operating conditions.

Table 14 summarizes the experiments carried out with Mn66FeTi7 with pine sawdust under similar conditions to those previously used with Fe and Mn based ores/minerals. About 180 hours of hot fluidization were accomplished, 41 h of which corresponded to biomass combustion. Good fluid dynamic performance and no agglomeration problems were observed during all the experiments. Steady state was usually reached after 20 min and maintained at least during 60 min.

The effect of different operating variables on the CO_2 capture efficiency and the total oxygen demand was analyzed, including the temperature in the air reactor and the air excess ratio, λ^*, calculated in Equation (14). Previous results using coal as fuel concluded the importance of these two particular variables on the molecular oxygen release of this oxygen carrier, since both variables affected the oxidation from spinel in the air reactor to bixbyite (Pérez-Vega et al. 2020).

$$\lambda^* = \frac{1-y_{O_2\ AR\ out}}{1-\frac{y_{O_2\ AR\ out}}{y_{O_2\ AR\ in}}} \qquad (14)$$

In the first series (M1-M3), conditions in the air reactor were set to about 880 ºC and low air excess ratio while the solid inventory in the fuel reactor was changed. In the second series (M4-M7) the solids inventory in the fuel reactor was maintained constant and the air excess ratio in the air reactor was changed while temperature remained at 880 ºC. The third series (M8-M11) analyzed the effect of the air excess ratio at two different specific solids inventories. Finally, the fourth series (M12-M16) set the values of air excess ratio and solids inventory while the temperature in the air reactor was increased to 930 ºC.

Table 14. Operating conditions with the Mn66FeTi7 in the 1 kW_{th} experimental unit.

Test	T_{FR} (ºC)	T_{AR} (ºC)	λ^* (-)	ϕ (-)	$\dot{m}_{OC}$ (kg/h)	$\dot{m}_{sf}$ (kg/h)	P_{th} (W_{th})	m^*_{FR} (kg/MW_{th})	$norm.\dot{m}_{OC}$ ((kg/s)/MW_{th})
Mn66FeTi7									
M1	930	880	**1.2**	2.6	5.3	0.130	692	**600**	2.1
M2	925	880	**1.1**	3.5	3.5	0.063	335	**1420**	2.9
M3	935	880	**1.2**	6.0	4.3	0.046	245	**1870**	4.9
M4	900	880	**1.4**	1.8	1.7	0.059	314	1575	1.5
M5	950	880	**1.4**	5.0	4.7	0.059	314	1515	4.1
M6	900	880	**1.8**	2.9	3.0	0.065	346	1330	2.4
M7	930	880	**1.9**	3.1	3.0	0.062	330	1400	2.5
M8	890	880	1.6	2.6	3.5	0.086	458	**1110**	2.1
M9	905	880	1.6	2.6	3.5	0.086	458	**1075**	2.1
M10	900	880	1.9	3.8	2.9	0.048	255	**1855**	3.1
M11	930	880	1.9	4.6	3.5	0.048	255	**1890**	3.8
M12	935	**930**	1.2	3.8	3.6	0.060	245	1310	3.1
M13	905	**930**	1.8	3.6	3.7	0.066	351	1240	3.0
M14	960	**930**	1.8	3.8	3.9	0.066	351	1240	3.1
M15	925	**930**	1.8	4.0	4.0	0.064	341	1485	3.3
M16	940	**930**	1.8	4.0	4.0	0.064	341	1385	3.3

Evaluation of Mn66FeTi7: CO_2 capture efficiency

The values of CO_2 capture efficiency under the different conditions in Table 14 were so close to 100 % that no influence of the operating conditions could be found. The high values of CO_2 capture efficiency reached were attributed to the almost full char conversion in the fuel reactor since almost no CO_2 was measured at the outlet of the air reactor.

Evaluation of Mn66FeTi7: Total oxygen demand

EFFECT OF THE SOLIDS INVENTORY

Figure 56 shows the results obtained with the Mn66FeTi7 oxygen carrier working under similar conditions of air excess ratio and solids inventory (M1) to those used with the Tierga ore and the manganese ores (MnGBHNE and MnSA). In this case, the temperature in the air reactor was maintained at 880 ºC. Working with specific solids inventories about 600-800 kg/MW_{th} (M1), the Mn66FeTi7 oxygen carrier performed similarly to Tierga (T2-T3) and MnGBHNE (G1-G2), yielding also high values of total oxygen demand (21-28%). Increasing the solids inventory to values about 1000-1400 kg/MW_{th} in the fuel reactor and keeping the rest of operating conditions constant, a further reduction in the oxygen demand was reached, as it is shown in Figure 56, point (M2). Working with 1870 kg/MW_{th} (M3) in the fuel reactor, an oxygen demand of about 12% was obtained. The increase in the solids inventory in the fuel reactor can be used as a measure for the oxygen demand reduction. However, similar results were obtained compared with the MnSA (S4-S3) despite the lower inventories used for this manganese ore, about 1000 kg/MW_{th}. Therefore, further optimization of the operating conditions of Mn66FeTi should be investigated in order to enhance the oxygen release potential of the Mn66FeTi7 material and a significant reduction in the oxygen demand compared to best values reached with iron or manganese ores could be expected.

EFFECT OF THE AIR EXCESS RATIO

In the second and third series of experiments in Table 14 several operating conditions affecting Mn66FeTi7 regeneration in the air reactor were analyzed. In the second series (M4-M7), the air excess in the air reactor was increased from 1.4 (M2) to 1.9 (M7) while the temperature in the air reactor was maintained at 880 ºC with an average solids inventory of about 1455 kg/MW_{th}. The results in Figure 57 show that the oxygen demand decreased when the air excess ratio was increased. The largest reductions in the oxygen demand were observed for λ^* = 1.8-1.9. Under these conditions, total oxygen demand values of 10.4 % (M7) were reached, which represents reductions of 35% with respect to the reference value with λ^* = 1.1 (M2).

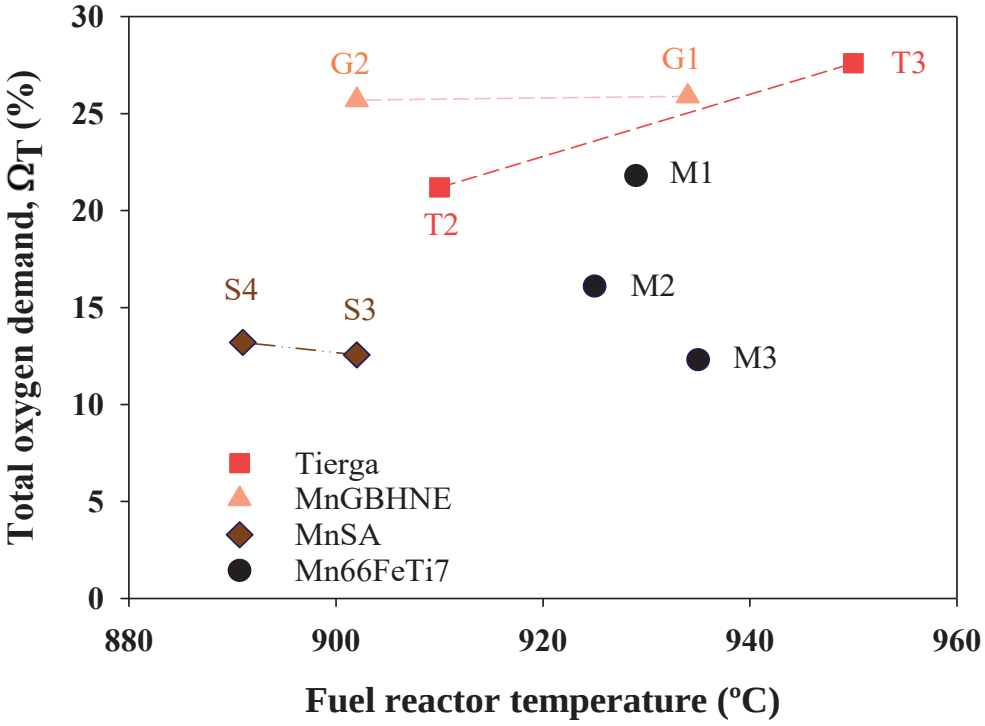

Figure 56. Effect of the specific solids inventory on the total oxygen demand with the Mn66FeTi7 with pine sawdust and comparison with Mn and Fe ores.

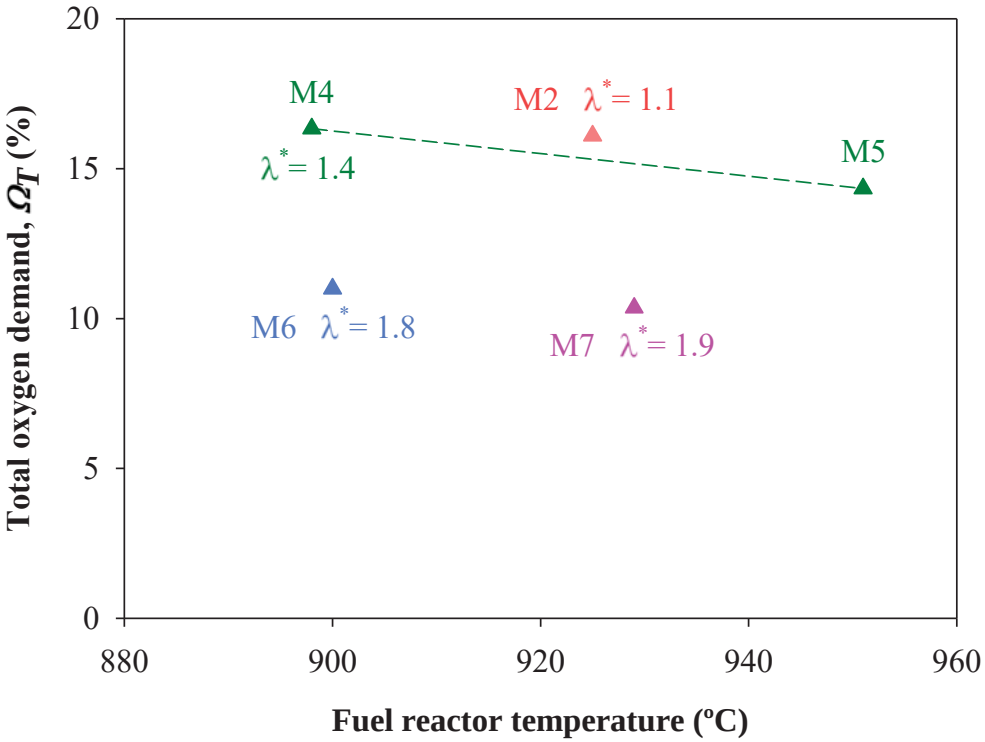

Figure 57. Effect of the air excess (λ^*) on the total oxygen demand with the Mn66FeTi7 with pine sawdust, T_{AR}≈ 880 ºC, m^*_{FR}≈ 1450 kg/MW_{th}.(M4-M7).

The effect of the air excess air ratio has been also assessed in the third series of the experimental campaign (M8-M11).The results shown in Figure 58 correspond to experiments performed under similar conditions to those shown in Figure 57 but with two different averaged values of solids inventories, i.e. 1095 kg/MW_{th} and 1875 kg/MW_{th}. When M4-M5 are compared to M8-M9 it can be observed that lower values of total oxygen demand were obtained despite the lower solids inventory available in the fuel reactor (1095 kg/MW_{th}). The combination of high air excess ratios (λ^* = 1.9) and high solids inventories (1875 kg/MW_{th}) can led to values of total oxygen demand as low as 4.6 % at 930 ºC (M11).

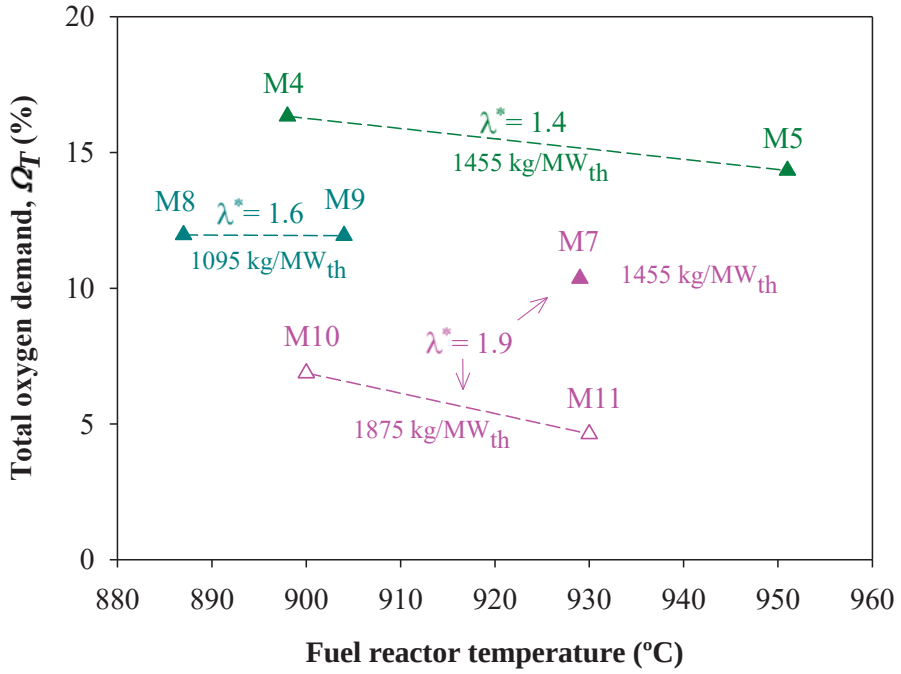

Figure 58. Effect of the air excess (λ^*) on the total oxygen demand with the Mn66FeTi7 with pine sawdust, T_{AR}=880 ºC (M8-M11).

EFFECT OF THE AIR REACTOR TEMPERATURE

All the experimental results shown in Figure 56 to 58 were obtained maintaining the temperature in the air reactor at approximately 880 ºC. The fourth experimental series, (M12-M16) was carried out increasing the temperature in the air reactor to 930 ºC. Under this conditions, two different air excess ratios were tested, i.e. 1.1-1.2 and 1.8. Results are shown in Figure 59. Tests corresponding to M2 and M12 were performed with a low air excess ratio (λ^* = 1.1-1.2) and an averaged solids

inventory about 1365 kg/MW_{th}. In this case, a slightly lower total oxygen demand was attributed to the experiment at 880 ºC in the air reactor. A similar comparison can be performed at higher air excess ratio, namely (λ^* = 1.8) and similar solids inventories for the tests M6 (1455 kg/MW_{th}), M13-M14 (1240 kg/MW_{th}) and M15-M16 (1435 kg/MW_{th}). Working at 930 ºC in the air reactor, a decrease in the total oxygen demand was observed from M13-M14 to M15-M16 when the solids inventory in the fuel reactor was slightly increased. Nevertheless, the lowest oxygen demand value was again obtained when the air reactor was operated at 880 ºC (M6-M7).

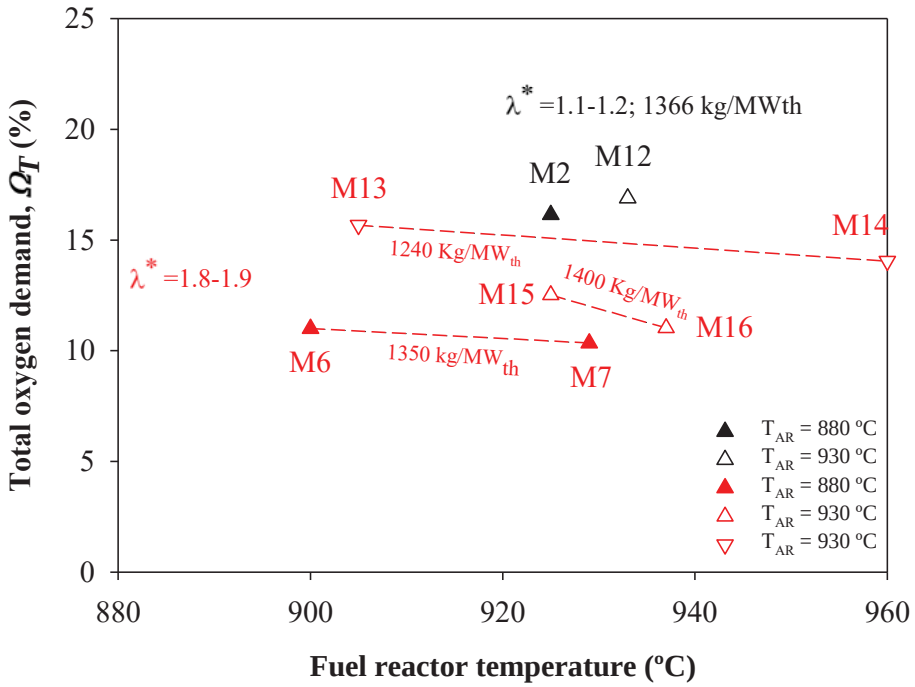

Figure 59. Effect of the air reactor temperature (T_{AR}) on the total oxygen demand with the Mn66FeTi7 with pine sawdust.

Further analysis of the total oxygen demand values obtained in the experimental series presented in Table 14 is shown in Figure 60 representing the total and partial oxygen demands attributed to each of the unburned compounds found at the fuel reactor exit, i.e. H_2, CO and CH_4 in the different experimental tests in Table 14. In Series I, the main contribution to the total oxygen demand value came from methane followed by CO regardless the solids inventory in the fuel reactor. In Series II and III this trend changed. When the air excess ratio was increased, methane

was better burned and its contribution to the total oxygen demand decreased and became closer to that of CO or even lower in some cases (see M10 and M11). These results demonstrate how the increased presence of molecular oxygen in the fuel reactor improved the oxygen demand by improving methane combustion.

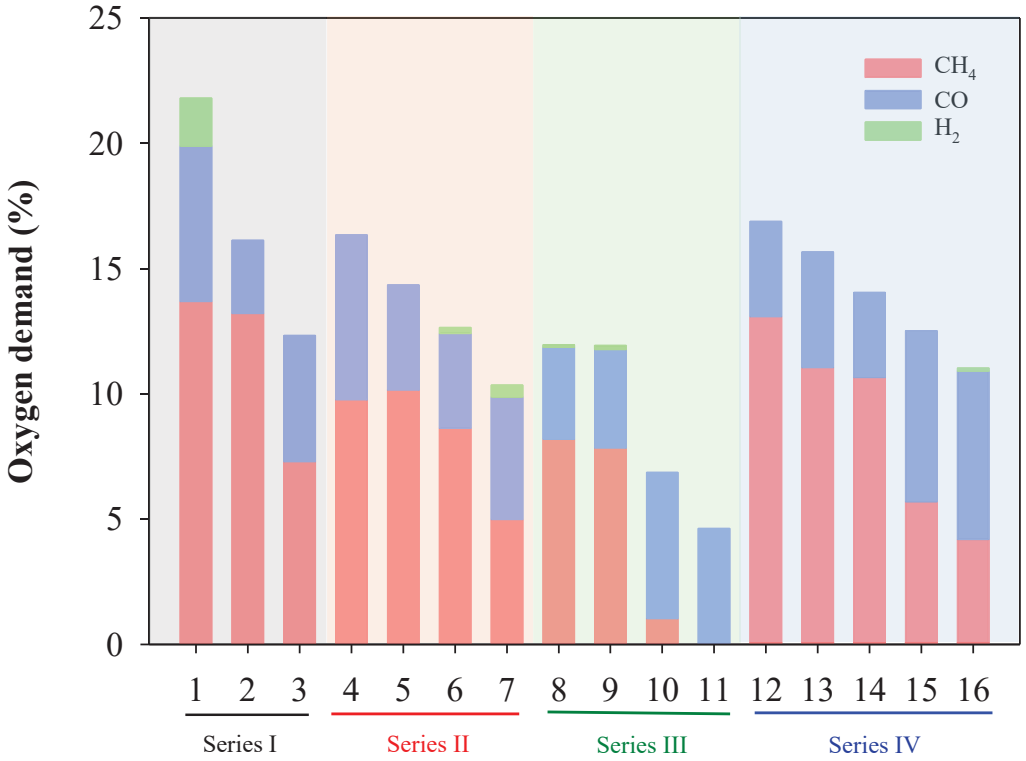

Figure 60. Comparison of partial oxygen demands for H_2, CO and CH_4 found at the fuel reactor exit in the different experimental tests in Table 14.

As a summary of the results shown in Figures 56 to 60, it was concluded that in order to maximize the oxygen release capacity of Mn66FeTi7 oxygen carrier in the fuel reactor and decrease the oxygen demand in biomass combustion, the air reactor should be operated with temperatures about 880 ºC and high air excess ratio, preferably about 1.8 or higher. Working under these operating conditions and using an averaged solids inventory of 1875 kg/MW_{th} in the fuel reactor, total oxygen demand values as low as 4.6% have been reached. Comparable values for the oxygen demand (3.4-6.7%) were reached recently by Schmitz et al. (2018) using a manganese-silicon-titanium oxygen carrier with the ability to release molecular oxygen. However, in this case, the fuel used was a low-volatile fuel (wood char).

3.1.2 Combustion under CLOU: Cu34Mn66

Biomass combustion under the CLOU mode has been reported to significantly reduce the total oxygen demand of the biomass combustion process compared to results under *i*G-CLC. Under the CLOU mode, the oxygen carrier releases molecular oxygen (O_2) that is able to easily react with the biomass devolatilization products in a similar way than in a conventional combustion. However, the oxygen carriers developed for the CLOU process (mainly based on copper oxides or perovskites) are commonly more expensive and with lower mechanical properties than those used under *i*G-CLC mode (Adánez et al. 2018). To reduce the high costs associated to copper oxides, mixed oxides have been proposed and among them, mixed oxides based on Cu-Mn have shown high oxygen uncoupling capability (Adánez-Rubio et al. 2016). Moreover, Cu-Mn mixed oxides have shown a lower temperature operating window than Cu-based oxygen carriers (750-850 ºC), see Figure 38, section 2.1.4.

In the present work, a mixed Cu-Mn oxide (Cu34Mn66) was used as oxygen carrier (**Papers IV and V**). Table 15 summarizes the experiments carried out with Cu34Mn66 with the three types of biomass (pine sawdust, olive stones and almond shells). A total of 65 h of biomass combustion were carried out with this oxygen carrier, without problems of agglomeration.

Figure 61 shows the gas concentrations in the outlet stream of the fuel and air reactors (dry basis) as a function of the operation time in the pine sawdust experiments, where the effect of the fuel reactor temperature was analysed (C5–C8). The fuel reactor temperature varied between 775 ºC and 850 ºC, and each temperature was maintained at a steady state for at least 60 min. No unburnt products (CH_4, CO or H_2) were detected in the gas outlet stream of the fuel reactor, even at the lower temperature (775 ºC). Therefore, all the volatiles were completely converted inside the fuel reactor by the molecular oxygen released by the oxygen carrier. It can be seen that an increase in the fuel reactor temperature resulted in an increase in the CO_2 concentration in the fuel reactor outlet gas stream. This was

caused by the increase in the char conversion inside the fuel reactor that decreased the CO_2 concentration at the air reactor outlet. Also worthy of note is the fact that that no gaseous oxygen was measured at the fuel reactor outlet which could be associated with the low fuel reactor temperature, together with the large proportion of volatiles in the biomass composition.

Table 15. Experimental conditions with Cu34Mn66 in the 1 kW_{th} experimental unit.

Test	FA (-)	T_{FR} (ºC)	T_{AR} (ºC)	$y_{O_2 in\ AR}$ (%)	ϕ (-)	$\dot{m}_{OC}$ (kg/h)	$\dot{m}_{sf}$ (kg/h)	P_{th} (W_{th})	m^*_{FR} (kg/MW_{th})	$norm.\dot{m}_{OC}$ ((kg/s)/MW_{th})
Pine sawdust										
C1	CO_2	850	800	21	**7.6**	**27.2**	0.082	435	2200	17.4
C2	CO_2	850	800	21	**5.3**	**19.3**	0.082	435	2200	12.3
C3	CO_2	850	800	21	**4.7**	**16.8**	0.082	435	2200	10.7
C4	CO_2	850	800	21	**2.3**	**8.7**	0.082	435	2200	5.6
C5	CO_2	**775**	800	21	3.9	22.5	0.14	740	1200	8.4
C6	CO_2	**800**	800	21	3.9	22.5	0.14	740	1200	8.4
C7	CO_2	**825**	800	21	3.9	22.5	0.14	740	1200	8.4
C8	CO_2	**850**	800	21	3.9	22.5	0.14	740	1200	8.4
C9	CO_2	800	800	10	3.9	22.5	**0.14**	740	1200	8.4
C0	CO_2	800	800	10	3.4	28.5	**0.19**	1000	900	7.9
C11	CO_2	800	800	10	2.6	28.5	**0.25**	1330	715	6.0
Olive stones										
C12	CO_2	**775**	800	21	3.0	20.3	0.173	860	1150	6.6
C13	CO_2	**800**	800	21	3.0	20.3	0.173	860	1150	6.6
C14	CO_2	**825**	800	21	3.0	20.3	0.173	860	1150	6.6
C15	CO_2	**850**	800	21	3.0	20.3	0.173	860	1150	6.6
Almond shells										
C16	CO_2	**775**	800	21	3.3	22.5	0.225	1040	760	6.0
C17	CO_2	**800**	800	21	3.3	22.5	0.225	1040	760	6.0
C18	CO_2	**825**	800	21	3.3	22.5	0.225	1040	760	6.0
C19	CO_2	**850**	800	21	3.3	22.5	0.225	1040	760	6.0

Figure 62 shows the combustion and CO_2 capture efficiencies, as well as the char conversion as a function of the fuel reactor temperature in experiments with the three types of biomass used in this work. It is remarkable that complete combustion of volatiles in the fuel reactor was obtained at such a low fuel reactor temperature as 775 ºC. The pine sawdust contained 81% volatile matter, therefore, even with this high volatile matter content, the results showed full combustion of the biomass in all the tests. The CO_2 capture efficiency with pine sawdust increased from 86% to about 98% when temperature in the fuel reactor increased from 775 to 850 ºC even without the use of carbon stripper in the 1 kW_{th} unit. However, the CO_2 capture efficiencies

obtained for almond shells and olive stones, were lower than those obtained for the pine sawdust. So, it seems that for types of biomass with lower reactivity than the pine sawdust, it would be necessary to increase the fuel reactor temperature or to install a carbon stripper to increase char conversion and thus reduce the amount of unburnt char transferred to the air reactor.

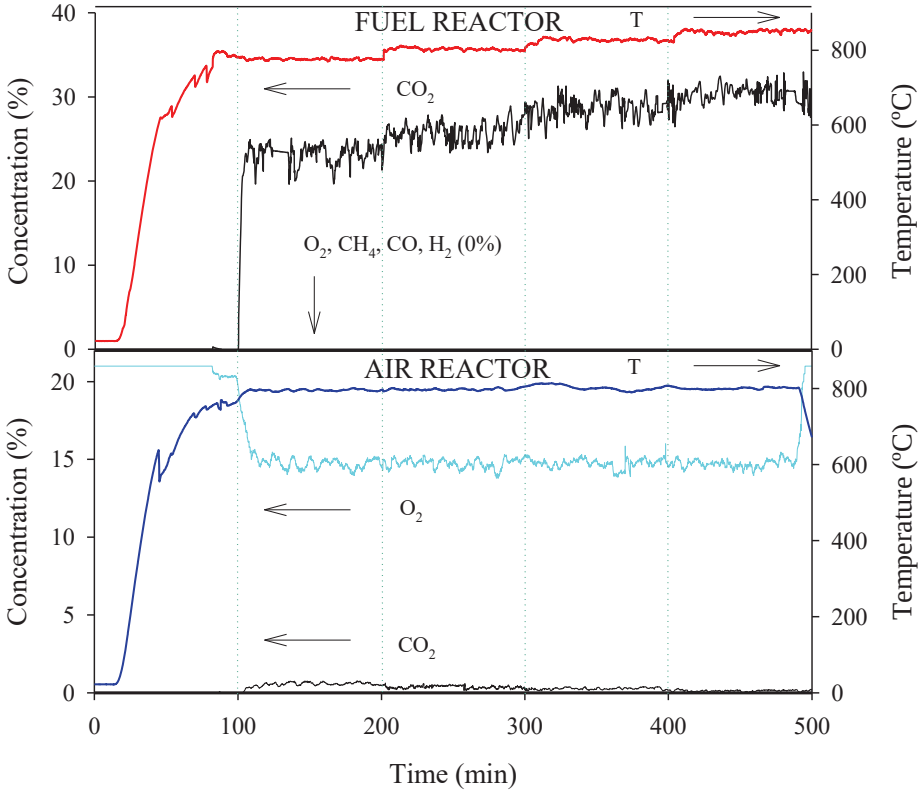

Figure 61. Evolution of the fuel and air reactors temperatures and gas outlet compositions in the 1 kW_{th} CLC unit. (Tests C5-C8).

Figure 63 shows the effect of the oxygen carrier-to-fuel ratio, ϕ, on the combustion and the CO_2 capture efficiencies (a) and on the char conversion (b) burning pine sawdust (C1–C4). Complete combustion to CO_2 and H_2O was always obtained in the fuel reactor. Therefore, the oxygen carrier under these conditions was able to generate enough oxygen, even with excess, in the fuel reactor stream to reach combustion efficiencies near to 100%. CO_2 capture efficiencies near 100% were also achieved. It was necessary to use ϕ values higher than 7 to observe a small reduction of the CO_2 capture efficiency from 100% to 99.6%, due to some unconverted char passed to the air reactor. It must be considered that the increase of ϕ was produced

by increasing the solids circulation rate, and then decreasing the residence time of char and oxygen carrier in the fuel reactor.

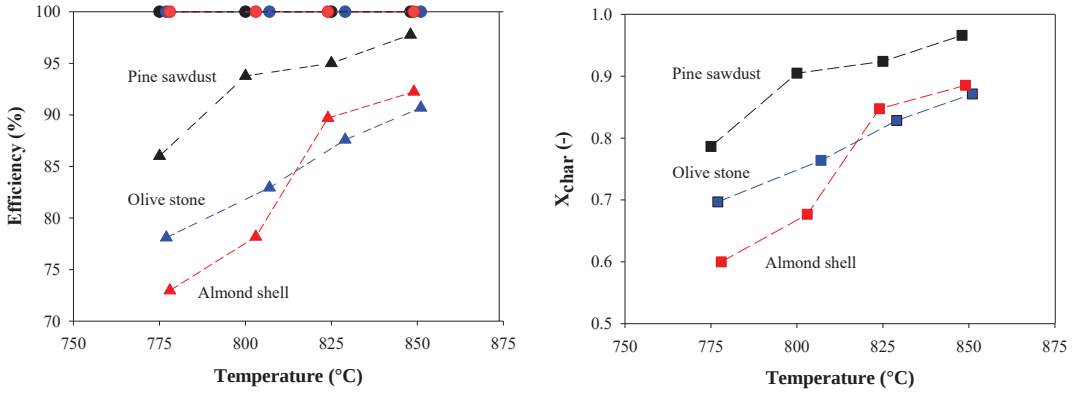

Figure 62. Effect of the fuel reactor temperature on the Combustion (●) and CO_2 capture (▲) efficiencies, and char conversion (■) for the three types of biomass: pine sawdust (C5–C8), almond shells (C12–C15) and olive stones (C16–C19).

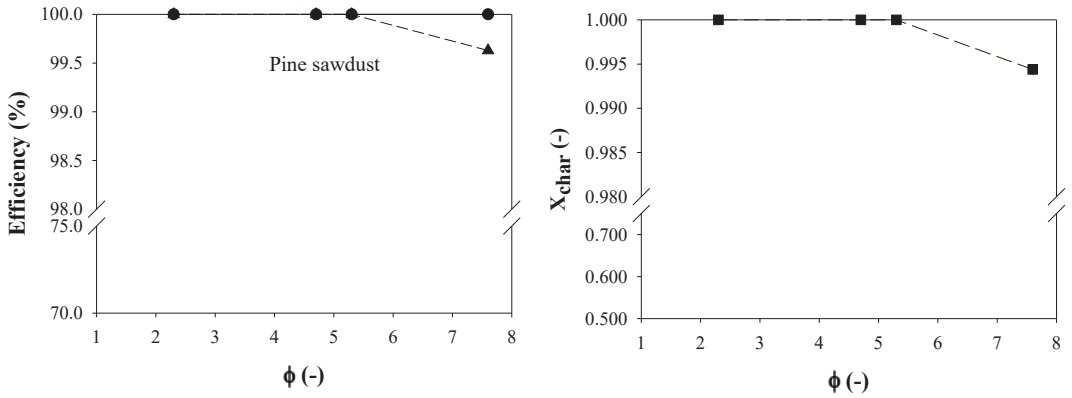

Figure 63. Effect of the oxygen to fuel ratio on the Combustion (●) and CO_2 capture (▲) efficiencies, and char conversion (■) in the 1 kW_{th} CLC unit (tests C1-C4, T_{FR}= 850 ºC).

Figure 64 shows the effect of the power input on the combustion and CO_2 capture efficiencies, and also on the char conversion at 800 ºC in the combustion of pine sawdust. It can be seen that the CO_2 capture efficiency decreased by increasing the power input from about 700 to 1300 W_{th}. When the biomass feeding rate increased, the CO_2 capture efficiency decreased as a result of the reduction in the

char conversion in the fuel reactor. Under these conditions, when the biomass feeding rate is increased, the ϕ value and the specific oxygen carrier inventory decreases. A decrease in the oxygen carrier-to-fuel ratio value increases oxygen carrier conversion in the fuel reactor, decreasing the rate at which O_2 is released by the Cu-Mn mixed oxide. Higher CO_2 capture efficiencies can be obtained increasing the fuel reactor temperature to 850 ºC, as it was seen, an optimum temperature to operate the fuel reactor with the Cu34Mn66 oxygen carrier (Adánez-Rubio et al. 2017a). It is important to highlight that even with a power input of 1330 W_{th} and a fuel reactor temperature as low as 800 ºC, a combustion efficiency near 100% was achieved.

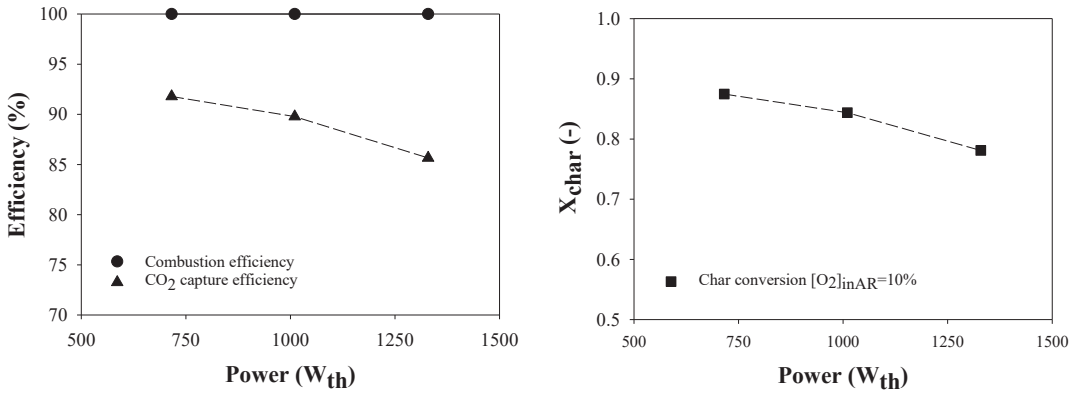

Figure 64. Effect of the power input on the Combustion (●) and CO_2 capture (▲) efficiencies, and char conversion (■) in the 1 kW_{th} CLC unit (C9–C11). T_{FR}=800 ºC, 10% O_2 in air reactor).

The results presented with the Cu34Mn66 synthetic oxygen carrier represent an important advance in the study of biomass fueled CLC. Throughout the experimental campaign, no unburnt gaseous compounds appeared at the fuel reactor outlet, despite the low temperatures used with this oxygen carrier, showing complete combustion efficiency in the fuel reactor, that is, the oxygen demand was near 0%. Compared to the number of studies concerning biomass combustion under iG-CLC, the number of studies under CLOU mode reported in literature is significantly less. Most of them use perovskite type oxygen carriers based on calcium manganates. Schmitz and Linderholm (2016) burned biochar in a 10 kW_{th} continuous unit with a bubbling fluidized bed reactor. Working at about 970 ºC, they reached values of CO_2

capture efficiency between 82 and 95.2% and the reported oxygen demand values were between 2.1 a 4.9%. Recently, Gogolev et al. (2019) also used a mixture of 80-90 wt% calcium manganite with 10-20 wt% ilmenite in the combustion of black wood pellets in a 100 kW_{th} continuous unit at temperatures close to 950 ºC. In this case, the fuel reactor was a circulating fluidized bed. Under these conditions, the lowest oxygen demand reported was about 3%.

3.1.3 Comparison of 1 kW_{th} experimental results

From the experimental results already presented, the high values obtained for the total oxygen demand can be pointed as the crucial parameter to be improved for the development of the bioCLC process as a BECCS technology. In this respect, a comparison of the oxygen demand values, obtained in the 1 kW_{th} CLC unit at comparable operating conditions for the different oxygen carriers (the Tierga ore, the manganese ores -MnGBHNE and MnSA- and the synthetic materials -Mn66FeTi7 and Cu34Mn66-) and using pine sawdust as fuel, is presented in Figure 65. CO_2 was used as fluidizing gas for all oxygen carriers, except for Tierga ore experimental campaign, which was carried out with water steam. However, no significant differences were observed in results using these two gasifying agents.

Figure 65 presents the total oxygen demand of the different oxygen carriers and also the partial oxygen demand of the different unburnt compounds (CH_4, CO and H_2). Starting with the ores results, lower amounts of hydrogen were obtained with the MnGBHNE compared to Tierga ore, achieving a total oxygen demand reduction despite the slightly higher amounts of CO measured. Total oxygen demand values continued decreasing using the MnSA oxygen carrier because of the negligible hydrogen detected as well as the CH_4 favoured oxidation (compared with both the Tierga and the MnGBHNE ores). Focusing on the synthetic Mn66FeTi7 oxygen carrier, initially similar oxygen demands to those obtained working with MnSA were reached. However, after optimization of the operating conditions, the oxygen demands with the Mn66FeTi7 oxygen carrier slightly decreased because this oxygen was able to release molecular oxygen, which improved the reaction rate with the unburnt compounds. Finally, the CLOU capacity of the Cu34Mn66 oxygen

carrier allowed to reach complete combustion of the volatiles in the fuel reactor, reaching an oxygen demand near to 0%.

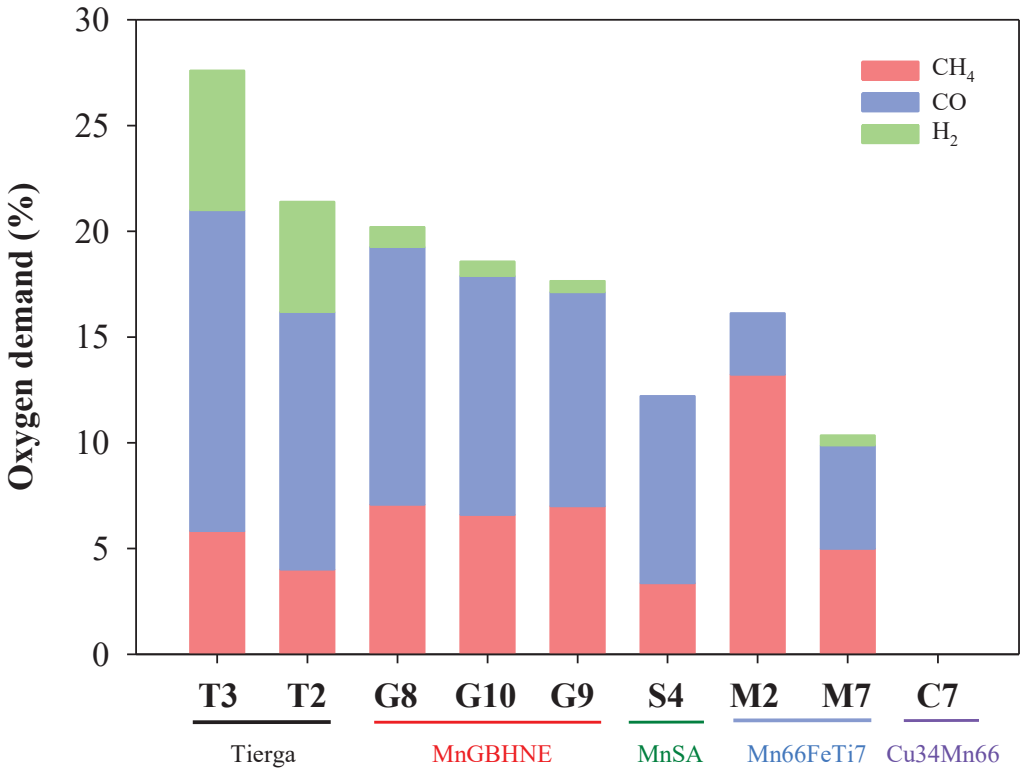

Figure 65. Effect of the different oxygen carrier used on the total oxygen demand (Ω_T) and the partial oxygen demands for the different oxygen carriers (T_{FR}≈ 900-950 ºC, m^*_{FR}≈ 650-1100 kg/MW_{th}, norm.$\dot{m}_{OC}$=3.9-4.9 kg/(s·MW_{th})).

3.1.4 Other aspects of the bioCLC process

3.1.4.1 Ash formation during combustion

The experience accumulated in the operation in fluidized bed boilers burning biomass shows that the characteristics of the biomass ash are important for the correct operation of the system. Alkali in biomass ash is released during combustion and could lead to problems such as corrosion and fouling of the boiler tubes. Moreover, some alkali present in biomass (mainly potassium) could react with the silica sand in the fluidized bed boiler forming sticky ash compounds, which can lead to

agglomeration of the bed. The most common configuration for a CLC system is two interconnected fluidized beds. Therefore, some of these problems previously encountered in biomass combustion in fluidized bed boilers can affect the performance of the bioCLC process. Nevertheless, as it was pointed by Pikkarainen et al. (2016) the risk of high-temperature corrosion of superheater tubes may be lower in bioCLC than in conventional biomass combustion since they might be placed in the air reactor and the alkali release would happen in the fuel reactor. Under this assumption, it would be possible to use higher steam values (temperature, pressure) in bioCLC improving the power generation efficiency from biomass.

There are many references available in literature concerning the effect of biomass ash in the bioCLC process. These studies refer to two aspects: effect on oxygen carrier reactivity and alkali emissions from the fuel/air reactors. The latter has been recently addressed by Gogolev et al. (2019) who explored the fate of alkali in the gaseous streams from fuel and air reactors from a 100 kW_{th} unit by on-line surface ionization measurements. The effect on the oxygen carrier reactivity has been evaluated with different types of oxygen carrier (mainly Mn and Fe-based) both in fixed (Haiming et al. 2015; Leion et al. 2017; Zevenhoven et al. 2018) or batch fluidized bed reactor (Song et al. (2016)) as well as continuous CLC units of different size (Haiming et al. 2011; Mendiara et al. 2013a; Adánez-Rubio et al. 2014; Niu et al. 2015; Schmitz et al. 2016; Sun et al. 2018; Gogolev et al. 2019; Hildor et al. 2019; Hanning et al. 2018).

The interaction of the oxygen carriers with alkali compounds in biomass ash showed widely different behavior. Mattison et al. (2019) impregnated two manganese ores and an iron-based waste material with alkali (K) in order to explore the behavior of oxygen carriers. The two manganese ores retained almost all alkali after redox testing in a batch fluidized bed reactor but the iron-based waste lost most alkali to the gas phase during testing. In the operation in continuous units, some authors found evidences of ash deposition on the oxygen carrier surface affecting its reactivity (Haiming et al. 2015), although some others did not report changes in the reactivity of the oxygen carriers used (Mendiara et al. 2013a; Adánez-Rubio et al.

2014; Pikkarainen et al. 2016). Regarding agglomeration, Haiming et al. (2015) found that SiO_2-rich biomass ash was likely to be converted into potassium silicates being the cause of serious particle sintering of oxygen carrier. Leion et al. (2017) also pointed to this effect of SiO_2 in the biomass ash. However, Zevenhoven et al. (2018) established from experiments with ilmenite in a fixed bed (crucible) that the agglomeration mechanisms depend on the major potassium compound found in the ash: KCl glued the particles together, whereas K_2CO_3 reacted with the bed particles. KH_2PO_4 reacted with the bed material and glued the particles together. K_2SO_4 remained non-reactive and did not influence the agglomeration of ilmenite bed particles.

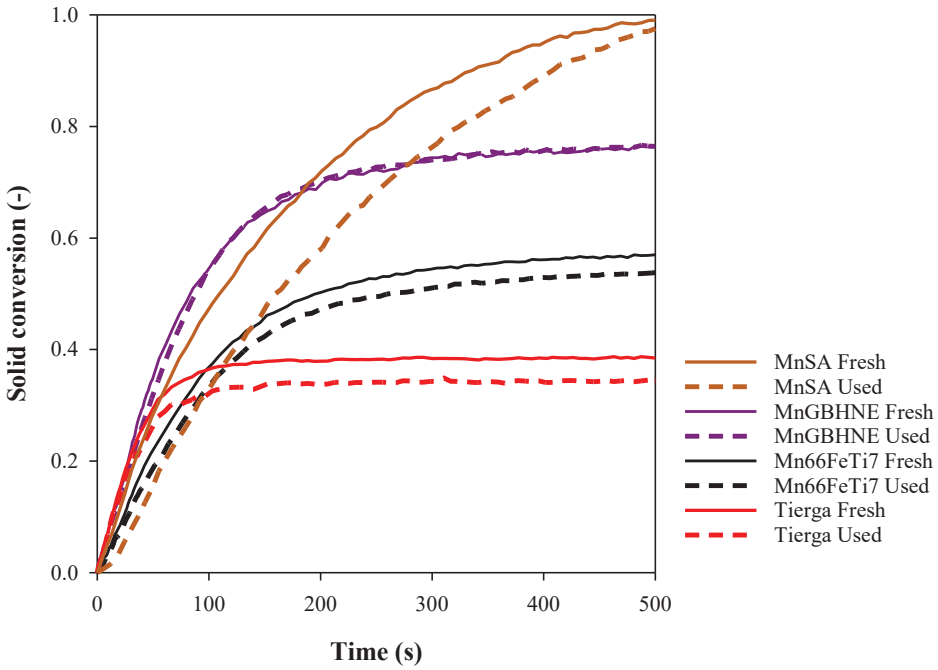

Figure 66. Conversion versus times curves obtained for fresh and used samples of the different oxygen carriers (T = 950 ºC, 15% CH_4 + 20 % H_2O).

In the present work, neither ash deposition on the oxygen carrier particles nor agglomeration problems during operation were found within the experimental campaigns in the 1 kW_{th} unit with any of the oxygen carriers tested. Moreover, the reactivity of the different oxygen carrier materials before and after the corresponding experimental campaigns carried out in the 1 kW_{th} CLC unit was evaluated in the TGA, already described in the experimental section. Figure 66 shows conversion

versus time curves obtained with the different oxygen carriers. No significant deactivation changes could be observed for any of the analyzed oxygen carriers. Slight reductions in the oxygen transport capacity can be observed in the case of the Tierga ore and the Mn66FeTi7 while similar behavior were obtained in the case of the manganese ores despite the initially lower conversion rate of the used MnSA.

Nevertheless, the influence of the presence in the biomass ash of alkali and alkaline earth metals on the fluidization behaviour and reactivity of the oxygen carriers tested was investigated in a batch fluidized bed reactor described in the experimental section during a 4-month stay at the Institute of Solids Process Engineering and Particle Technology in Hamburg Technological University (Germany). In a previous study carried out in the same batch fluidized bed reactor used at Hamburg University, Song et al. (2016) studied the effect of the addition of NaCl to the oxygen carrier fluidization at temperatures over the salt's melting point. Pressure drop variations in the fluidized bed were analyzed as an important and representative variable of the fluidization behavior. In this study, about 280 g of iron ore were used as bed material and three additions of 0.5 g each of sodium chloride were carried out at 900°C. It was observed an important pressure drop variation during the experimental procedure and agglomerates were found in the analysis of the samples. It was assumed that the salt acted as glue for the iron ore particles, causing agglomeration that produced the pressure drop. Moreover, sodium chloride was found in SEM analysis presented by Song et al. (2016) on the oxygen carrier particles surfaces.

During the research stay at Hamburg University similar experiments were performed with Tierga ore, ilmenite, MnGBHNE and a synthetic iron-based oxygen carrier (Fe20γAl) and three different salts (NaCl, KCl and $CaCl_2$). A total of 5 g of each salt were gradually added to each oxygen carrier, using two different oxygen carrier reduction conversion degrees (50 and 75 %) at 950 ºC. Figure 67 presents an example of the pressure drop variations measured in the fluidized bed in a test at 950 ºC during three $CaCl_2$ additions to a Tierga ore bed identified by (a). As it can be observed, high-pressure drop oscillations were observed just during the salt

introduction. After that, a slight increase of the pressure drop of the fluidized bed was measured to finally return to previous values. No significant changes were found for the bed pressure drop despite the higher salt amounts added compared to Song et al. (2016). This behaviour was observed for all the salt additions and all the oxygen carriers tested. In this way, no defluidization problems were found analysing the fluidized bed pressure drop variations.

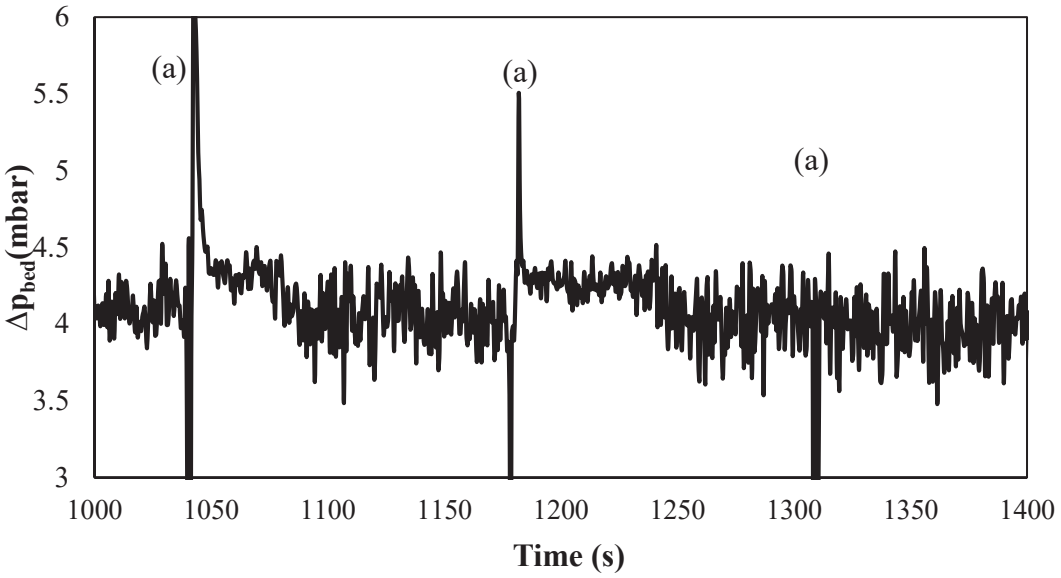

Figure 67. Fluidized bed pressure drop using 250 g of iron ore (Tierga) at 950ºC with $CaCl_2$

In addition to fluidization properties, no significant changes in the reactivity for any of the oxygen carriers used during the redox cycles carried out for the salt addition experiments were observed. Moreover, no visible agglomeration for any tested oxygen carrier and salt was observed, neither in the oxygen carrier samples extracted online from the fluidized bed nor after the experiments during the oxygen carrier batch change nor in the SEM analyses carried out to the samples extracted from the bed. SEM images also show no salt deposition on the oxygen carrier particles surface. As an example, Figure 68 presents the SEM image (a) and an element mapping (b) for the Fe20γAl oxygen carrier after KCl addition, where it can be observed that K on the surface of the oxygen carrier is almost not detected.

It should be considered that results reported to date in batch fluidized bed reactors or continuous CLC units regarding biomass ash effect on bioCLC performance may be limited by the number of hours of continuous operation reached (Mendiara et al. 2018a). Longer operating periods under similar conditions to those existing in a chemical looping unit would be needed in order to establish solid conclusions. In this respect, the oxygen carrier-aided combustion (OCAC) process can be of great interest. In the OCAC process, biomass is combusted in a fluidized bed using an oxygen carrier as bed material. In this case, the combustion efficiency of the process is improved, although combustion is performed with air, and therefore CO_2 capture is not achieved. The operational experience gained through the OCAC process can offer information on what happens to the oxygen carrier particles during their long exposure to ash in a combustion environment. Recent results were obtained in a 12 MW_{th} CFB boiler at Chalmers University where a Fe-based waste material from the steel industry and a manganese ore were tested as oxygen carriers and the effect of biomass ash evaluated. In both cases potassium as well as silicon and calcium were found to be deposited on the oxygen carrier surface (Hanning et al. 2019; Hildor et al. 2019).

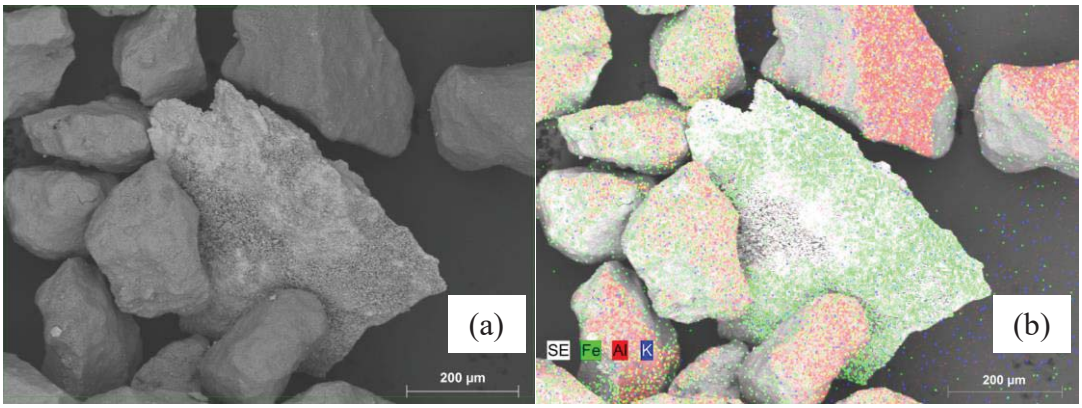

Figure 68. SEM image after the addition of about 5 g of KCl for the Fe20γAl.

3.1.4.2 NO_x emissions

During the experimental campaigns carried out with the different oxygen carrier materials attention was paid to the possible emissions generated in the bioCLC process, especially NO_x emissions. One of the advantages of CLC over conventional

combustion is the reduction in NO_x (Ishida and Jin 1996) formation due to two reasons. First, the lower combustion temperatures used in the bioCLC process compared to conventional combustion avoid thermal NO_x formation. Thus, NO_x emission will mainly come from the fuel nitrogen. Second, since the nitrogen fuel released to the fuel reactor stream will be capture, the only NO_x considered as emissions would be those appearing in the air reactor outlet stream. This NO_x would be formed in the combustion of the unconverted char that may reach the air reactor. In the specific case of the bioCLC process, the unconverted char in the air reactor is minimal since high CO_2 capture efficiencies are reached in the process, as it has been outlined before. Considering this, the presence of NO_x in both fuel and air reactor streams has been analysed in all the experimental campaigns performed with the five oxygen carriers and the three types of biomass studied. The main results and conclusions about NO_x emissions are summarized next. Some of these conclusions were already outlined in **Paper VI**.

The first consideration when analysing NO_x emissions results is the operating mode under which they were obtained, i.e. *i*G-CLC or CLOU. The optimal temperature range for each process used in the fuel reactor is different and this fact can affect the nitrogen chemistry occurring in the fuel reactor. Performance results from the experiments were discussed in detail in Figure 69 for the experiments with Tierga ore (as reference results for the *i*G-CLC mode) and with Cu34Mn66 (CLOU mode) in order to be afterwards correlated to the results obtained in the analysis of pollutant emissions. It can be seen under the *i*G-CLC mode high values of CO_2 capture efficiencies were obtained with all the types of biomass. The values increase with the fuel reactor temperature reaching almost 100% at 980ºC. These values for CO_2 capture efficiencies are correlated to those calculated for the char conversion in the fuel reactor, which also increase with the fuel reactor temperature from 70-80 to almost 100%. In *i*G-CLC, low combustion efficiencies (about 70%) were found for all the types of biomass tested mainly due to the fraction of volatiles released by the biomass that are not burnt by the oxygen carrier. In the CLOU experiments also shown in Figure 69, the CO_2 capture efficiencies increased with temperature because of the char reactivity increase at higher temperatures in the fuel reactor and therefore, less unconverted char reaches the air reactor. With this Cu-Mn based oxygen carrier

values of CO_2 capture efficiencies about 98% at 850ºC were obtained. In order to increase the values of the CO_2 capture efficiencies a carbon stripper would be needed. The combustion efficiencies for CLOU experiments in Figure 69 were always close to 100% even at the lowest temperature (775ºC), due to the release of gaseous oxygen in the fuel reactor.

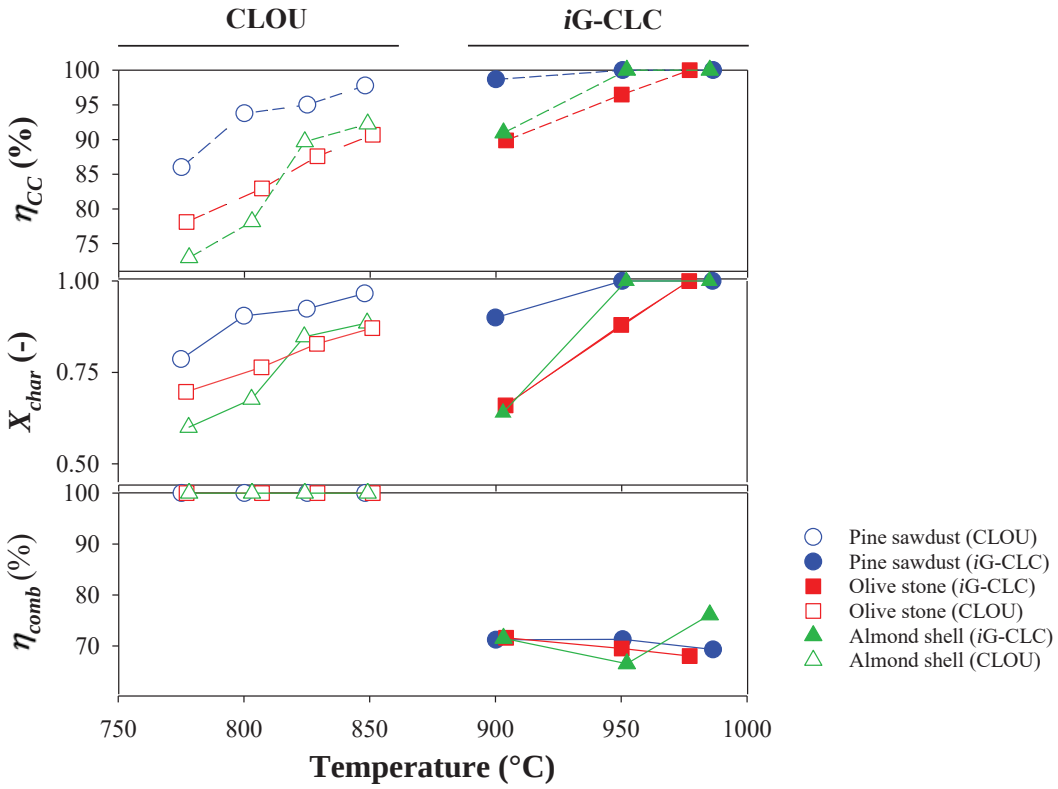

Figure 69. Effect of the fuel reactor temperature on the combustion ($\eta_{comb,FR}$) and CO_2 capture efficiencies (η_{CC}) and char conversion ($X_{char,FR}$) for iG-CLC (filled symbols) and CLOU (open symbols) burning pine sawdust, olive stones and almond shells.

***Fuel-N distribution** between fuel and air reactors*

There is some information in literature about the fate of fuel-N in CLC processes, mainly referred to coal as fuel (Adánez et al. 2018). The majority of the *i*G-CLC studies carried out conclude that most of fuel-N is released in the fuel reactor as N_2 and only low amounts of NO_x can be found (Mendiara et al. 2014b). In the air reactor, the fuel-N in the unconverted char that may reach the air reactor is released

as NO. According to the composition of the different types of biomass in Table 8, the highest nitrogen content is observed for pine sawdust (0.3 wt%), while olive stones and almond shells are reported 0.2 wt%. Fuel-N in biomass is released during biomass devolatilization. The dominant nitrogenous volatile species are NH_3 and HCN (Werther et al. 2000). Both can evolve to either N_2 or NO, depending on the combustion conditions. On the other hand, char-bound nitrogen can evolve to NO, N_2O or N_2. However, at temperatures higher than 900ºC N_2O decomposes to N_2 (Glarborg et al. 2003). In the experiments performed under both *i*G-CLC and CLOU modes, different atmospheres can be found in the fuel reactor when biomass devolatilization takes place. In the experiments with NO_x measurement, CO_2 was supplied to the fuel reactor as gasifying/fluidizing agent. Therefore, in *i*G-CLC a reducing environment is generated due to the presence of gasification products (H_2 and CO). However, oxygen is present in the reacting atmosphere under CLOU operation. In both processes, N_2 from air is not present, which is an important difference compared to the conventional combustion in air.

Figure 70 presents fuel-N distribution between fuel and air reactors in the experiments under *i*G-CLC and CLOU modes with the different oxygen carrier using pine sawdust, although similar conclusions could be obtained with the olive stones and almond shells (**Paper VI**). Despite the different operating temperature under *i*G-CLC and CLOU, 900 ºC were chosen for comparison in *i*G-CLC and 850 ºC for the CLOU mode of operation. As a general conclusion shown in Figure 70, for both operating modes, the most of the nitrogen in the fuel was released in the fuel reactor, in line with the results previously reported in literature for CLC using coal as fuel (Adánez et al. 2018). Moreover, nitrogen emissions in the air reactor were only measured using the Tierga ore and the Cu34Mn66 at those conditions. In this way, the high CO_2 capture efficiencies reached with all the oxygen carriers used avoided the nitrogen emissions at these conditions with the manganese ores and the Mn66FeTi7. Moreover, the temperature increase slightly reduces the amount of char achieving the air reactor, being necessary temperatures higher than 850 ºC with the Cu34Mn66 and 900 ºC with the rest of the used oxygen carriers (Tierga, MnGBHNE, MnSA and Mn66FeTi7) to obtain negligible nitrogen emissions in the air reactor.

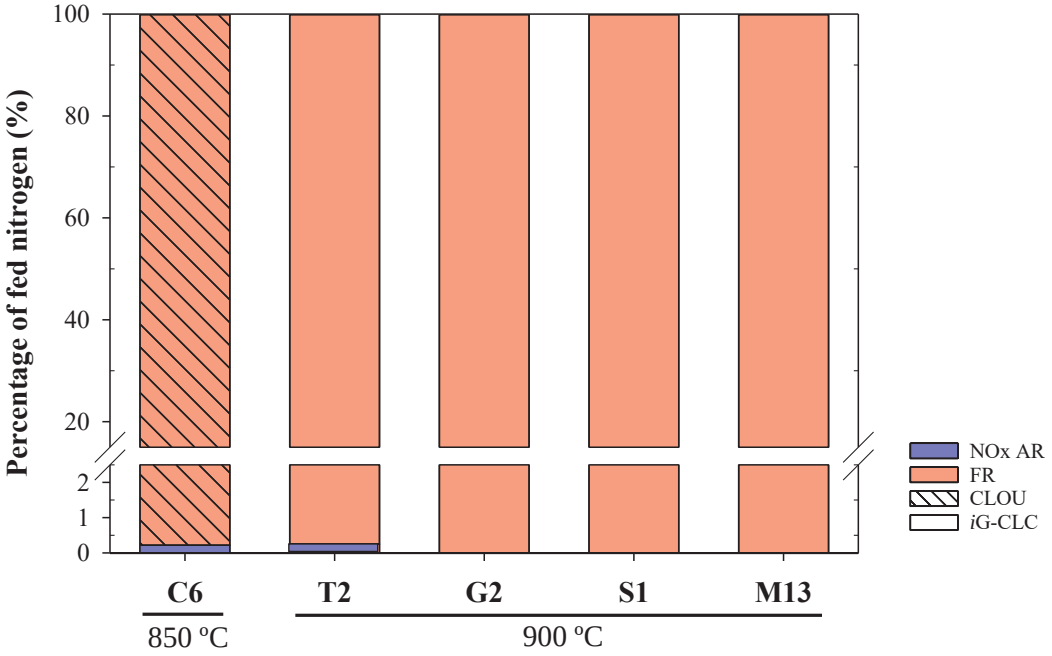

Figure 70. Fuel-N distribution between the fuel and the air reactor for iG-CLC and CLOU processes burning pine sawdust (m^*_{FR}≈ 650-1250 kg/MW_{th}, norm.$\dot{m}_{OC}$=2.5-3.9 kg/(s·MW_{th})).

*Evolution of nitrogen species in the **fuel reactor***

Neither under *i*G-CLC nor under CLOU mode the presence of NH_3 or HCN was detected at the fuel reactor outlet. As it is shown in Table 16, only N_2, NO_x and N_2O were identified depending on the conditions. This indicated that all the nitrogen released as NH_3 or HCN in the devolatilization was converted via homogenous or heterogeneous reactions.

Table 16. Nitrogen species found at the fuel reactor outlet in the iG-CLC and CLOU experiments.

***i*G-CLC**	N_2, NO_x
CLOU	N_2, NO_x, N_2O

Both under *i*G-CLC and CLOU, the major nitrogen species found in the fuel reactor was N_2, followed by NO_x and by certain amounts of N_2O, the later only in the case of CLOU experiments with the Cu34Mn66. The presence of N_2O can be attributed to the temperature range of operation (775-850ºC) and the release of

molecular oxygen in the fuel reactor atmosphere (Glarborg et al. 2003). Nevertheless, the concentration of N_2O in the fuel reactor outlet stream in the CLOU experiments decreased with temperature to values close to zero at 850ºC.

Among de different types of biomass, the nitrogen measured in the fuel reactor as N_2 in the experiments at the highest temperature (980 ºC) with the pine sawdust, olive stones and almond shells, were respectively, 97.2, 96.7 and 94.6 wt% with the Tierga ore under *i*G-CLC. The corresponding percentages under the CLOU mode with the Cu34Mn66 operating at 850ºC were respectively 97.3, 92.0 and 81.5 wt%, maintaining the same order of biomass types.

Regarding the amount of NO present in the fuel reactor outlet stream the value of the NO_x/C molar ratio was calculated in the experiments with pine sawdust in order to determine whether this ratio was lower than that recommended for CO_2 concentrated streams to be transported and stored with each oxygen carrier. The quality of the CO_2 to be captured can be affected by the presence of different compounds in the outlet stream from the fuel reactor. Steam, N_2, O_2, CO, H_2, CH_4 and other hydrocarbons, SO_2, particles and also NO_x levels should be controlled in order to ensure that the captured CO_2 stream can be transported and safely stored. To date, no legal requirements exist and only recommendations have been outlined for the quality of CO_2 (de Visser et al. 2008). The limit marked by these recommendations regarding NO_x/C molar ratio content in the CO_2 stream is 280 ppm, calculated with values in Table 4, see section 1.4. Figure 71 shows the different trends in the evolution of the molar ratio NO_x/C (expressed in ppm) with the fuel reactor temperature for both *i*G-CLC and CLOU. All the experiments presented were performed at comparable conditions with any of the oxygen carriers used, the ratio was well below the recommended value. The NO_x/C ratio increased with temperature in CLOU since more oxygen was released by the oxygen carrier with the increase of the fuel reactor temperature (Adánez-Rubio et al. 2017a). The presence of gaseous oxygen in the fuel reactor atmosphere favours fuel-N oxidation to NO (Williams et al. 2012).

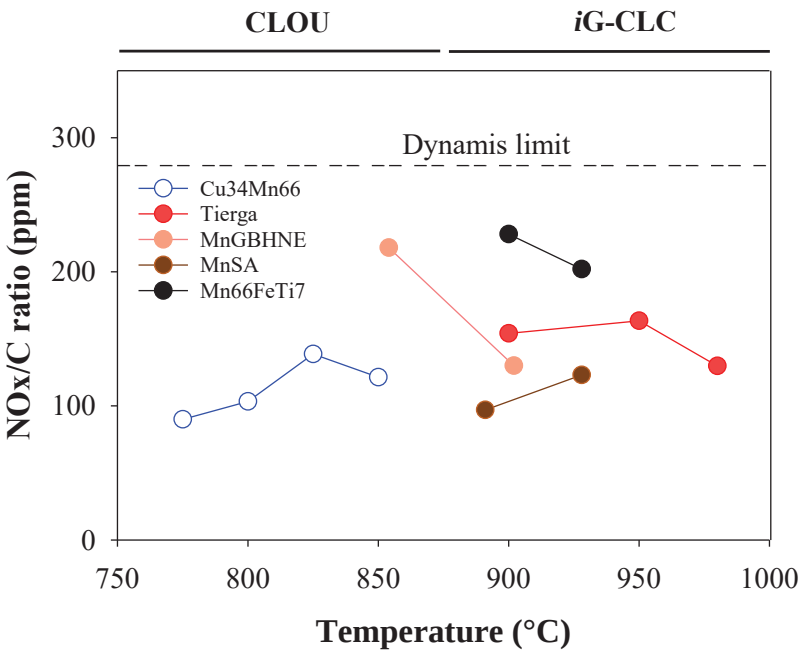

Figure 71. Effect of the fuel reactor temperature on the molar ratio NO_x/C for CLOU (open symbols) and iG-CLC (filled symbols) in experiments using pine sawdust ($norm.\dot{m}_{OC}$=3.1-3.9 kg/(s·MW_{th})).

*Evolution of nitrogen species in the **air reactor***

Both during *i*G-CLC and CLOU operation, the main nitrogen species besides N_2 found at the air reactor outlet was NO. In this case, no N_2O was detected. This NO is originated in the oxidation of the fuel-N present in the unconverted char that reaches the air reactor. Figure 72 shows the evolution of the NO concentration with the fuel reactor temperature. The NO concentrations have been normalized to 6% O_2 in the stream, as it is indicated in the legal emission limit. Results in Figure 72 correspond to pine sawdust but the trends for both operating modes, *i*G-CLC and CLOU, are the same for all the types of biomass tested. The NO emissions decreased when the fuel reactor temperature was increased. The reason for this trend is that an increase in the fuel reactor temperature enhances the char gasification. If more char is converted, less unconverted char is transferred to the air reactor. Thus, the fuel-N released in the air reactor is decreased. It should be taken into account that the NO present in the outlet stream of the air reactor can be considered an emission to the atmosphere and therefore, the levels should fulfil those specified in the current

legislation (European Council 2010). The Directive 2010/75/EU on industrial emissions (integrated pollution prevention and control) sets the NO_x emission most restrictive limit to 150 mg/Nm^3 (normalized to 6% O_2) for new installations in the EU and for the highest power (> 300 MW). Values shown in Figure 72 presented NO_x levels at the air reactor outlet in the range of 0-10 mg/Nm^3 for the CLOU and *i*G-CLC experiments with pine sawdust, then lower than legal limits. Thus, no emission problems could be anticipated when biomass was used as fuel in a CLC system. Moreover, these values were obtained in the absence of a carbon striper. If there was a carbon stripper, this would decrease the unconverted char bypassed to the air reactor and hence the NO_x formed in the air reactor.

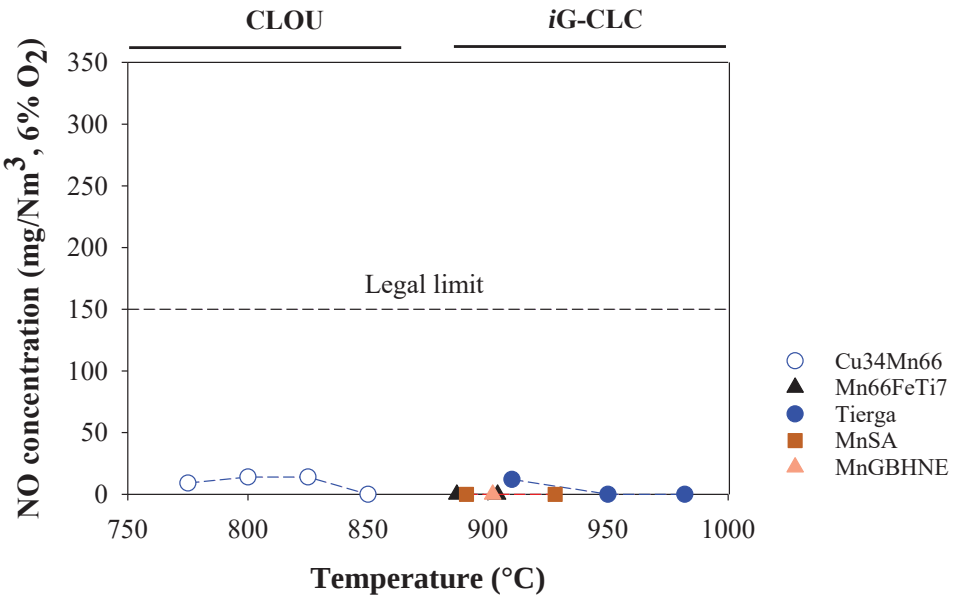

Figure 72. Effect of the fuel reactor temperature on the NO_x concentrations in mg/Nm^3 (6% O_2) at the air reactor outlet for CLOU (open symbols) and iG-CLC (filled symbols) processes burning pine sawdust.

3.1.4.3 Tar formation

Another aspect of the bioCLC process that was analysed in the present work was tar formation. Traditionally, tar formation control during gasification represented one of the main challenges in the use of biomass. Tar has been reported to cause fouling problems downstream of the gasification chamber and strict limits have been imposed for its presence when the syngas produced is intended to be used

for energy generation or chemicals production. In the case of the CLC process, scarce information about tar formation can be found. The presence of tar is limited to the fuel reactor outlet and it is therefore affecting the quality of the CO_2 stream there generated and the further operations prior to CO_2 storage (compression and transport). In the recommendations summarized by de Visser about CO_2 quality (de Visser et al. 2008), there is no clear reference to tar. Nevertheless, in order to set a range of values for safe operation, the limit given by (Reed et al. 1987) for compressing and piping any distance a biomass gasification gas can be used. According to these authors, the tar content should be lower than 0.5 g/Nm^3. The main results and conclusions about tar formation are summarized next. Some of these conclusions were already outlined in **Paper VI**.

In the experiments under *i*G-CLC and CLOU modes, the tar compounds at the fuel reactor outlet were detected and quantified. In these experiments, steam was used in the fuel reactor as fluidizing agent in *i*G-CLC and nitrogen in CLOU. Figure 73 plotted the tar compounds grouped as primary, secondary tertiary and alkyl-tertiary tars (Evans and Milne 1987a, 1987b) and also includes lineal hydrocarbons. Figure 73 shows the concentration values in the experiments with the different oxygen carriers tested, the three ores (iron and manganese based) and the Mn66FeTi7 at about 900-950 ºC and the synthetic Cu34Mn66 at the highest temperature evaluated (825 ºC), all using pine sawdust.

Focusing in the *i*G-CLC measurements, Figure 73, it can be seen that similar types of compounds were obtained for both iron and MnGBHNE ores. Moreover, tertiary compounds were the major tar compounds followed by the alkyl-tertiary and secondary tars with both oxygen carriers. At these conditions, the total tar values obtained for the iron ore almost doubled those obtained for the MnGBHNE (3.8 g/Nm^3 and 1.9 g/Nm^3) mostly because of the reduction in the presence of alkyl-tertiary tar compounds. Furthermore, in the case of the iron ore, no significant differences were found among types of biomass, see (**Paper VI**). Similar behavior was found in the tar formation between S4 and P15, obtaining similar tar types despite the lower amount produced with the Mn66FeTi7 (0.4 g/Nm^3 and 0.2 g/Nm^3 respectively).

Recently, results from operation the in a boiler/gasifier loop (12 and 2-4 MW_{th}, respectively) at Chalmers University of Technology using ilmenite and a manganese ore as oxygen carriers with wood pellets reported 21-22 g tar per kg dry-ash-free fuel at 830 ºC (Berdugo Vilches et al. 2017). The values obtained in the present work were 8-13 times lower than those previously reported. Besides the different methodology employed in the tar collection and analysis, the differences can be also attributed to the higher temperatures used in the fuel reactor during gasification in the present work.

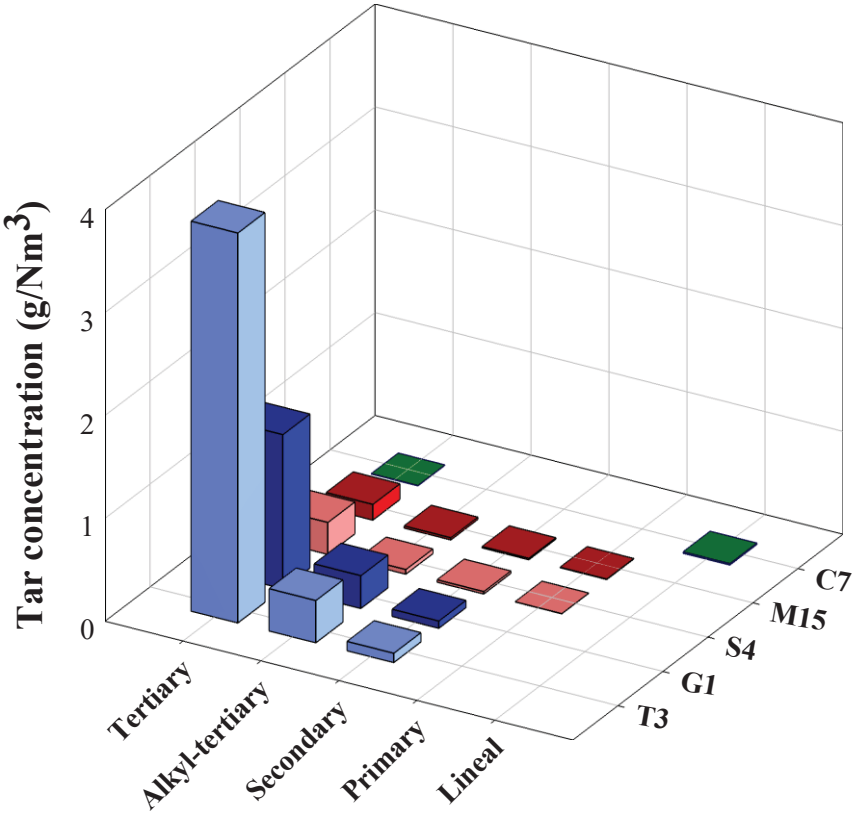

Figure 73. Effect of the fuel reactor temperature on the tar concentration using pine sawdust under CLOU and iG-CLC.

The tar concentration values obtained under *i*G-CLC were higher than those considered adequate to avoid operational problems derived from tar condensation and subsequent polymerization leading to fouling. Nevertheless, no fouling problems downstream can be anticipated in CLC due to the tar presence. In an industrial CLC unit tar compounds would be burned in the oxygen polishing step after the fuel reactor. The amount of tar found in the experimental campaign performed, <

5 g/Nm^3, would represent an increase of about 1% in the total oxygen demand from the unburnt compounds in the fuel reactor outlet. Tertiary tars showed the higher concentrations with all the oxygen carriers used, showing also the major differences among oxygen carriers. Comparing both operating CLC modes, significant differences were found. First of all, the different levels of tar found. The values determined for CLOU were about two orders of magnitude lower (< 0.02 g/Nm^3) in a lower fuel reactor temperature interval (775-850ºC). These tar levels are so low that it should not represent a problem in the CO_2 transport-storage chain. Tar composition obtained in CLOU experiments showed some differences with respect to that obtained in *i*G-CLC. In the CLOU experiments, low amounts of naphthalene were found but certain quantities of linear or branched hydrocarbons are detected, such as dodecane or tetradecane. This may indicate a different mechanism for the consumption/reforming of the tar under CLOU environment when it is compared to *i*G-CLC. In any case, the combustion of biomass using both of any combustion modes results in lower tar content in the product gas stream than in conventional processes such as biomass air-fired gasification. Note that for an air-blown circulating fluidized bed (CFB) gasifier a typical tar content of about 10 g/Nm^3 has been reported (Anis and Zainal 2011).

3.2 Scale-up of the bioCLC process: Operation in a 20 kW_{th} unit

The experience gained in the evaluation of the bioCLC process in the 1 kW_{th} continuous unit is of great value for the scaling-up of the technology. The principal conclusion drawn from the experimental campaigns carried out was the need to reduce the high oxygen demand values obtained in the bioCLC process. This high oxygen demand values found, associated to the high volatile content of biomass. The high oxygen demand is a drawback in the development of the bioCLC process as costly measures should be taken in order to reach complete combustion of the fuel.

Bearing this idea in mind, an experimental campaign based on the Tierga ore as oxygen carrier was designed to be performed at the 20 kW_{th} CLC unit existing at the *Instituto de Carboquímica* (ICB-CSIC) (García-Labiano et al. 2018). As it was mentioned, this unit consists of two interconnected circulating fluidized beds acting as fuel and air reactors, respectively. Table 17 summarizes the experiments carried out with Tierga ore and olive stones. The solid fuel conversion values obtained were in the range of 75-91%, which means that about 9-25% of the carbon in biomass leaked from the fuel reactor cyclone as elutriated char particles. A total of 60 hours of continuous hot fluidization were carried out, of which 20 hours corresponded to biomass combustion by *i*G-CLC mode using both H_2O and CO_2 as gasifying agent.

Table 17. Experimental conditions with the Tierga ore in the 20 kW_{th} experimental unit.

Test	FA (-)	T_{FR} (ºC)	T_{AR} (ºC)	ϕ (-)	τ_{FR} (s)	$\dot{m}_{OC}$ (kg/h)	$\dot{m}_{sf}$ (kg/h)	P_{th} (kW_{th})	m^*_{FR} (kg/MW_{th})	$norm.\dot{m}_{OC}$ ((kg/s)/MW_{th})
H1	H_2O	900	1000	1.1	164	60	1.1	5.1	540	3.1
H2	H_2O	900	1000	1.8	122	115	1.3	6.1	630	2.9
H3	H_2O	900	1000	1.8	158	90	1.0	4.8	850	4.9
H4	CO_2	900	1000	**1.8**	212	115	1.4	6.5	1000	1.5
H5	H_2O	900	1000	2.4	230	115	1.0	4.8	1550	4.1
H6	CO_2	900	1000	**2.4**	135	170	1.4	6.5	1035	3.0
H7	CO_2	900	1000	5.4	65	375	1.4	6.5	1050	3.1

Figure 74 shows the time evolution with the temperature and gas concentrations in both the fuel (dry and nitrogen free) and air reactors during tests H2-H4. The unit operation was smooth and the response to a gas flow change was quite quick. Solid flows and pressure drops were kept stable during the steady state operation. Steady state was usually reached on 20-30 min after operating conditions modification for every test, with roughly stable concentration values of CO_2, CO, H_2 and CH_4 in the fuel reactor, and O_2 and CO_2 in the air reactor. H4 uses CO_2 as gasifying agent, this explains the strong gap of unburned products (H_2, CO and CH_4) in the fuel reactor only because of the dilution process. It has to be considered that plots in Figure 74 correspond to dry and nitrogen free basis.

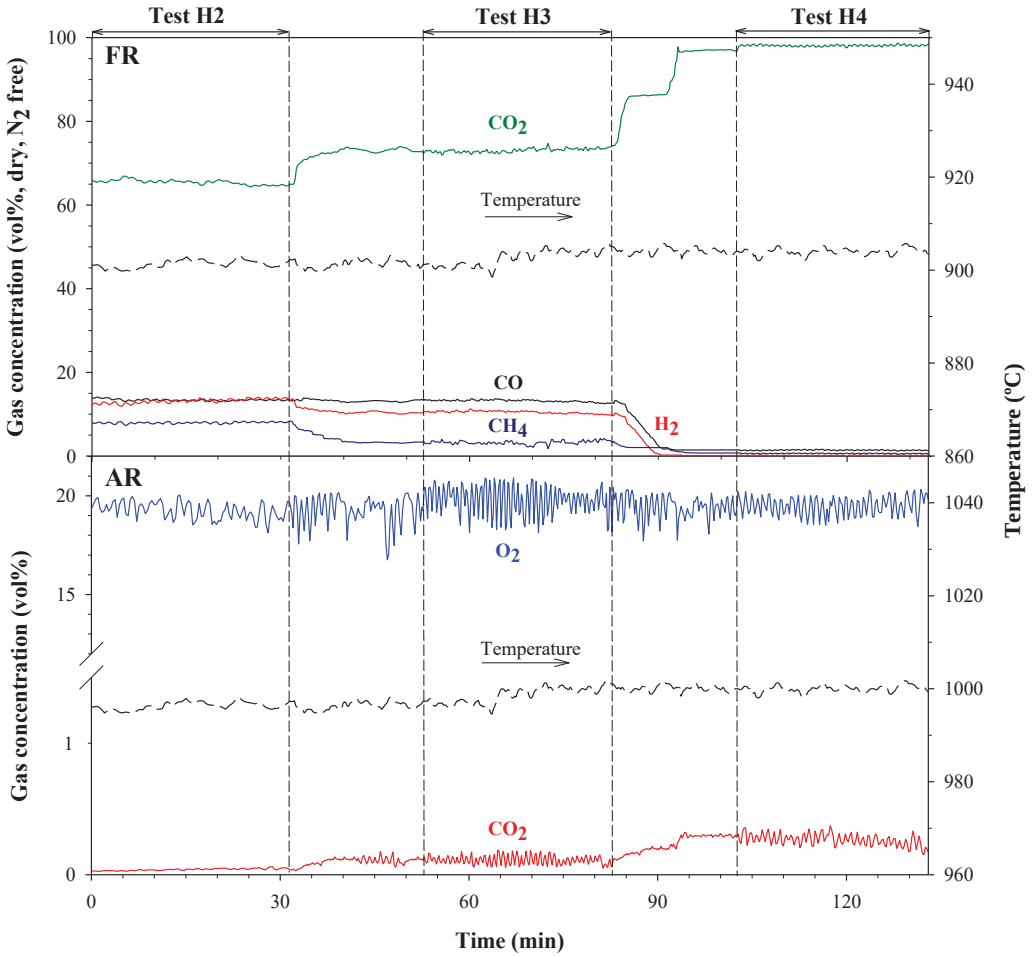

Figure 74. Time evolution of the temperature and gas concentrations in both fuel and air reactors during test H2, H3 and H4. Gas concentration values in the fuel reactor are given in dry basis and N_2-free.

Evaluation of the CO_2 capture efficiency

CO_2 capture efficiency is usually affected by several operating conditions in *i*G-CLC mode, such as the fuel reactor temperature, the carbon stripper separation efficiency and the solids circulation rate. It should be remembered that during the experimental campaign both the fuel reactor temperature and the carbon stripper separation efficiency were maintained. The fuel reactor temperature was set to 900 ºC to clearly observe changes on total oxygen demand as a consequence of the variations in the ϕ parameter and the specific solids inventory in the fuel reactor. In the latter case, the carbon stripper separation efficiency was set keeping constant the gas velocity at 0.35 m/s. This value should be enough to separate and return the unconverted char particles to the fuel reactor (Abad et al. 2015a). Therefore, the CO_2

capture efficiency could only be affected by the solids circulation rate during this experimental campaign.

The solids circulation rate was modified in the range 60-375 kg/h, see Table 17. Figure 75 shows the variation of CO_2 capture efficiency as a function of the solids circulation rate in experiments using olive stones as solid fuel. Clearly, the CO_2 capture efficiency in the unit decreased as the solids circulation rate was increased, independently of the gasifying agent used. This is because a lower circulating solids flux entails higher residence times for the char particles in the fuel reactor, see Table 17. In addition, the type of gasifying agent used was also considered when CO_2 capture efficiency was assessed. No clear differences were found for the CO_2 capture efficiency in those tests where steam was introduced both to the fuel reactor and the carbon stripper in comparison with similar tests carried out with CO_2. Therefore, the use CO_2 as gasifying agent seems cannot be discarded considering the energy penalty of the use of H_2O. In this sense, solids circulation rates up to 150 kg/h should be maintained at 900 ºC to achieve CO_2 capture efficiencies above 95%, although these values would be improved operating at higher temperatures.

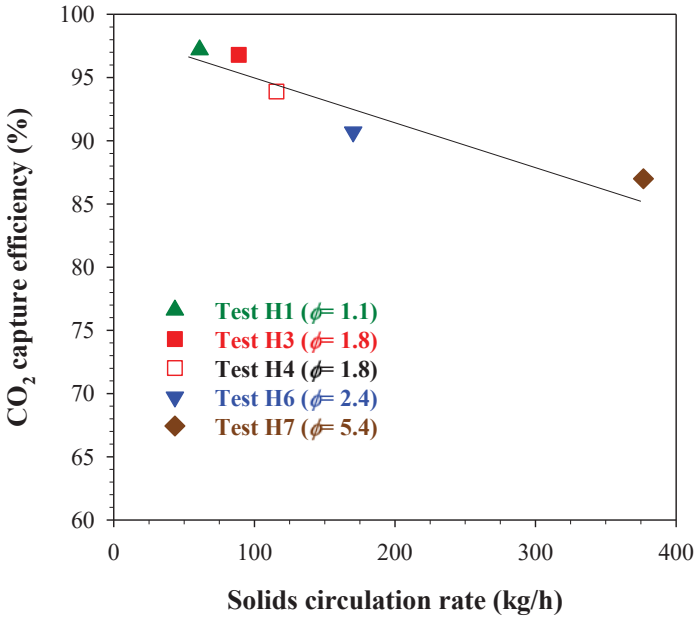

Figure 75. Effect of solids circulation rate on CO_2 capture efficiency during tests burning olive stones.

Evaluation of the Total oxygen demand

The total oxygen demand depends mainly of both the availability of oxygen and the solids inventory into the fuel reactor (Cuadrat et al. 2012; García-Labiano et al. 2013). Therefore, the effect of the oxygen carrier to fuel ratio (ϕ) and the specific solids inventory in the fuel reactor (m^*_{FR}) on the total oxygen demand was analyzed, see Figure 76.

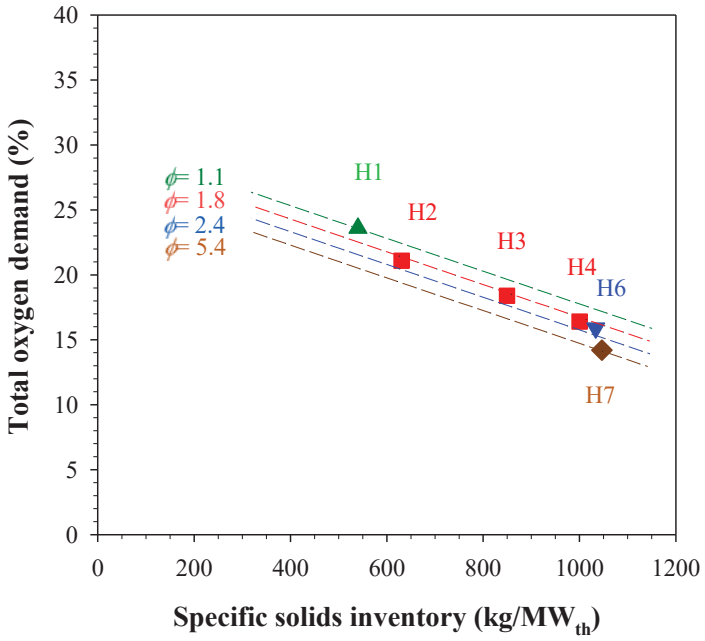

Figure 76. Effect of oxygen carrier to fuel ratio (ϕ) and specific solids inventory in the fuel reactor (m^*_{FR}) on total oxygen demand (Ω_T).

It was observed that when both the ϕ parameter and the specific solids inventory in the fuel reactor were increased, the total oxygen demand decreased. This can be observed comparing the tests H1 and H3, since they were performed feeding similar biomass to the CLC unit (~1 kg/h) and using steam as gasifying agent. The total oxygen demand decreased by 5 points (from 23.6% to 18.4%) when increasing the ϕ parameter from 1.1 to 1.8 and the solids inventory in the fuel reactor from 540 kg/MW$_{th}$ to 850 kg/MW$_{th}$. The lowest total oxygen demand value (Ω_T = 14.8%) was obtained in test H7, which represents one of the lowest oxygen demand value obtained during biomass combustion by *i*G-CLC in a continuous CLC unit (Schmitz and Linderholm 2018; Pikkarainen and Hiltunen 2017), excepting those tests using wood char as fuel (Linderholm and Schmitz, 2016; Schmitz et al. 2016).

Effect of the oxygen carrier to fuel ratio on the total oxygen demand

Figure 76 shows that the total oxygen demand was clearly decreased when the oxygen carrier to fuel ratio was increased. For a correct evaluation of the isolated effect of the ϕ parameter on the total oxygen demand, the rest of the operating conditions must be maintained constant. It was previously observed that the specific solids inventory in the fuel reactor greatly affected the total oxygen demand. But it should be also considered that other operating conditions such as the biomass feeding rate (m_{sf}) could affect the total oxygen demand by modifying the amount of unburned gases inside the fuel reactor. Thus, test H4, tests H6 and H7 were selected, since they were carried out at same fuel power input (6.5 kW_{th}), using the same gasifying agent (CO_2), and with a similar specific solids inventory (m^*_{OC} ~1000kg/MW_{th}). Increasing the ϕ value from 1.8 (test H4) to 2.4 (test H6) a decrease of the total oxygen demand by 2.5 points was achieved. Subsequently, the increase in the ϕ value from 2.4 to 5.4 in test H7 allowed a decrease of 1 additional point. Considering that volatile matter is the most influencing parameter on total oxygen demand, these results confirm that the decrease of the total oxygen demand observed when the ϕ parameter was increased was mainly due to the improvement on the volatile matter conversion to CO_2 and H_2O. This is in agreement with the work of Pérez-Vega et al. (2016), who observed a similar behavior burning coal by in the same CLC unit.

Effect of the fuel reactor specific solids inventory on the total oxygen demand

The isolated analysis of the effect of the specific solids inventory in the fuel reactor on the oxygen demand would require modifying other operating conditions, such as solids circulation rate, fuel power input, or total solids inventory in the CLC unit. Thus, the results obtained are consequence of the combined effect of several operating conditions. However, it should be kept in mind that the operating parameter that mainly affects to the total oxygen demand is the oxygen carrier to fuel ratio. Thus, tests H2, H3 and H4 were selected because of the oxygen carrier to fuel ratio was set to 1.8 and the solids inventory in the fuel reactor was varied between 630 and 1000 kg/MW_{th}.

In test H2, a total oxygen demand of 21.1% was obtained for a specific solids inventory in the fuel reactor of 630 kg/MW_{th}. Figure 76 shows that total the oxygen demand decreased by 2.5 points in test H3 when increasing the specific solids inventory up to 850 kg/MW_{th}. In this case, the effect could be increased by the lower fuel power input used in test H3. It should be considered that a lower biomass feeding rate generates a lower amount of unconverted gases inside the fuel reactor, which could cause a decrease of the total oxygen demand. However, in test H4 the total oxygen demand decreased by 2 points with respect to test H3, in spite of the increase the biomass feeding rate in the CLC rig.

Further improvement in the performance of the 20 kW_{th} unit will look for an increase of the CO_2 capture efficiency. For that, it would be necessary to raise both the fuel reactor temperature and the carbon stripper separation efficiency (e.g., by increasing the gas velocity). The increase of the fuel reactor temperature will drive to higher biomass char gasification rate but it will also to increase the reaction rate between the oxygen carrier and the gases present into the fuel reactor, which could reduce the total oxygen demand.

CONCLUSIONS

One of the actions for climate change mitigation is the substitution of fossil fuels by biofuels such as biomass in many thermo-chemical processes. Furthermore, when biofuels are combined with CCS processes, a negative emission technology known as BECCS is obtained. This group of technologies are able to produce energy while the CO_2 is captured, thus obtaining and selling carbon credits. The present work focused on the use of solid biofuels in a combustion technology with inherent carbon capture such as Chemical Looping Combustion (CLC) technology- the bioCLC process. A correct management of biomass resources converts biomass in an almost neutral fuel regarding CO_2 emissions. The work was carried out at the *Instituto de Carboquímica* in Zaragoza (Spain), including a four-month stay at the Institute of Solids Process Engineering and Particle Technology in the *Technische Universität Hamburg* (TUHH) in Hamburg (Germany). The experimental campaigns performed with different oxygen carriers and three types of biomass (pine sawdust, olive stones and almond shells) involved more than 220 h of continuous biomass combustion in both 1 kW_{th} and 20 kW_{th} continuous CLC units. This way, both *i*G-CLC and CLOU

operation modes were studied and the integration of biomass in CLC processes was assessed.

Five oxygen carriers were tested: three ores based in Fe or Mn (Tierga ore, MnGBHNE and MnSA) and the other two synthetic oxygen carriers (Fe-Mn and Mn-Cu mixed oxides: Mn66FeTi7 and Cu34Mn66). In this sense, the evaluation of the bioCLC performance was carried out and the effect of different operating variables was analyzed. Despite the different behavior of the oxygen carriers any of them could be dismissed for the bioCLC. Among types of biomass, no significant differences were obtained in the CLC performance with both CO_2 and steam as gasifying agents.

Almost 100% of CO_2 capture efficiency was obtained with all the low-cost oxygen carriers (Tierga, MnGBHNE and MnSA ores) without carbon stripper in the 1 kW_{th} CLC unit at different operating conditions. Focusing on the synthetic oxygen carriers, values about 100% of CO_2 capture efficiency were obtained during all the experimental campaign with the Mn66FeTi7 between 890 and 960 ºC into the fuel reactor. This fact confirmed the higher reactivity of the Mn66FeTi7 with the char since no CO_2 was measured in the air reactor outlet. CO_2 capture efficiency reached values up to 98% at operating temperatures in the fuel reactor as low as 850 ºC with Cu34Mn66.

High values of total oxygen demand (20-30 %) were observed for the Tierga ore. Slightly better values were obtained working the MnGBHNE at similar conditions, mainly because of the higher reactivity of with H_2. The higher reactivity of the MnSA compared with the MnGBHNE further contributed on the total oxygen demand reduction, reaching the lowest values in the present study working under *i*G-CLC mode (10.2 % with about 750 kg/MW_{th} and 930 ºC). Thus, this newly identified manganese mineral can be thought as an interesting low-cost oxygen carrier for further scale up. The molecular oxygen releasing capacity of Mn66FeTi7 could reduce the total oxygen demand values achieved with the Fe or Mn-based minerals. The oxygen release was favored by a low temperature of operation in the air reactor (880 ºC) and a high air excess ratio (λ^*=1.9). Under these conditions, oxygen demand

values of 4.6% were obtained with averaged solids inventories of 1875 kg/$MW_{th.}$ The best results regarding oxygen demand were obtained with the Cu34Mn66 working under CLOU mode. In this case, no gaseous unburnt compounds were present in the fuel reactor outlet, even at the lowest temperature studied (775 ºC).

The possibility of dry recycling the outlet stream of the fuel reactor to the fuel reactor was evaluated in this work as a design solution for further oxygen demand reduction. In the conditions evaluated in this work, it is possible about a 30% reduction in the oxygen demand when the fuel reactor outlet stream is recirculated.

The presence of NO_x and tar in the outlet streams of fuel and air reactor was studied under both *i*G-CLC and CLOU operation modes. During all the experiments, most the fuel-N appeared as N_2 at the fuel reactor outlet with only little presence of NO. About air reactor emissions, NO_x concentrations never exceeded the legal limits for power plants. Working under *i*G-CLC mode, naphthalene was the major tar compound found in all the studied cases and for all the types of biomass. The tar contribution to the total oxygen demand was estimated about 1% of the oxygen needed to fully burn the fuel. Under CLOU mode, insignificant tar amounts were found although in this case also linear or branched hydrocarbons were detected.

Finally, biomass fueled CLC was demonstrated in a 20 kW_{th} unit at 900 ºC using the Tierga iron ore with olive stones. CO_2 capture efficiencies above 95% were commonly obtained achieving values about 99.9% in some specific conditions. Total oxygen demands about 15-20% with specific solids inventory in the fuel reactor about 1000 kg/MW_{th} were achieved. All these results demonstrate the promising possibilities of biomass fueled CLC (bioCLC) as a BECCS technology.

ABBREVIATIONS

AAEM	*Alkali and alkaline earth metals*
AR5	*Fifth Assessment Report*
BECCS	*Biomass energy with CO_2 Capture and Storage*
BET	*Brunauer-Emmett-Teller*
BFB	*Bubbling fluidized bed*
BP	*British Petroleum*
B2DS	*Beyond the two degrees scenario*
CCS	*CO_2 Capture and Storage*
CCU	*CO_2 Capture and Utilization*
CFB	*Conference of the Parties*
CFB	*Circulating Fluidized bed*
CFCs	*Chlorofluorocarbon Substances*
CL	*Chemical Looping*
CLC	*Chemical Looping Combustion*
CLG	*Chemical Looping Gasification*
CL*a*OU	*Chemical Looping Combustion assisted by Oxygen Uncoupling*
CLOU	*Chemical Looping Combustion with Oxygen Uncoupling*
CLC	*Chemical Looping Reforming*
COP	*Conference of the parties*
CUT	*Chalmers University of Technology*
DAC	*Direct Air Capture*
DACCS	*Direct Air CO_2 Capture and Storage*
EOR	*Enhancing Oil Recovery*
EU	*European Union*
EuTrace	*European Transdisciplinary Assessment on Climate Engineering*

FA	*Fluidizing Agent*
FID	*Flame ionization detector*
GDP	*Gross Domestic Product*
GHG	*Greenhouse Gases*
GISS	*Goddard Institute for Space Studies*
GNI	*Gross National Income*
GWP	*Global Warming Potential*
HUT	*Hamburg University of Technology*
ICB-CSIC	*Instituto de Carboquímica – Consejo Superior de Investigaciones Científicas*
IEA	*International Energy Agency*
*i*G-CLC	*In situ Gasification-Chemical Looping Combustion*
IPCC	*Intergovernmental Panel on Climate Change*
LCA	*Life Cycle Analysis*
LHV	*Low Heating Value (kJ/kg)*
MSW	*Municipal Solid Waste*
NDC	*Nationally Determined Contribution*
NDIR	*Nondispersive infrared sensor*
NET	*Negative Emission Technology*
OECD	*Organization for Economic Co-operation and Development*
RCP	*Representative Concentration Pathway*
SEM	*Scanning electronic microscopy*
SINTEF	*Stiftelsen for industriell og teknisk forskning*
SRM	*Solar Radiation Management*
STP	*Standard temperature and pressure*
SB	*Spouted bed*
SU	*Southeast University*

TCD	*Thermal conductivity* detector
TGA	*Thermogravimetric Analyzer*
TUD	*Darmstadt* University *of Technology*
UN	*United Nations*
UNEP	*United Nations Environmental Program*
UNFCCC	*United Nations Framework Convention on Climate Change*
USA	*United States of America*
VTT	VTT *Technical Research Centre of Finland*
XRD	*X-Ray Diffractometer*
2DS	*Two degrees scenario*

SYMBOLS

F_i	*mol/s*	*Molar flow of component i in the air reactor outlet*
g	*m/s²*	*Gravity*
m	*kg*	*Oxygen carrier mass at any time*
m^*	*kg/MW$_{th}$*	*Specific solids inventory*
m_{OC}	*kg*	*Mass of oxygen carrier*
m_{Ox}	*kg*	*Oxygen carrier mass fully oxidized*
m_{Red}	*kg*	*Oxygen carrier mass fully reduced*
$\dot{m}_{OC}$	*kg/s*	*Oxygen carrier circulating rate*
$\dot{m}_{sf}$	*kg/s*	*Solid fuel mass flow*
M_i	*kg/mol*	*Molecular mass of component i*
$norm.\dot{m}_{OC}$	*kg/(s·MW$_{th}$)*	*Normalized solids circulation rate*
P_{th}	*MW$_{th}$*	*Power input*
R_{OC}	-	*Oxygen transport capacity*
S	*m²*	*Surface area*
t	*s*	*Time*
T	*K*	*Temperature*
X_{char}	-	*Char conversion*
X_{Ox}	-	*Oxygen carrier conversion for oxidation*
X_{Red}	-	*Oxygen carrier conversion for reduction*
χ	-	*Conversion*
y_{O_2}	-	*Oxygen concentration*

Greek letters

ΔP	*Pa*	*Pressure drop*
ϕ	-	*Oxygen carrier to fuel molar ratio*
λ^*	-	*Air excess in the air reactor*
η_{CC}	-	*CO_2 capture efficiency*
$\eta_{comb,FR}$	-	*Combustion efficiency*
τ_{FR}	*s*	*Mean residence time of particles in the fuel reactor*
Ω_{sf}	*kg/kg*	*Stoichiometric oxygen for the solid fuel full conversion*
Ω_T	-	*Total oxygen demand*
Ω_{tar}	-	*Tar oxygen demand*

Subscripts

AR	*Air reactor*
elu	*Elutriated*
FR	*Fuel reactor*
in	*Inlet*
OC	*Oxygen carrier*
out	*outlet*
sf	*Solid fuel*
vol	*Volatiles*

REFERENCES

Abad, A., Adánez-Rubio, I., Gayán P., García-Labiano, F., de Diego, L. F. and Adánez, J. **2012**. "Demonstration of Chemical-Looping with Oxygen Uncoupling (CLOU) Process in a 1.5 kW_{th} Continuously Operating Unit Using a Cu-Based Oxygen-Carrier." International Journal of Greenhouse Gas Control 6 (January): 189–200.

Abad, A., Pérez-Vega, R., de Diego, L. F., García-Labiano, F., Gayán, P. and Adánez, J. **2015a**. "Design and Operation of a 50 kW_{th} Chemical Looping Combustion (CLC) Unit for Solid Fuels." Applied Energy 157: 295–303.

Abad, A., Adánez, J., Gayán, P., de Diego, L. F., García-Labiano, F. and Sprachmann, G. **2015b**. "Conceptual Design of a 100 MW_{th} CLC Unit for Solid Fuel Combustion." Applied Energy 157: 462–74 .

Abad, A., Gayán, P., Mendiara, T., Bueno, J. A., García-Labiano, F., de Diego, L. F. and Adánez, J. **2018**. "Assessment of the Improvement of Chemical Looping Combustion of Coal by Using a Manganese Ore as Oxygen Carrier." Fuel Processing Technology 176 (July): 107–18.

Adánez, J., de Diego, L. F., García-Labiano, F. and Gayán, P., Abad, A. and Palacios, J. M. **2004**. "Selection of Oxygen Carriers for Chemical-Looping Combustion." Energy Fuels 18: 371–77.

Adánez, J., Abad, A., García-Labiano, F., Gayán, P. and L. F. de Diego. **2012**. "Progress in Chemical-Looping Combustion and Reforming Technologies." Progress in Energy and Combustion Science 38 (2): 215–82.

Adánez, J., Abad, A., Mendiara, T., Gayán, P., de Diego, L. F. and García-Labiano, F. **2018**. "Chemical Looping Combustion of Solid Fuels." Progress in Energy and Combustion Science 65 (March): 6–66.

Adánez, J., and Abad, A. **2019**. "Chemical-Looping Combustion: Status and Research Needs." Proceedings of the Combustion Institute 37 (4): 4303–17.

Adánez-Rubio, I., Abad, A., Gayán, P., de Diego, L. F., García-Labiano, F. and Adánez, J. **2014**. "Biomass Combustion with CO_2 Capture by Chemical Looping with Oxygen Uncoupling (CLOU)." Fuel Processing Technology 124 (August): 104–14.

Adánez-Rubio, I., Abad, A., Gayán, P., Adánez I., de Diego, L. F., García-Labiano, F. and Adánez, J. **2016**. "Use of Hopcalite-Derived Cu–Mn Mixed Oxide as Oxygen Carrier for Chemical Looping with Oxygen Uncoupling Process." Energy & Fuels 30 (7): 5953–63.

Adánez-Rubio, I., Abad, A., Gayán, P., García-Labiano, F., de Diego, L. F., and Adánez, J. **2017a**. "Coal Combustion with a Spray Granulated Cu-Mn Mixed Oxide for the Chemical Looping with Oxygen Uncoupling (CLOU) Process." Applied Energy 208 (December): 561–70.

Adánez-Rubio, I., Izquierdo, M. T., Abad, A., Gayán, P., de Diego, L. F. and Adánez J. **2017b**. "Spray Granulated Cu-Mn Oxygen Carrier for Chemical Looping with Oxygen Uncoupling (CLOU) Process." International Journal of Greenhouse Gas Control 65 (October): 76–85.

Adánez-Rubio, I., Abad, A., Gayán, P., de Diego, L. F. and Adánez, J. **2018**. "CLOU Process Performance with a Cu-Mn Oxygen Carrier in the Combustion of Different Types of Coal with CO_2 Capture." Fuel 212 (January): 605–12.

ALINNE. **2019**. "Análisis Del Potencial de Desarrollo de Tecnologías Energéticas. Captura, Transporte, Almacenamiento, Usos y Transformación Del CO_2." Ejercicio APTE 2017-2018, 1–45.

Anis, S. and Zainal Z. A. **2011**. "Tar Reduction in Biomass Producer Gas via Mechanical, Catalytic and Thermal Methods: A Review." Renewable and Sustainable Energy Reviews 15 (5): 2355–77.

Azimi, G., Rydén, M., Leion, H., Mattisson, T. and Lyngfelt, A. **2013**. "$(Mn_zFe_{1-z})_yO_x$ Combined Oxides as Oxygen Carrier for Chemical-Looping with Oxygen Uncoupling." AIChE Journal 59 (2): 582–88.

Berdugo Vilches, T., Rydén, M. and Thunman, H. **2017**. "Experience of More than 1000 h of Operation with Oxygen Carriers and Solid Biomass at Large Scale." Applied Energy 190 (March): 1174–83.

BP. **2019**. "BP Energy Outlook 2019 Edition." BP Energy Outlook 2019. https://www.bp.com/content/dam/bp/business-sites/en/global/corporate/pdfs/energy-economics/energy-outlook/bp-energy-outlook-2019.pdf.

Brown, A. and Le Feuvre, P. **2017**. "Technology Roadmap: Delivering Sustainable Bioenergy." International Energy Agency (IEA), 94.

Cabello, A., Gayán, P., García-Labiano, F., de Diego, L.F., Abad, A. and Adánez, J. **2016**. "On the Attrition Evaluation of Oxygen Carriers in Chemical Looping Combustion." Fuel Processing Technology 148 (July): 188–97.

Consoli, C. **2019**. "2019 Perspective. Bioenergy and Carbon Capture and Storage." Global CCS Institute, 1–14.

Cook, E. L. **1971**. "The Flow of Energy in an Industrial Society." Scientific American 225 (3): 135-42.

Cuadrat, A., Abad, A., García-Labiano, F., Gayán, P., de Diego, L. F. and Adánez, J. **2011**. "The Use of Ilmenite as Oxygen-Carrier in a 500 W_{th} Chemical-Looping

Coal Combustion Unit." International Journal of Greenhouse Gas Control 5: 1630–42.

Cuadrat, A., Abad, A., García-Labiano, F., Gayán, P., de Diego, L. F. and Adánez J. **2012**. "Effect of Operating Conditions in Chemical-Looping Combustion of Coal in a 500 W_{th} Unit." International Journal of Greenhouse Gas Control 6: 153–63.

Ehrlich, P. R., Kareiva, P. M. and Daily, G. C. **2012**. "Securing Natural Capital and Expanding Equity to Rescale Civilization." Nature 486 (7401): 68–73.

European Commission. **2018**. Final Report of the High-Level Panel of the European Decarbonisation Pathways Initiative. 978–92–79–96826–6.

European Council. **2010**. "Directive 2010/75/EU Industrial Emissions." Official Journal of the European Union. https://doi.org/10.3000/17252555.L_2010.334.eng.

Evans, R. J. and Milne, T. A. **1987a**. "Molecular Characterization of the Pyrolysis of Biomass." Energy & Fuels 1 (2): 123–37.

Evans, R. J. and Milne, T. A. **1987b**. "Molecular Characterization of the Pyrolysis of Biomass. 2. Applications." Energy & Fuels 1 (4): 311–19.

Fourier, J. B. J. **1824**. "Remarques Générales Sur Les Températures Du Globe Terrestre Et Des Espaces Planétaires." Annales de Chimie et de Physique 27: 136–67.

Fuss, S., Lamb, W. F., Callaghan, M. W., Hilaire, J., Creutzig, F., Amann, T., Beringer, T. et al. **2018**. "Negative Emissions—Part 2: Costs, Potentials and Side Effects." Environmental Research Letters 13 (6): 063002.

García-Labiano, F., de Diego, L. F., Gayán, P., Abad A. and Adánez, J. **2013**. "Fuel Reactor Modelling in Chemical-Looping Combustion of Coal: 2-Simulation and Optimization." Chemical Engineering Science 87: 173–82.

García-Labiano, F., Pérez-vega, R., Pérez-Astray, A., Mendiara, T., de Diego, L. F. and Izquierdo, M. T. **2018**. "Chemical Looping Combustion of Biomass in a 50 kW_{th} Unit." In 5th CLC Conference, Park City, Utah, USA.

Gaston, K. J. and Spicer, J. I. **2009**. Biodiversity: An Introduction. Planet Earth. Second edition. University of Chicago Press, Chicago, 2008 . 217 pp. https://doi.org/10.1111/j.1442-9993.2009.01985.x.

Gayán, P., Abad, A., de Diego, L. F., García-Labiano, F. and Adánez, J. **2013**. "Assessment of Technological Solutions for Improving Chemical Looping Combustion of Solid Fuels with CO_2 Capture." Chemical Engineering Journal 233 (November): 56–69.

Ge, H., Guo, W., Shen, L., Song, T. and Xiao, J. **2016**. "Biomass Gasification Using Chemical Looping in a 25 kW_{th} Reactor with Natural Hematite as Oxygen Carrier." Chemical Engineering Journal 286 (February): 174–83.

Glarborg, P, Jensen, A. D. and Johnsson, J. E. **2003**. "Fuel Nitrogen Conversion in Solid Fuel Fired Systems." Progress in Energy and Combustion Science 29 (2): 89–113. https://doi.org/10.1016/S0360-1285(02)00031-X.

Gogolev, I., Linderholm, C., Gall, D., Schmitz, M., Mattisson, Pettersson, T., J. B. C. and Lyngfelt, A. **2019**. "Chemical-Looping Combustion in a 100 kW Unit Using a Mixture of Synthetic and Natural Oxygen Carriers – Operational Results and Fate of Biomass Fuel Alkali." International Journal of Greenhouse Gas Control 88 (September): 371–82.

Guandalini, G., Romano, M. C., Ho, M., Wiley, D., Rubin, E. S. and Abanades, J. C. **2019**. "A Sequential Approach for the Economic Evaluation of New CO_2 Capture Technologies for Power Plants." International Journal of Greenhouse Gas Control 84 (May): 219–31.

Haiming G., Shen, L., Xiao, J., Zhang, S. and Song, T. **2011**. "Chemical Looping Combustion of Biomass/Coal with Natural Iron Ore as Oxygen Carrier in a Continuous Reactor." Energy & Fuels 25 (1): 446–55.

Haiming, G., Shen, L., Zhong, Z., Zhou, Y., Liu, W., Niu, X., Ge, H., Jiang, S. and Wang L. **2015**. "Interaction between Biomass Ash and Iron Ore Oxygen Carrier during Chemical Looping Combustion." Chemical Engineering Journal 277 (October): 70–78.

Hanning, M., Frick, V., Mattisson, T., Rydén, M. and Lyngfelt, A. **2016**. "Performance of Combined Manganese–Silicon Oxygen Carriers and Effects of Including Titanium." Energy & Fuels 30 (February): 1171–82.

Hanning, M., Corcoran, A., Lind, F. and Rydén, M. **2018**. "Biomass Ash Interactions with a Manganese Ore Used as Oxygen-Carrying Bed Material in a 12 MW_{th} CFB Boiler." Biomass and Bioenergy 119 (December): 179–90.

Haus, J., Feng, Y., Hartge, E. U., Heinrich, S. and Werther, J. **2018**. "High Volatiles Conversion in a Dual Stage Fuel Reactor System for Chemical Looping Combustion of Wood Biomass." In , 1–13. I International Conference on CO_2 Negative Emissions. 22-24 May 2018, Goteborg, Sweeden.

Hildor, F., Mattisson, T., Leion, H., Linderholm, C. and Rydén, M. **2019**. "Steel Converter Slag as an Oxygen Carrier in a 12 MW_{th} CFB Boiler – Ash Interaction and Material Evolution." International Journal of Greenhouse Gas Control 88 (September): 321–31.

Hosseini, D., Imtiaz, Q., Abdala, P. M., Yoon, S., Kierzkowska, A. M., Weidenkaff, A. and Müller, C. R. **2015**. "CuO Promoted Mn_2O_3 -Based Materials for Solid Fuel Combustion with Inherent CO_2 Capture." Journal of Materials Chemistry A 3 (19): 10545–50.

IDAE. **2011**. "Plan de Energías Renovables 2011-2020." Instituto para la Diversificación y Ahorro de la Energía: 1–824.

IEA. **2016**. "Energy Technology Perspectives 2016: Towards Sustainable Urban Energy Systems" OECD/IEA, no. May. 1–418.

IEA. **2018**. "Global Energy and CO_2 Status Report." OECD/IEA, no. March. 1–28 https://www.iea.org/publications/freepublications/publication/GECO2017.pdf

INC. **2018**. "Nuts and Dried Fuits Statistical Yearbook 2017/2018.". International Nut and Dried Fruit Council Foundation. 1–80.

IOOC. **2018**. International Olive Oil Council. http://www.internationaloliveoil.org

IPCC. **2005**. B. Metz, O. Davidson, H. de Coninck, M. Loos and L. Meyer (Eds.) "Carbon Dioxide Capture and Storage" Cambridge University Press, UK. 431 pp. Cambridge University Press, The Edinburgh Building Shaftesbury Road, Cambridge.

IPCC. **2013**. "Summary for Policymakers. In: Climate Change 2013: The Physical Science Basis." Contribution of Working Group I to the Fifth Assessment Report of the Intergovernmental Panel on Climate Change.

IPCC. **2014**. Climate Change 2014: Synthesis Report. Contribution of Working Groups I, II and III to the Fifth Assessment Report of the Intergovernmental Panel on Climate Change. Core Writing Team, Pachauri, R.K. and Meyer, L.A. Geneva, Switzerland. 1–151.

Ishida, M., Zheng, D. and Akehata, T. **1987**. "Evaluation of a Chemical-Looping-Combustion Power-Generation System by Graphic Exergy Analysis." Energy 12 (2): 147–54.

Ishida M. and Jin, H. **1996**. "A Novel Chemical-Looping Combustor without NO_x Formation." https://doi.org/10.1021/IE950680S.

Ishida M., Jin, H. and Okamoto, T. **1996**. "A Fundamental Study of a New Kind of Medium Material for Chemical-Looping Combustion." Energy & Fuels 10 (4): 958–63.

Jackson, R. **2019**. "Eunice Foote, John Tyndall and a Question of Priority." Notes and Records: The Royal Society Journal of the History of Science, February.

Jiang, S., Shen, L., Niu, X., Ge, H. and Haiming G. **2016**. "Chemical Looping Co-Combustion of Sewage Sludge and Zhundong Coal with Natural Hematite as the Oxygen Carrier." Energy and Fuels 30: 1720–29.

Jiang, S. Shen, L., Yan, J., Ge H. and Song, T. **2018**. "Performance in Coupled Fluidized Beds for Chemical Looping Combustion of CO and Biomass Using Hematite as an Oxygen Carrier." Energy & Fuels 32 (12): 12721–29.

Jing, D, Arjmand, M., Mattisson, T., Rydén, M., Snijkers, F., Leion, H. and Lyngfelt, A. **2014**. "Examination of Oxygen Uncoupling Behaviour and Reactivity towards Methane for Manganese Silicate Oxygen Carriers in Chemical-Looping Combustion." International Journal of Greenhouse Gas Control 29 (October): 70–81.

Jones, P. D. and Harpham, C. **2013**. "Estimation of the Absolute Surface Air Temperature of the Earth." Journal of Geophysical Research: Atmospheres 118 (8): 3213–17.

Kander, A., Malanima, P. and Warde, P. **2014**. Power to the People: Energy in Europe over the Last Five Centuries. Princeton and Oxford: Princeton University Press, 457 pp.

Keeling, C. D., Piper, S. C., Bacastow, R. B., Wahlen, M., Whorf, T. P., Heimann, M. and Meijer, H. A. Atmospheric CO_2 and $^{13}CO_2$ exchange with the terrestrial biosphere and oceans from 1978 to 2000: observations and carbon cycle implications, 83–113, in "A History of Atmospheric CO_2 and its effects on Plants, Animals, and Ecosystems", **2005**. Ed. Ehleringer, J.R., T. E. Cerling, M. D. Dearing, Springer, New York.

Kobayashi, N. and Fan, L. S. **2011**. "Biomass Direct Chemical Looping Process: A Perspective." Biomass and Bioenergy 35 (3): 1252–62.

Kramp, M. **2014**. "Chemical Looping Combustion in Interconnected Fluidized Bed Reactors: Simulation and Experimental Validation." 181 pp, Dissertation Technische Universität Hamburg-Harburg (2014). Ed. Dr. Hut.

Kump, L. R., Kasting, J. F. and Crane R. G. **2004**. "The Earth System. " Prentice Hall; 2 edition (August 16, 2003), 432 p.

Langørgen, Ø., and Saanum, I. **2018**. "Chemical Looping Combustion of Wood Pellets in a 150 kW_{th} CLC Reactor." In, 1–10. Gothemborg, Sweeden.

Leion, H., Jerndal, E., Steenari, B. M., Hermansson, S., Israelsson, M., Jansson, E., Johnsson, M., et al. **2009a**. "Solid Fuels in Chemical-Looping Combustion Using Oxide Scale and Unprocessed Iron Ore as Oxygen Carriers." Fuel 88 (10): 1945–54.

Leion, H., Larring, Y., Bakken, E., Bredesen, R., Mattisson, T. and Lyngfelt, A. **2009b**. "Use of $CaMn_{0.875}Ti_{0.125}O_3$ as Oxygen Carrier in Chemical-Looping with Oxygen Uncoupling." Energy & Fuels 23 (10): 5276–83.

Leion, H., Mattisson, T. and Lyngfelt A. **2011**. "Chemical Looping Combustion of Solid Fuels in a Laboratory Fluidized-Bed Reactor." Oil & Gas Science and Technology – Revue d'IFP Energies Nouvelles 66 (2): 201–8.

Leion, H., Knutsson P. and Steenari B.M. **2017**. "Experimental Evaluation of Interactions between K, Ca, and P and Mn/Si-Based Oxygen Carriers." In 25th

European Biomass Conference and Exhibition Proceedings. Stockholm (Sweden).

Lewis, W. K., and Gilliland, E. R. **1954**. "Production of Pure CO_2," November. https://patents.google.com/patent/US2665972A/en.

Linderholm, C., Schmitz, M., Knutsson, P., Källén, M. and Lyngfelt A. **2014**. "Use of Low-Volatile Solid Fuels in a 100 KW Chemical-Looping Combustor." Energy and Fuels 28: 5942–52.

Linderholm, C. and Schmitz, M. **2016**. "Chemical-Looping Combustion of Solid Fuels in a 100 kW Dual Circulating Fluidized Bed System Using Iron Ore as Oxygen Carrier." Journal of Environmental Chemical Engineering 4: 1029–39.

Lyngfelt, A. and Leckner, B. **2015**. "A 1000 MW_{th} Boiler for Chemical-Looping Combustion of Solid Fuels – Discussion of Design and Costs." Applied Energy 157: 475–87.

Malanima, P. **2014**. "The Basic Environmental History." Edited by Mauro Agnoletti and Simone Neri Serneri. Springer International, Environmental History, 4 (10): 52-5302-52–5302.

Mattisson, T., Lyngfelt, A. and Leion, H. **2009**. "Chemical-Looping with Oxygen Uncoupling for Combustion of Solid Fuels." International Journal of Greenhouse Gas Control 3 (1): 11–19.

Mattison, T., Hildor, F., Li, Y. and Linderholm, C. **2019**. "Negative Emissions of Carbon Dioxide through Chemical-Looping Combustion (CLC) and Gasification (CLG) Using Oxygen Carriers Based on Manganese and Iron." Mitigation and Adaptation Strategies for Global Change, April, 1–21.

Mei, D., Mendiara, T., Abad, A., de Diego, L. F., García-Labiano, F., Gayán, P., Adánez, J. and Zhao, H. **2015**. "Evaluation of Manganese Minerals for Chemical Looping Combustion." Energy and Fuels 29 (10): 6605–15.

Mei, D., Mendiara, T., Abad, A., de Diego, L. F., García-Labiano, F., Gayán, P., Adánez, J. and Zhao, H. **2016**. "Manganese Minerals as Oxygen Carriers for Chemical Looping Combustion of Coal." Industrial and Engineering Chemistry Research. 8 June 201655, (22): 6539–46.

Mendiara, T., Pérez, R., Abad, A., de Diego, L. F., García-Labiano, F., Gayán, P. and Adánez, J. **2012**. "Low-Cost Fe-Based Oxygen Carrier Materials for the *i*G-CLC Process with Coal. 1." Industrial and Engineering Chemistry Research 51: 16216–29.

Mendiara, T., Abad, A., de Diego, L. F., García-Labiano, F., Gayán, P. and Adánez, J. **2013a**. "Biomass Combustion in a CLC System Using an Iron Ore as an Oxygen Carrier." International Journal of Greenhouse Gas Control 19: 322–30.

Mendiara, T., de Diego, L. F., García-Labiano, F., Gayán, P., Abad, A. and Adánez, J. **2013b**. "Behaviour of a Bauxite Waste Material as Oxygen Carrier in a 500 W_{th} CLC Unit with Coal." International Journal of Greenhouse Gas Control 17: 170–82.

Mendiara, T., de Diego, L.F., García-Labiano, F., Gayán, P., Abad, A. and Adánez, J. **2014a**. "On the Use of a Highly Reactive Iron Ore in Chemical Looping Combustion of Different Coals." Fuel 126 (June): 239–49.

Mendiara, T., Izquierdo, M.T., Abad, A., de Diego, L.F., García-Labiano, F., Gayán, P., and Adánez, J. **2014b**. "Release of Pollutant Components in CLC of Lignite." International Journal of Greenhouse Gas Control 22 (March): 15–24.

Mendiara, T., García-Labiano, F., Abad, A., Gayán, P., de Diego, L. F., Izquierdo, M. T. and Adánez J. **2018a**. Negative CO_2 emissions through the use of biofuels in chemical looping technology: A review, 232 Applied Energy 657–84.

Mendiara, T., Pérez-Astray, A., Izquierdo, M.T., Abad, A., de Diego, L. F., García-Labiano, F., Gayán, P. and Adánez J. **2018b**. "Chemical Looping Combustion of Different Types of Biomass in a 0.5 kW_{th} Unit." Fuel 211 (January): 868–75.

Miller, R. L., Schmidt, G. A., Nazarenko, L. S., Tausnev, N., Bauer, S. E., del Genio, A. D. Kelley, M. et al. **2014**. "CMIP5 Historical Simulations (1850-2012) with GISS ModelE2." Journal of Advances in Modeling Earth Systems 6 (2): 441–78.

Mohammad P., N., Leion, H., Rydén, M. and Mattisson T. **2013**. "Combined Cu/Mn Oxides as an Oxygen Carrier in Chemical Looping with Oxygen Uncoupling (CLOU)." Energy & Fuels 27 (10): 6031–39.

Moldenhauer, P, Linderholm, C., Rydén, M. and Lyngfelt A. **2019**. "Avoiding CO_2 Capture Effort and Cost for Negative CO_2 Emissions Using Industrial Waste in Chemical-Looping Combustion/Gasification of Biomass." Mitigation and Adaptation Strategies for Global Change, March, 1–24.

Neves, D., Thunman, H., Matos, A., Tarelho, L. and Gómez-Barea A. **2011**. "Characterization and Prediction of Biomass Pyrolysis Products." Progress in Energy and Combustion Science 37 (5): 611–30.

Nigam, P. S. and Singh A. **2011**. "Production of Liquid Biofuels from Renewable Resources." Progress in Energy and Combustion Science 37 (1): 52–68.

Niu, X., Shen, L., Haiming G., Jiang, S. and Xiao J. **2015**. "Characteristics of Hematite and Fly Ash during Chemical Looping Combustion of Sewage Sludge." Chemical Engineering Journal 268: 236–44.

Ohlemüller, P., Ströhle, J. and Epple B. **2017**. "Chemical Looping Combustion of Hard Coal and Torrefied Biomass in a 1 MW_{th} Pilot Plant." International Journal of Greenhouse Gas Control 65: 149–59.

Pérez-Astray, A, Mendiara T, Abad A, García-Labiano F, de Diego L. F., Izquierdo M. T., Adánez J. **2019a**. "Manganese Ores as Low-Cost Oxygen Carriers for Biomass Chemical Looping Combustion in a 0.5 kW_{th} Unit". Submitted to Fuel Processing Technology.

Pérez-Astray, A, Mendiara T, Abad A, García-Labiano F, de Diego L. F., Izquierdo M. T., Adánez J. **2019b**. "CLC of Biomass as a BECCS Technology Using a Manganese-Iron Mixed Oxide". Submitted to Sep. Purif. Technol.

Pérez-Vega, R., Abad, A., Izquierdo, M. T., Gayán, P., de Diego, L. F. and Adánez J. **2019**. "Evaluation of Mn-Fe Mixed Oxide Doped with TiO_2 for the Combustion with CO_2 Capture by Chemical Looping Assisted by Oxygen Uncoupling." Applied Energy 237: 822–35.

Pérez-Vega, R., Abad A., García-Labiano, F., Gayán, P., de Diego, L. F., Adánez, and Adánez J. **2016**. "Coal Combustion in a 50 kW_{th} Chemical Looping Combustion Unit: Seeking Operating Conditions to Maximize CO_2 Capture and Combustion Efficiency." International Journal of Greenhouse Gas Control 50 (July): 80–92.

Pérez-Vega, R., Abad, A., Gayán, P., García-Labiano, F., Izquierdo, M. T., de Diego, L. F. and Adánez J. **2020**. "Coal Combustion via Chemical Looping Assisted by Oxygen Uncoupling with a Manganese‑iron Mixed Oxide Doped with Titanium." Fuel Processing Technology 197 (January): 106184.

Pikkarainen, T., Teir, S. and Hiltunen I. **2016**. "Piloting of Bio-CLC for BECCS." 4th International Conference on Chemical Looping. Nanjing (China).

Pikkarainen, T., Hiltunen, I. **2017**. "Chemical Looping Combustion of Solid Biomass Performance of Ilmenite and Braunite as Oxygen Carrier Materials." European Biomass Conference and Exhibition Proceedings 2017 (June): 1837–44.

Priddle, R. **2016**. "World Energy Outlook- Special Report Energy and Air Pollution." IEA, 266. https://doi.org/10.1021/ac00256a010.

Quéré, C. Le, Andrew, R. M., Friedlingstein, P., Sitch, S., Hauck, J., Pongratz, J., Pickers, P. A. et al. **2018**. "Global Carbon Budget 2018." Earth System Science Data 10 (4): 2141–94.

Rayner, S., Heyward, C., Kruger, T., Pidgeon, N., Redgwell, C. and Savulescu, J. **2013**. "The Oxford Principles." Climatic Change 121 (3): 499–512.

Reed, T. B., Levie, B. and Graboski, M. S. **1987**. "Fundamentals, Development and Scaleup of the Air-Oxygen Stratified Downdraft Gasifier." Richland, WA (United States).

Richter, H. J. and Knoche K. F. **1983**. "Reversibility of Combustion Processes." American Chemical Society. Chapter 3, 71–85.

Rodhe, H., Charlson, R., and Crawford E. **1997**. "Svante Arrhenius and the Greenhouse Effect." Ambio. vol. 26: 2-5.

Rydén, M., Leion, H., Mattisson, T. and Lyngfelt A. **2014**. "Combined Oxides as Oxygen-Carrier Material for Chemical-Looping with Oxygen Uncoupling." Applied Energy 113: 1924–32.

Sajen, S., Singh, S. K., Mungse, P., Rayalu, S., Watanabe, K., Saravanan, G. and Labhasetwar N. **2016**. "Mechanically Stable Mixed Metal Oxide of and Mn as Oxygen Carrier for Chemical Looping Syngas Combustion." Energy & Fuels 30 (9): 7596–7603.

Schäfer, S., Lawrence, M., Stelzer, H., Born, W., Low, S., Schäfer, S., Lawrence, M., et al. **2015**. "The European Transdisciplinary Assessment of Climate Engineering (EuTRACE) Away from Earth," 170. http://www.iass-potsdam.de/sites/default/files/files/rz_150715_eutrace_digital.pdf.

Schmidt, G. A., Kelley, M., Nazarenko, L., Ruedy, R., Russell, G. L., Aleinov, I., Bauer, M. et al. **2014**. "Configuration and Assessment of the GISS ModelE2 Contributions to the CMIP5 Archive." Journal of Advances in Modeling Earth Systems 6 (1): 141–84.

Schmitz, M. Linderholm, C., Hallberg, P., Sundqvist, S. and Lyngfelt, A. **2016**. "Chemical-Looping Combustion of Solid Fuels Using Manganese Ores as Oxygen Carriers." Energy & Fuels 30 (2): 1204–16.

Schmitz, M. and Linderholm C. J. **2016**. "Performance of Calcium Manganate as Oxygen Carrier in Chemical Looping Combustion of Biochar in a 10 KW Pilot." Applied Energy 169 (May): 729–37.

Schmitz, M. and Linderholm C. J. **2018**. "Chemical Looping Combustion of Biomass in 10- and 100-KW Pilots – Analysis of Conversion and Lifetime Using a Sintered Manganese Ore." Fuel 231 (November): 73–84.

Schmitz, M., Linderholm, C. J. and Lyngfelt, A.. **2018**. "Chemical Looping Combustion of Four Different Solid Fuels Using a Manganese-Silicon-Titanium Oxygen Carrier." International Journal of Greenhouse Gas Control 70 (March): 88–96.

Schramski, J. R., Gattie, D. K. and Brown J. H. **2015**. "Human Domination of the Biosphere: Rapid Discharge of the Earth-Space Battery Foretells the Future of Humankind." Proceedings of the National Academy of Sciences 112 (31): 9511–17.

Shen, L., Wu, J., Xiao, J., Song, Q. and Xiao R. **2009**. "Chemical-Looping Combustion of Biomass in a 10 kW_{th} Reactor with Iron Oxide as an Oxygen Carrier." Energy and Fuels 23: 2498–2505.

Shulman, A., Cleverstam, E., Mattisson, T.and Lyngfelt A. **2009**. "Manganese/Iron, Manganese/Nickel, and Manganese/Silicon Oxides Used in Chemical-Looping With Oxygen Uncoupling (CLOU) for Combustion of Methane." Energy & Fuels 23 (10): 5269–75.

Shulman, A., Cleverstam, E., Mattisson, T. and Lyngfelt A. **2011**. "Chemical – Looping with Oxygen Uncoupling Using Mn/Mg-Based Oxygen Carriers – Oxygen Release and Reactivity with Methane." Fuel 90 (3): 941–50.

Sikarwar, Vi. S., Zhao, M., Fennell, P. S., Shah, N. and Anthony E. J. **2017**. "Progress in Biofuel Production from Gasification." Progress in Energy and Combustion Science 61 (July): 189–248.

Simell, P., Ståhlberg, P., Kurkela, E., Albrecht, J., Deutsch, S. and Sjöström K. **2000**. "Provisional Protocol for the Sampling and Anlaysis of Tar and Particulates in the Gas from Large-Scale Biomass Gasifiers. Version 1998." Biomass and Bioenergy 18 (1): 19–38.

Song, T., Hartge, E. U., Heinrich, S., Shen, L. and Werther J. **2016**. "Chemical Looping Combustion of High Sodium Lignite in the Fluidized Bed: Combustion Performance and Sodium Transfer." In 4th International Conference on Chemical Looping, 70:22–31.

Staffell, I., Jansen, M., Chase, A., Cotton, E. and Lewis, C. **2018**. "Energy Revolution : A Global Outlook Headline Messages." Drax: Selby, 1–39. https://www.drax.com/wp-content/uploads/2018/12/Energy-Revolution-Global-Outlook-Report-Final-Dec-2018-COP24.pdf.

Sun, Y., Jiang, E., Xu, X., Wang, J. and Li Z. **2018**. "Supplied Oxygen Properties of $NiO/NiAl_2O_4$ in Chemical Looping Re-Forming of Biomass Pyrolysis Gas: The Influence of Synthesis Method." ACS Sustainable Chemistry & Engineering 6 (11): 14660–68.

Team, ESRL. 2019. "ESRL Global Monitoring Division - Global Greenhouse Gas Reference Network." 2019. https://www.esrl.noaa.gov/gmd/ccgg/trends/global.html.

UNEP. **2018**. The Emissions Gap Report 2018. Nairobi: United Nations Environment Programme.

UNFCCC. **2015**. "Paris Agreement." UNFCCC. https://doi.org/FCCC/CP/2015/L.9.

Vangkilde-Pedersen, T., Anthonsen, K. L., Smith, N., Kirk, K., Neele, F., van der Meer, B., Le Gallo, Y., et al. **2009**. "Assessing European Capacity for Geological Storage of Carbon Dioxide–the EU GeoCapacity Project." Energy Procedia (1): 2663–70.

Virginie, M., Adánez, J., Courson, C., de Diego, L. F., García-Labiano, F., Niznansky, D., Kiennemann, A., Gayán, P. and Abad, A. **2012**. "Effect of Fe–

Olivine on the Tar Content during Biomass Gasification in a Dual Fluidized Bed." Applied Catalysis B: Environmental 121–122 (June): 214–22.

Visser, E., de Hendriks, C., Barrio, M., Mølnvik, M. J., de Koeijer, G., Liljemark, S. and Le Gallo, Y. **2008**. "Dynamis CO_2 Quality Recommendations." International Journal of Greenhouse Gas Control 2 (4): 478–84.

Werther, J., Saenger, M., Hartge, E. U., Ogada, T. and Siagi, Z. **2000**. "Combustion of Agricultural Residues." Progress in Energy and Combustion Science 26 (1): 1–27.

Wiesenthal, T., Mourelatou, A., Petersen, J. E. and Taylor P. **2006**. "How Much Bioenergy Can Europe Produce without Harming the Environment?" Eea No. 7 (7): 1–72. http://reports.eea.europa.eu/eea_report_2006_7/en.

Williams, A., Jones, J.M., Ma, L. and Pourkashanian M. **2012**. "Pollutants from the Combustion of Solid Biomass Fuels." Progress in Energy and Combustion Science 38 (2): 113–37.

Belotskaia E. D., Galkin I. V., Galkina A. A., Geller E. I., Gimadi V. I., Grigoriev L. M., et al. **2016**. "Global and Russian Energy Outlook 2016." Edited by The Analytical Center for the Government of the Russian Federation, November 2016, Moscow, 1-198

Yan, J., Shen, L., Jiang, S., Wu, J., Shen, T., and Song, T. **2017**. "Combustion Performance of Sewage Sludge in a Novel CLC System with a Two-Stage Fuel Reactor." Energy & Fuels 31 (11): 12570–81.

Zapatero, M. A., Reyes, J. L., Martínez, R., Suárez, I., Arenillas, A. and Perucha, M. A. **2008**. "Estudio Preliminar de Las Formaciones Favorables Para El Almacenamiento Subterráneo de CO_2 En España." Instituto Geológico y Minero de España, 1-135.

Zevenhoven, M., Sevonius, C., Salminen, P., Lindberg, D., Brink, A., Yrjas, P. and Hupa, L. **2018**. "Defluidization of the Oxygen Carrier Ilmenite – Laboratory Experiments with Potassium Salts." Energy 148 (April): 930–40.

APPENDIX - PAPERS